ユーザ中心の無線システムに向けて：カスタマイズと持続可能性のための再構成可能なインテリジェント表面の最適化

Towards User-centric Wireless Systems: Optimizing Reconfigurable Intelligent Surfaces for Customization and Sustainability

YUYIN MA

Department of Sciences and Informatics
Muroran Institute of Technology

This dissertation is submitted for the degree of
Doctor of Philosophy of Engineering

August 2024

Declaration

I hereby declare that this thesis is my own work and effort and that it has not been submitted anywhere for any award. Wherever contributions of others are involved, every effort is made to indicate this clearly, with due reference to the literature, and acknowledgement of collaborative research and discussions.

YUYIN MA
August 2024

Acknowledgements

Firstly, I extend my sincere gratitude to my supervisor, Prof. Mianxiong Dong, for his unwavering support during my Ph.D. studies and research endeavors. His patience, motivation, and profound expertise have been invaluable assets. Under his guidance, I have gained invaluable insights into the research process, academic writing, presentation skills, and more.

Besides my supervisor, I would like to thank the rest of my thesis committees: Prof. Sato Kazuhiko, Prof. Kaoru Ota, and Prof. Yusheng Ji, for their insightful comments and encouragement, but also for the hard questions which encouraged me to widen my research from various perspectives.

I am grateful to Prof. Kaoru Ota, Prof. He Li, and Prof. Jianwen Xu for their invaluable support of my scientific research. Particularly, I extend my heartfelt gratitude to Prof. Kaoru Ota for her extensive assistance in various aspects of my research.

I would like to acknowledge the financial support from the China Scholarship Council (CSC), which enables me to concentrate on my studies without worrying about tuition and living expenses.

Last but not least, I extend my deepest gratitude to my family and parents for their unwavering spiritual support throughout my Ph.D. journey.

YUYIN MA
August 2024

Abstract

Reconfigurable intelligent surfaces (RISs) have emerged as a promising technology for future wireless communication systems due to their passive meta-elements, slim design, high integration, cost-effectiveness, and ease of deployment. However, optimizing beamforming at RISs, transmission power at access points (APs), deployment locations of multiple RISs, and association relationships between RISs and IoT devices are crucial for various RIS-assisted wireless communication networks. Therefore, this dissertation presents effective solutions to maximize the achievable rates, enhance the coverage probability, minimize power consumption, and optimize the quality of experience (QoE).

In this dissertation, four major tasks are proposed on the various multi-RIS-assisted wireless communication scenarios. The first task investigates the influence of multiple RIS on the average achievable rate in indoor communication wireless networks. The second task focuses on exploring the relationships between coverage probability and deployment locations of multiple RIS in outdoor scenarios to maximize coverage while satisfying the network cost constraint. Moreover, the second task introduces a method based on approximate cell decomposition to calculate coverage probability quantitatively. The third task is to optimize power consumption, which consists of exploring the association relationships and minimizing the overall power consumption. Finally, the last task investigates the RIS deployed in the wireless VR THz communication systems to maximize the QoE by jointly optimizing the beamforming vectors at multiple RISs, the transmit power of AP, and the rendering capacity allocation among VR users. To solve the issue, the issue is decomposed into two stages: stage-1 aims to minimize BER and maximize the data rate, while stage-2 aims to maximize rendering capacity among virtual objects.

Table of contents

List of figures **xiii**

List of tables **xvii**

1 Introduction **1**

1.1 Background 1

1.2 System Outline and Challenges 3

1.2.1 The Maximization of Achievable Rate in Multi-RIS-Assisted Indoor Wireless Networks 3

1.2.2 The Enhancement of Coverage in Multi-RIS-Assisted Outdoor Wireless Communication Networks 4

1.2.3 The Optimization of Power in Multi-RIS-Assisted Indoor Communication Networks 4

1.2.4 QoE Optimization for VR Services in Multi-RIS-Assisted Terahertz Wireless Networks 5

1.3 Organization 5

2 The Maximzation of Achievable Rate in Multi-RIS-Assisted Indoor Wireless Networks **7**

2.1 Motivation 7

2.2 Related Work 8

2.3 System Model and Problem Formulation 10

2.4 Proposed Multi-verse Optimizer Algorithm 11

2.5 Numerical Results and Analysis 15

2.5.1 Simulation Settings 15

2.5.2 Performance Evaluation 16

2.6 Conclusion 18

3 The Enhancement of Coverage in Multi-RIS-Assisted Outdoor Wireless Communication Networks 21
3.1 Motivation . . . 21
3.2 Related Work . . . 23
3.3 System Model and Problem Formulation . . . 25
3.3.1 Multi-RIS-assisted Wireless Communication Scenario . . . 25
3.3.2 RIS Model . . . 27
3.3.3 Path Loss Model . . . 27
3.3.4 Coverage Probability Analysis . . . 29
3.3.5 Network Cost Analysis . . . 34
3.3.6 Problem Formulation . . . 34
3.4 Coverage Probability Maximization Algorithm Design . . . 35
3.4.1 Rule-based Algorithm to Obtain Feasible Solutions . . . 35
3.4.2 Branch-and-Bound Algorithm to Optimize RISs Deployment Locations 35
3.5 Simulation Results . . . 38
3.5.1 Coverage Enhancement for Multi-RIS Deployment . . . 38
3.5.2 Performance Evaluation vs. Number of OBs, BSs, and RISs . . . 40
3.5.3 Comparison Algorithms . . . 43
3.6 Conclusion . . . 45

4 The Optimization of Power in Multi-RIS-Assisted Indoor Communication Networks 47
4.1 Motivation . . . 47
4.2 Related Work . . . 49
4.3 System Model and Problem Formulation . . . 50
4.3.1 System Model . . . 50
4.3.2 Signal Model . . . 52
4.3.3 Path Loss and Number of Elements Model . . . 53
4.3.4 Communication Region and Coverage Rate . . . 54
4.3.5 Power Consumption Model . . . 55
4.3.6 Problem Formulation . . . 56
4.4 Solution to Power Minimization Problem . . . 57
4.4.1 Coverage-Based Association Strategy Design . . . 57
4.4.2 Phase-Based Power Consumption Optimization Design . . . 61
4.5 Numerical Experiments . . . 61
4.5.1 Coverage Rate Performance . . . 62
4.5.2 Performance evaluation for different deployment strategy . . . 64

4.5.3 Comparison Algorithms 65
4.6 Conclusion 69

5 QoE Optimization for VR Services in Multi-RIS-Assisted Terahertz Wireless Networks 71
5.1 Motivation 71
5.2 Related Work 74
5.3 System Model 76
5.3.1 Scenario Description 76
5.3.2 Uplink BER Performance 76
5.3.3 Downlink Transmission Rate 81
5.3.4 MEC Rendering 82
5.4 Problem Formulation and Decomposition 83
5.4.1 Quality of Experience Analysis 83
5.4.2 Problem Formulation 84
5.4.3 Problem Decomposition 85
5.5 QoE Optimization for VR Users in Multi-RIS-Assisted Wireless THz Networks 86
5.5.1 Minimization BER and Maximization Data Rate at Stage-I 86
5.5.2 Maximization Rendering Capacity Allocation at Stage-II 90
5.6 Simulation Results 91
5.7 Conclusion 97

6 Conclusions and Future Directions 99

References 101

7 Appendix 113
7.1 Proof of Virtual LoS Link Probability 113
7.2 Proof of Reflection Probability 113

List of figures

2.1 The multi-RIS assisted multi-user indoor wireless communication system model. 10
2.2 Convergence of the MVO algorithm for different values of K, L, N. The system parameters are set as $M = 16$, $C = 2$. 16
2.3 The average achievable rate versus the number of the phase shifts states C for $M = 16$, $L = 4$, $K = 3$. 16
2.4 The average achievable rate versus the number of reflecting elements N, where $M = 16$, $C = 2$, $K = 2$. 17
2.5 The average achievable rate versus the number of mobile uers N, where $M = 16$, $C = 2$, $N = 32$, $L = 4$. 18

3.1 The system model of wireless communication networks assisted by multiple RISs. (a) The scenario graph. (b) The view graph. 26
3.2 Examples of coverage probability calculation. (a) The coverage calculation without RIS. (b) The coverage calculation for deploying RIS. 30
3.3 The setup for the fourth condition. 33
3.4 An example of the Rule-based method. 36
3.5 Tree structure of the proposed B&B algorithm. 36
3.6 A realization of the coverage regions with the density of BS $\lambda_{BS} = 10/\text{km}^2$, the density of obstacles is $\lambda_{OB} = 400/\text{km}^2$, and the RIS density is $\lambda_{RIS} = \mu\lambda_{OB}$. Fig. 3.6(a) is a scenario diagram. Fig. 3.6(b)-(f) are the coverage diagrams. The μ varies as follows: (a) $\mu = 0$, (b) $\mu = 0$, (c) $\mu = 0.1$, (d) $\mu = 0.2$, (e) $\mu = 0.4$, (f) $\mu = 0.8$. 39
3.7 The number of RISs after pruning versus the number of BSs, where $\lambda_{OB} = 700/\text{km}^2$. 40
3.8 The coverage probability versus the number of OBs, where $\lambda_{BS} = 14/\text{km}^2$. 41
3.9 The coverage probability and network cost versus the different number of OBs and RIS density for $\lambda_{BS} = 14/\text{km}^2$. 41

3.10 The coverage probability and network cost versus the different number of BS and RIS density for $\lambda_{OB} = 700/\text{km}^2$. 42
3.11 The coverage probability and network cost versus the different number of BSs and OBs. 42
3.12 The coverage probability and network cost versus the number of OBs, where $\lambda_{BS} = 14/\text{km}^2$, $\lambda_{RIS} = 0.5 \cdot \lambda_{OB}/\text{km}^2$. 43
3.13 The coverage probability and network cost versus the number RISs, where $\lambda_{BS} = 14/\text{km}^2$, $\lambda_{OB} = 700/\text{km}^2$. 44

4.1 System model. 51
4.2 Improved cooling parameter ν and coverage convergence of coverage for different oscillation period c. 63
4.3 The association relationships between RISs and IoT devices for different cases in indoor wireless communication environment with 200 m $\times$ 200 m. (a) Case I: $B = 2, K = 30, R = 20, OB = 40$; (b) Case II: $B = 2, K = 60, R = 20, OB = 40$; (c) Case III: $B = 2, K = 30, R = 40, OB = 40$;(d) Case IV: $B = 4, K = 30, R = 20, OB = 40$; (e) Case V: $B = 2, K = 30, R = 20, OB = 80$. 63
4.4 The coverage rate of LoS and RIS-aided for different cases. 63
4.5 The coverage rate and power consumption for various deployment strategies. 65
4.6 The coverage rate and power consumption *vs.* the number of elements, where $N = 100, N = 200, N = 300$, and $N = 400$, respectively. 66
4.7 The coverage rate and power consumption *vs.* the number of devices, where $K = 10, K = 30, K = 50$, and $K = 70$, respectively. 67
4.8 The coverage rate and power consumption *vs.* the number of obstacles, where $OB = 20, OB = 40, OB = 60$, and $OB = 80$, respectively. 68
4.9 The coverage rate and power consumption *vs.* the number of obstacles, where $R = 10, R = 20, R = 30$, and $R = 40$, respectively. 68

5.1 Structure and contributions of this paper. Part I introduces the scenario and system model, which includes uplink BER, downlink transmission rate, and MEC rendering. Part II presents the problem formulation and algorithm design. Part III demonstrates our proposed approach performance versus several simplified schemes regarding average data rate and QoE. 73
5.2 Multi-RIS-assisted THz wireless VR system in the indoor environment. . . 77
5.3 A top view of considered multi-RIS-assisted wireless VR system. 92

5.4 BER performance of single/multiple RIS-assisted THz wireless VR network. (a) Case of a single RIS with different reflective elements. (b) Case of multiple RIS with same reflective elements $N = 20$. 93
5.5 The effect of rendering capacity on the average QoE in the considered multi-RIS-assisted THz wireless VR system. 93
5.6 The effect of the number of RIS on the downlink data rate from AP to the users and the average QoE among VR users in the considered multi-RIS-assisted THz wireless VR system. 94
5.7 The effect of the number of reflecting elements on the downlink data rate from AP to the users and the average QoE among VR users in the considered multi-RIS-assisted THz wireless VR system. 95
5.8 The effect of the total transmit power on the downlink data rate from AP to the users and the average QoE among VR users in the considered multiple RIS-assisted THz wireless VR system. 96
5.9 The effect of the number of VR users on the downlink data rate from AP to the users and the average QoE among VR users in the considered multiple RIS-assisted THz wireless VR system. 97

List of tables

2.1 Solution updation 15

3.1 Symbols and descriptions 38

4.1 Symbols and descriptions 62

Chapter 1

Introduction

1.1 Background

The exponential data growth in the internet era with limited spectrum resources has derived a strong desire for future wireless communication speed, quality, and security [19]. To fill this vision, reconfigurable intelligent surfaces (RISs), also known as intelligent reflecting surfaces (IRS) and large intelligent surfaces (LIS) [21], have emerged as an up-and-coming paradigm for wireless communication, offering significant advantages over traditional solutions like adding base stations (BSs) or relays in many tasks, e.g., improving data transmission, enhancing coverage, reducing energy consumption and system costs [20]. The square metal arrays controlled by a digital microcontroller in an RIS produce different amplitudes and phase shifts on the incident signal, intending to enhance the signal quality at receivers [91]. In the absence of complicated signal processing, coding, and decoding procedures, RISs enable telecom operators to control the whole propagation environment by modeling the objects and regulating the electromagnetic response in a controlled environment. The advantages of RIS are summarized as follows:

- **Easy to deploy:** RISs comprise passive elements and a micro-digital controller. RISs can be placed on various objects, including the facades of buildings, indoor walls [68], trees, billboards, the facades of high-speed rail, vehicle windows, and unmanned aerial vehicles (UAV).

- **Spectral efficiency enhancement:** RISs adjust signal transmission path and beamforming through multipath propagation, enabling more mobile users and data transmission within the same spectrum resource. This enhancement in spectrum efficiency can boost communication system capacity and throughput to satisfy growing communication demands.

- **Signal and coverage enhancement:** By manipulating the phase shifts of reflective elements, RISs control signal propagation direction and beamforming. Typically, obstacles like taller buildings obstruct the Line-of-sight (LoS) links between the base stations (BSs) and mobile users. The RIS-assisted virtual LoS links are established to enhance coverage and signal strength.
- **Power Reduction:** Compared to traditional methods involving increased transmit power of BSs or BS quantity, RISs optimize propagation paths and reduce signal power consumption. Therefore, RIS usage can more efficiently curtail power consumption and enhance system energy utilization.
- **Cost Effectiveness:** RIS deployment and maintenance costs are relatively low, yet they offer more efficient communication services, thereby reducing overall communication expenses.
- **Privacy Protection:** By controlling the signal direction and beamforming, RISs mitigate the risk of signal leakage and eavesdropping, safeguarding user privacy and communication content.
- **Compatibility:** As RISs only reflect Wireless electromagnetic (EM) waves, they support full-duplex (FD) and full-band transmission. Moreover, RIS-enhanced wireless networks seamlessly integrate with existing wireless network standards and hardware.

Most recent studies have investigated RIS because of the aforementioned advantages and characteristics, focusing on exploring their various application scenarios under different assumptions. For example, RIS-assisted cellular networks are proposed, where RISs are installed on the obstacles between BSs and mobile users. Therefore, the quality of service (QoS) in heterogeneous networks and the latency in mobile edge computing (MEC) networks are improved [12, 6]. On the other hand, RISs serve as signal reflection hubs to support large-scale connectivity through interference mitigation technology in device-to-device (D2D) communication networks [13], or RISs can be employed in the physical layer security (PLS) by intelligently designing wireless beamforming to eliminate interference signals [96]. RIS-assisted indoor communications are also being explored, with RISs strategically placed on walls to improve the QoS in indoor environments with high data rate demands, such as virtual reality (VR) applications. Moreover, to ensure full coverage in block-sensitive scenarios like visible light communications [83] and wireless fidelity (WiFi) networks, a concatenated virtual RIS-aided LoS link can be established between access points (APs) and mobile users. This setup allows for LoS propagation links between APs and RISs, as well as between RISs and users. Additionally, RISs hold the potential for optimizing the performance of various

wireless networks, including UAV-enabled networks [46], cellular-connected UAV networks [54], autonomous vehicular networks, autonomous underwater vehicle (AUV) networks, and intelligent robotic networks, by harnessing the benefits offered by RIS technology.

Therefore, RIS technology has emerged as a promising solution in various application domains, especially in wireless communication systems. However, several challenges persist in the deployment of RIS in different scenarios. The first challenge is to investigate the influence of multiple RIS in indoor walls on the average achievable rate. The second challenge is to explore coverage probability in outdoor wireless communication networks with the assistance of large-scale RISs. The third challenge is to minimize overall power consumption while optimizing association relationships between multiple RISs and several IoT devices. The fourth challenge is to enhance the QoE for VR services in wireless Terahertz networks by jointly optimizing the passive beamforming at the RISs, the transmission power, and rendering capacity allocation among VR users.

1.2 System Outline and Challenges

In this section, four major challenges in the dissertation are briefly introduced, and the following chapters will discuss these research problems in detail.

1.2.1 The Maximization of Achievable Rate in Multi-RIS-Assisted Indoor Wireless Networks

Technological development in the creation of programmable metamaterial has aided progress in the development of the Reconfigurable Intelligent Surface (RIS), which has been considered one of the fundamental technologies for future wireless communication systems. In this paper, we investigate the problem of maximizing the average achievable rate for multiple users indoor wireless communication environment assisted by multiple RISs. Unlike most existing works considering single-RIS single-user scenarios or single-RIS multi-user scenarios, the multi-RIS can reflect the signals from several transmission links in all destinations. The average achievable rate maximization problem for indoor communication systems is solved by optimizing the phase shifts of reflective elements. Thus, we propose a Multi-verse Optimizer approach to solve the problem. Our simulation results demonstrate that a communication system with multiple RISs provides considerable achievable rate gains relative to baseline schemes.

1.2.2 The Enhancement of Coverage in Multi-RIS-Assisted Outdoor Wireless Communication Networks

As one innovative paradigm, reconfigurable intelligent surface (RIS) has been applied to enhance coverage in wireless communication networks by providing a virtual connection between the transmitter and the receiver in scenarios where line-of-sight (LoS) is obstructed. In this work, the issue of optimizing multi-RIS deployment locations is considered to enhance coverage while reducing network costs. We first develop a method based on approximate cell decomposition to quantitatively calculate the coverage probability in RIS-assisted outdoor wireless communication networks. Then we propose a RIS location optimization strategy, Rule-based and Brand-and-Bound-based (B&B), called R&B algorithm to strike a balance between coverage probability and network cost. The Rule-based algorithm is applied to obtain feasible solutions, and the B&B algorithm is proposed to optimize the RISs deployment locations to enhance coverage probability while satisfying network cost constraints. Numerical results show that the proposed method outperforms the other baseline schemes to trade off coverage probability and network cost in a multi-obstacle wireless communication environment with sufficient RIS.

1.2.3 The Optimization of Power in Multi-RIS-Assisted Indoor Communication Networks

Reconfigurable intelligent surfaces (RISs) have been proposed to mitigate power consumption in wireless communication systems by dynamically adjusting the signal propagation direction between transmitters and receivers. In this paper, the problem of optimizing the power consumption and IoT device coverage rate in an indoor communication scenario is considered. An adaptive hybrid optimization strategy (AHOS) based on the association between RISs and devices is proposed to maximize the device coverage rate. We then aim to minimize system power consumption by optimizing the phase shifts of multiple RISs using the relaxation transformative method while satisfying the coverage constraint. Extensive simulation results demonstrate that, in an indoor environment with several obstacles, the proposed algorithm achieves higher coverage compared to a solution without RIS and exhibits lower power consumption compared to strategies relying more on BS.

1.2.4 QoE Optimization for VR Services in Multi-RIS-Assisted Terahertz Wireless Networks

The immersive experience and 360-degree visual stimulation offered by virtual reality (VR) have contributed to its widespread adoption in games, education, and healthcare. The quality of experience (QoE), as a significant performance indicator, is used to measure user experience from subjective and objective perspectives and is required to satisfy high data rate, low delay, and high reliability in the wireless VR system. To achieve a higher data rate for VR users, a terahertz (THz) network is deployed. However, THz frequency experiences severe signal attenuation due to complex indoor obstacles, which can be alleviated by utilizing a reconfigurable intelligent surface (RIS) equipped with programmable metamaterial reflective elements. Taking inspiration from these considerations, this paper investigates a new framework for indoor multi-user multi-RIS-assisted THz wireless VR systems. Based on the scenario, an optimization problem is formulated to maximize the QoE by jointly optimizing the passive beamforming at RIS, the transmit power allocation among VR users, and the rendering capacity allocation among virtual objects. To achieve an optimal solution, we decompose the optimization problem into two stages: stage-1 aims to minimize BER and maximize data transmission rate, while stage-2 aims to maximize rendering capacity among virtual objects. Objective function conversion and alternative optimization (AO) methods are employed to address the two problems. Extensive simulations are conducted to validate the feasibility of the proposed system model and to showcase the superior performance of the proposed method in terms of QoE compared to other baseline methods.

1.3 Organization

The rest of this dissertation is organized as follows. We briefly introduce the trendency of VR games in Chapter 2. This chapter also includes the analyzation of user concerns of different language regions. We discuss the UX in VR games of different age groups in Chapter 3, which considers the avatar, self-presentation, harassment behaviors, and physical effects. Chapter 4 shows the exploration of Cybersickness in VR games. We conclude this dissertation in Chapter 5.

Chapter 2

The Maximzation of Achievable Rate in Multi-RIS-Assisted Indoor Wireless Networks

2.1 Motivation

Along with the gradual solidification of the fifth-generation (5G) standardization, academics and industry have turned their attention to sixth-generation (6G) wireless communication technology [19]. It has been demonstrated that multiple-input multiple-output (MIMO) has been achieved successfully in the 5G era with high data rates, low latency, and secure transmission as a potential approach for supporting large numbers of users. However, insufficient coverage is a challenging problem with the current communication systems, especially in the indoor environment. The high signal loss caused by the walls can lower the signal strength received from an outdoor Base Station (BS) within a building to an unacceptably low level. There is the fact that BSs can not increase transmission power in an unlimited manner to improve signals received in trouble zones. A better solution is to provide more dense transmission points in these areas. That is to say, additional BSs or multiple relays are deployed, which benefits users but is a high cost in terms of the cumbersome location-finding procedure, the heavy backhaul, execution, as well as power-consuming [37].

The reconfigurable intelligent surface (RIS), also called large intelligent surface (LIS), has been widely used as a cost-effective method for overcoming non-line-of-sight (NLoS) transmission and increasing the coverage of blind areas. Meanwhile, RIS has been proven to reduce spectral inefficiency, energy consumption, and security threats and improve reliability

in communication networks [92] [59]. Therefore, RIS has been considered a potential technique for the forthcoming 6G communication systems.

This paper discusses a multi-RIS-assisted multiple mobile users' indoor wireless communication network. An AP generates signals reflected by the RISs, resulting in a favorable RSS distribution. To optimize the average achievable rate of all mobile users, we formulate the optimization problem. Furthermore, optimizing discrete phase shifts of all RIS elements is an NP-hard problem. We first derive the fitness function and then propose a multi-verse optimizer (MVO) algorithm to solve the problem efficiently. Overall, the primary contributions of this article can be summarized as follows.

- We investigate the achievable rate maximization problem of multiple users' indoor wireless communication assisted by the multi-RIS. This article is an early attempt to focus on a multi-user, multi-RIS-assisted communication scenario.
- We introduce the MVO algorithm to maximize the achievable rate by optimizing phase shifts of RIS elements. As far as we know, this study is the first work that uses the MVO algorithm in a multi-user indoor wireless environment by assisting multiple RISs.
- We analyze the convergence and the optimality of the MVO algorithm, discuss the performance of the proposed optimization scheme, and verify the effectiveness of the proposed approach through simulations.

2.2 Related Work

The RIS is an artificial surface consisting of electromagnetic material with a significant number of square metal arrays, each of which can be controlled through a digital microcontroller to produce various amplitudes and phases on incident signals [91]. To enhance the achievable rates, the signals from several transmission links are aligned at the intended receiver by regulating the phase shifts of RIS elements [69], which is a breakthrough feature that has never been applied in any the modern wireless communication networks. In addition, metasurfaces can be covered on existing infrastructure, such as building walls and UAV surfaces, reducing operational costs and the complexity of RIS deployment. As a result, RIS has excellent potential in a variety of applications because they offer a cost-effective way to regulate the radio propagation environment without having to deploy extra energy-intensive and high-priced communication facilities, such as amplify-and-forward relays. Nowadays, owing to the aforementioned attractive characteristic, RIS has been widely investigated and

applied in many wireless communication systems, e.g., OFDM, NOMA, Multi-antenna Communication.

Given the fact that RIS has gained significant attention over the last few years, the majority of the current work has been focused on hardware development, such as reflect-arrays and metasurfaces, as well as executing end-to-end experiment tests. In addition, some studies have been conducted to enhance the performance of RIS-enabled communication systems. Aiming at the energy efficiency (EE) maximization problem, Huang *et al.* [37] studied a multiple users MISO wireless communication network with RIS-assisted and proposed a method that is a solution for the joint design of transmission power for each mobile user and phase shifts of reflecting elements. Yu *et al.* [98] devoted their efforts to enhance the achievable sum rate of the wireless communication system by cooperatively optimizing the transmission beamforming vectors, the artificial noise (AN) covariance matrix, and phase shifts of RIS elements while ensuring secrecy restrict for any eavesdroppers. The machine learning technique is also exploited in RIS-assisted wireless communication systems. For example, Huang *et al.* [38] proposed using deep reinforcement learning (DRL) technology to design and optimize transmit beamforming and phase shifts. In addition, In addition, Mao *et al.* [57] combined RIS with edge computing to improve the security of task offloading.

All the works mentioned above focus on RIS-aided outdoor wireless communication systems. Nevertheless, several wireless communication technologies have been presented to enhance signals focusing on the indoor environment over the last few decades. For example, Zhang *et al.* [102] presented an alternating optimization algorithm to maximize energy efficiency for the MISO system by RIS-assisted consisting of passive reflection elements. Venkat Arun *et al.* [4] put forward a system called RFocus that shifts the beamforming functions into the surrounding environment. RFocus comprises a 2D surface with a rectangular metamaterial of simple components, including an RF switch. These elements either transmit or reflect electrical signals. An algorithm based on a majority vote maximizes received signal strength (RSS) at a target user, determined by the state of the reflecting elements using a software controller. Huang *et al.* [36] formulated a coordinated fingerprint database as training data for an offline phase. On the other hand, the authors developed an approach for deploying RIS in the indoor wireless communication environment to configure them online using deep learning efficiently. To the best of our knowledge, however, most studies of RIS have failed to consider the scenario of multi-user multi-RIS-assisted communication systems in indoor environments.

2.3 System Model and Problem Formulation

In this paper, we analyze an indoor wireless communication environment with one AP, multiple RISs, and multiple mobile users, as shown in Fig.2.1. The AP has M antenna elements and communicates with K users. A RIS consists of N reflective elements and one microcontroller which can regulate the operation of the RIS. In general, building facades are equipped with multiple RISs to assist this wireless communication.

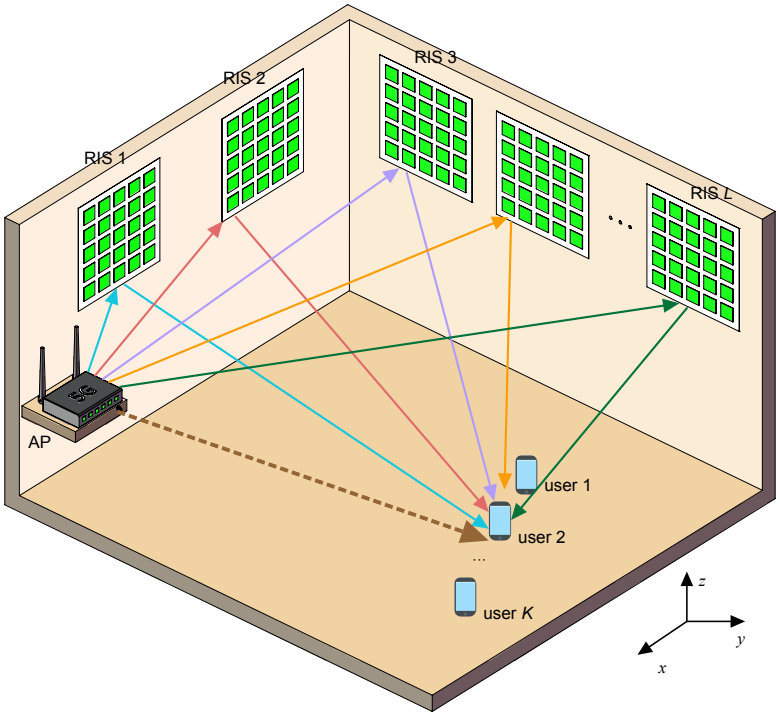

Fig. 2.1 The multi-RIS assisted multi-user indoor wireless communication system model.

With $\mathbf{h}_k \in \mathbb{C}^{1\times M}$, we represent the direct communication channel between AP and the mobile user k, where $k = 1,2,\ldots,K$. Additionally, $\mathbf{H}_{k,l} \in \mathbb{C}^{1\times N}$ represents the channel between the user k and the RIS l, and the notion $\mathbf{G}_l \in \mathbb{C}^{N\times M}$ represents the channel between AP and the l-th RIS. It can be shown that the baseband representation of the received signal strength at the k-th mobile user is expressed by

$$y_k = \sum_{l=1}^{L} (\mathbf{H}_{k,l}\mathbf{\Phi}\mathbf{G}_l + \mathbf{h}_k)\mathbf{x} + n_k \tag{2.1}$$

where l is the number of RIS, and $\mathbf{x} \triangleq \sqrt{\frac{p_k}{M}}\mathbf{1}_M x_k, \in \mathbb{C}^{M\times 1}$ indicates the transmission signal from AP to all the users, which satisfies $\mathbb{E}[|x_k|^2] = p_k \leq P_k$, p_k denotes the transmission

power of user k and P_K denotes the maximum power of user k. In addition, $n_k \sim \mathscr{CN}(0,\delta^2)$ means Gaussian white noise with variance δ^2, and $\mathbf{\Phi} \triangleq \text{diag}[\phi_1,\phi_2,\ldots,\phi_{\text{N}}], \in \mathbb{C}^{\text{N}\times\text{N}}$ denotes a diagonal matrix including the phase shifts $\phi_n, \forall n = 1,2,\ldots,N$, applied at the RIS reflecting elements.

Each of the reflecting elements is assumed to have C states with the same amplitude ratio and a uniform phase shift interval $\Delta\theta = \frac{2\pi}{C}$. As a result, the n-th element's phase shift can be expressed as

$$\phi_n = \alpha_n e^{jc_n\Delta\theta} \tag{2.2}$$

where the amplitude ratio $\alpha_n \in [0,1], n = 1,2,\ldots,N$ is a constant and $c_n \in \{1,\ldots,C\}$. The subsequent analysis focuses on communication performance differences caused by the phase shifts of RIS. Hence, we assume $\alpha_n = 1$. In this study, c_n is used to represent the n-th element's phase shift for convenience. Thus, $\mathbf{c} = \{c_1,c_2,\ldots,c_N\}$ can be utilized to represent the vector of phase shifts.

From (2.1), it is obvious that the SINR at the k-th user is given by

$$\gamma_k = \sum_{l=1}^{L} \frac{p_k \mid \mathbf{H}_{k,l}\mathbf{\Phi}\mathbf{G}_l + \mathbf{h}_k \mid^2}{\sum_{i=1,i\neq k}^{K} p_i \mid \mathbf{H}_{i,l}\mathbf{\Phi}\mathbf{G}_l + \mathbf{h}_i \mid^2 + \delta_2} \tag{2.3}$$

Hence, the achievable sum rate, as given in (2.4), is obtained as

$$\mathscr{R} = \sum_{k=1}^{K} \log_2(1+\gamma_k) \tag{2.4}$$

In this paper, using the MVO algorithm, we aim to find out what is the optimal $\mathbf{\Phi}$ to maximize the system average achievable rate at a particular channel state information (CSI). Therefore, we can formulate the optimization problem as follows.

$$\begin{aligned} \max\ & f_{obj} = \frac{1}{K}\cdot\mathscr{R}(\mathbf{G}_l,\mathbf{H}_{k,l},\mathbf{h}_k,\mathbf{\Phi}) \\ s.t.\quad & 0 \le \phi_n \le 2\pi \\ & p_k \le P_k \end{aligned} \tag{2.5}$$

2.4 Proposed Multi-verse Optimizer Algorithm

Our objective in this paper is to design the optimal multiple RISs configuration for maximizing the system average achievable rate in a multi-user indoor wireless communication environment.

In this section, we present the proposed MVO algorithm for designing RIS elements with phase shifts. The algorithm was proposed by Mirjalili *et al.* in 2016 [61], which is based on astrophysics. Within the algorithm, white holes, black holes, and wormholes were presented by the authors. In the search space, white holes and black holes handle exploration, while wormholes handle development. In addition, some novel conceptions are presented, e.g., a universe that matches a candidate solution of all phase shifts, an individual from the universe that matches a solution variable, and the inflation rate matches the fitness value. A detailed description of the proposed method can be found in Algorithm 1, which can be divided into the following steps:

1) Initialization: We assumed that a population consists of p universes and d dimensional target space while initialing them.

$$\boldsymbol{U} = \begin{bmatrix} u_1^1 & u_1^2 & \cdots & u_1^d \\ u_2^1 & u_2^2 & \cdots & u_2^d \\ \vdots & \vdots & \ddots & \vdots \\ u_p^1 & u_p^2 & \cdots & u_p^d \end{bmatrix} \tag{2.6}$$

where d corresponds to the number of phase shifts of all RIS elements.

2) Selection: We used the roulette mechanism to build mathematical models between white holes and black holes; all universes are ranked according to their inflation rate (fitness value) in each iteration and while a roulette mechanism selects a white hole.

$$u_i^j = \begin{cases} u_k^j, & r_1 < NI(\boldsymbol{U}_i) \\ u_i^j, & r_1 \geq NI(\boldsymbol{U}_i) \end{cases} \tag{2.7}$$

where u_i^j indicates the position of the j-th black hole of the i-th universe, and $NI(\boldsymbol{U}_i)$ is the normalized inflation rate of the i-th universe, $r_1 \in [0,1]$ is a random number. In addition, u_k^j is the j-th black hole of the k-th universe selected as a white hole by the roulette mechanism.

3) Update: Update the position of black holes in the current optimal universe.

if $r_2 < WEP$,

$$u_i^j = \begin{cases} u_{best}^j + TDR \times ((ub_j - lb_j) \times r_4 + lb_j), & r_3 < H \\ u_{best}^j - TDR \times ((ub_j - lb_j) \times r_4 + lb_j), & r_3 \geq H \end{cases} \tag{2.8}$$

if $r_2 \geq WEP$,

$$u_i^j = u_i^j \tag{2.9}$$

Algorithm 1 Multi-verse Optimization Algorithm (MVO)

Input:

$\mathbf{G}_l$, $\mathbf{H}_{k,l}$, $\mathbf{h}_k$, T, p, ub, lb, d, f_{obj}.

Output:

U_{best}, f_{obj}^{best}.

Initialize the p universes, (2.6).
Setting $wep_{min} = 0.2$ and $wep_{max} = 1$.
while $t < T + 1$ **do**
  Compute WEP by (2.11);
  Compute TDR by (2.10);
  for $i = 1$ to p **do**
    Compute Inflation rate f_{obj}^{i} for each universe by (2.5);
    if $f_{obj}^{i} > f_{obj}^{best}$ **then**
      $f_{obj}^{best} \leftarrow f_{obj}^{i}$;
      $U_{best} \leftarrow U_i$;
    end if
  end for
  $SU \leftarrow$ Sorted all universes;
  $NI \leftarrow$ Normalized all universes;
  for $i = 2$ to p **do**
    Back_index $\leftarrow i$;
    for $j = 1$ to d **do**
      $r_1 \leftarrow random[0,1]$;
      if $r_1 < NI(U_i)$ **then**
        White_index $\leftarrow$ Roulette selection, (2.7);
        U_i(Back_index, j)$\leftarrow SU$(White_index, j);
      end if
      $r_2 \leftarrow random[0,1]$;
      if $r_2 < WEP$ **then**
        $r_3, r_4 \leftarrow random[0,1]$;
        $U_{ij} \leftarrow$ Update the position of black hole, (2.8);
      end if
    end for
  end for
end while
return U_{best}, f_{obj}^{best}.

where TDR (Travelling Distance Rate) is a dynamic parameter, WEP stands for wormhole existence probability, u_{best}^{j} is the j-th object of the greatest universe, H is the threshold, and here we set $H = 0.5$ according to experience [77]. In addition, the upper and lower limits of j-th solution variable are expressed by ub_j and lb_j, respectively. r_2, r_3, and r_4 are three random values from 0 to 1.

The TDR is a critical factor in helping to transport individuals in the universe through the wormholes into the best universe available at present. Furthermore, the TDR grows with the number of iterations to accomplish more explicit development.

$$TDR = 1 - \frac{t^{1/w}}{T^{1/w}} \tag{2.10}$$

where t represents the current iteration number, and T represents the maximum iteration number. w denotes the ability to implement local searches throughout the optimization process. A higher w value can reach more precise local search capabilities as the number of iterations grows. w is set to 6 in this paper.

The wormhole existence probability, WEP, increases monotonously throughout the optimization process. As a result, the MVO algorithm focuses on exploitation over the iterations.

$$WEP = wep_{min} + t \times (\frac{wep_{max} - wep_{min}}{T}) \tag{2.11}$$

where wep_{min} and wep_{max} denote the minimum and maximum of the WEP, respectively. This paper set wep_{min} to 0.2, wep_{max} to 1.

The overall steps of the MVO algorithm are summarized below. Set the parameters and randomly generate a few universes within the constraints as potential solutions. Next, the universe with a high fitness value transports individual variables to the universe with a low fitness value through white and black hole tunnels, part of the optimization process. Simultaneously, every universe has an opportunity to travel through the wormhole to the best universe. Finally, the termination condition is met, resulting in the output of the ideal universe and its fitness value. In addition, an example is shown in Table 2.1 about the process of the current universe p towards the best universe p_{best} thorough white holes, black holes, and wormholes. It is important to note that the universe individual is set to the boundary value if it is beyond its boundary constraint. Otherwise, it remains the value obtained from the update process. As shown in Table 2.1, when the universe p is updated according to (2.8) and (2.9), its first individual is calculated as 8.232, which exceeds the boundary value 2π. Thus, the first object of the universe p is set to 2π. On the other hand, the universe p's fourth object has a value of 1.6 between 0 and 2π, so it is still at 1.6.

Table 2.1 Solution updation

Update process	Individual variable ϕ_n
Current universe p	$\{3\pi/2, \pi/2, 2\pi, 0, 3\pi/4, 3\pi/4\}$
Best universe p_{best}	$\{3\pi/2, 7\pi/4, \pi/4, \pi, \pi, 5\pi/4\}$
$NI(p), NI(p_{best})$	$\boxed{0.63}$, 0.78
Random number $r_1 \in [0,1]$	0.75, $\boxed{0.38}$, 0.67, $\boxed{0.49}$, $\boxed{0.16}$, 0.98
Update universe p, (2.7)	{ $3\pi/2$, $\boxed{7\pi/4}$, 2π, $\boxed{\pi}$, $\boxed{\pi}$, $3\pi/4$ }
WEP and TDR, (2.10), (2.11)	0.2016, 0.6450
Random number $r_2 \in [0,1]$	$\boxed{0.11}$, 0.50, 0.78, $\boxed{0.13}$, 0.48, 0.60
Random number $r_3 \in [0,1]$	$\boxed{0.19}$, 0.40, 0.52, $\boxed{0.54}$, 0.96, 0.14
Random number $r_4 \in [0,1]$	$\boxed{0.97}$, 0.79, 0.88, $\boxed{0.38}$, 0.18, 0.52
Update universe p, (2.8), (2.9)	{ $\boxed{2\pi}$, $\boxed{7\pi/4}$, 2π, $\boxed{1.60}$, $\boxed{\pi}$, $3\pi/4$ }

2.5 Numerical Results and Analysis

This section verifies the effectiveness of the multi-RIS-aided indoor wireless communication based on the proposed MVO approach. We introduce the simulation settings and analyze the results in terms of the average achievable rate.

2.5.1 Simulation Settings

We have simulated an indoor scenario with one AP and K single-antenna mobile users identical to the one shown in Fig.2.1. The multiple RISs with N reflective elements are painted on the facade of the room wall, while one AP with $M = 16$ antenna arrays is coated on the left side of the room wall. We randomly generate channel matrixes $\mathbf{H}_{k,l}$, $\mathbf{G}_l$, and $\mathbf{h}_k$. To verify whether multiple RIS sufficiently increased received signal strength, we assumed only RIS could offer signal reflections and neglected reflections from the floor, ceiling, windows, *etc.*

We selected two benchmark methods for comparison. Baseline 1 emphasizes a simple design and does not consider iterative optimization of RIS elements' phase shifts. For baseline 2, we estimate the performance of indoor wireless communication systems without RIS deployment.

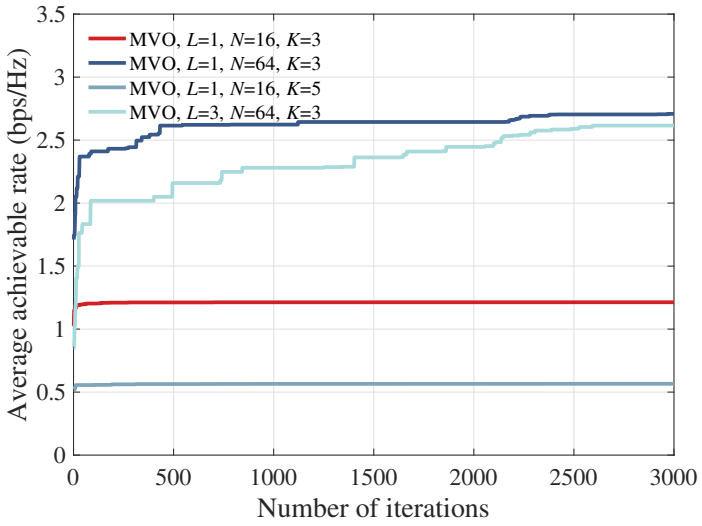

Fig. 2.2 Convergence of the MVO algorithm for different values of K, L, N. The system parameters are set as $M = 16$, $C = 2$.

2.5.2 Performance Evaluation

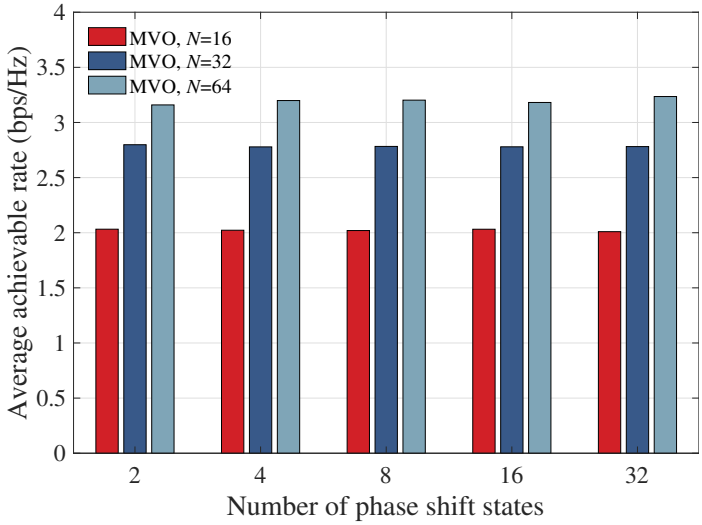

Fig. 2.3 The average achievable rate versus the number of the phase shifts states C for $M = 16$, $L = 4$, $K = 3$.

We start with Fig.2.2, which shows the convergence of the proposed approach for various numbers of mobile users K, RIS L, and reflecting elements N. As shown in Fig.2.2, the MVO algorithm has monotonic convergence for the different number of users, RISs, and reflective elements. Specifically, for $L = 1, N = 16, K = 5$ and $L = 1, N = 16, K = 3$, the proposed approach all converge after approximately 10 iterations. For increasing RISs

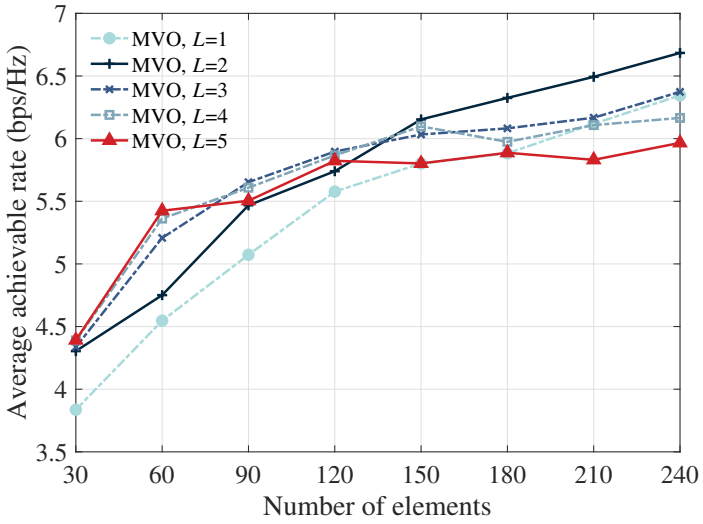

Fig. 2.4 The average achievable rate versus the number of reflecting elements N, where $M = 16, C = 2, K = 2$.

and reflective elements, i.e., the cases $L = 3, N = 64, K = 3$ and $L = 1, N = 64, K = 3$, the MVO algorithm requires more iterations to achieve convergence because the number of the individual variables from universes in problem (2.5) increases with the number of RIS L and reflective elements N. To sum up, the convergence of the MVO approach is more sensitive to the number of RIS and reflective elements while less sensitive to the number of mobile users.

Fig.2.3 depicts the average achievable rate against the number of the phase shift states, C. The graph above shows that the average achievable rate increases when the number of reflecting elements N rises for different states of phase shifts. However, there is almost no increase in the achievable rate for different phase shift states C when the reflecting elements N are fixed. That is to say, the proposed algorithm is finally able to obtain the optimal achievable rate for different phase shift states through continuous optimization and iteration.

We exhibit the average achievable rate versus the number of reflecting elements N, in Fig.2.4. For the different numbers of RIS L, all cases display the same trend: the achievable rate increases as increasing N, especially $L \leq 2$. Increasing N up to a certain number does maximize the achievable rate by designing phase shifts. However, the achievable rate eventually decreases when the number of N increases beyond certain values, which is because there is more interference among multiple channels between the RISs and the mobile users. Interestingly, for $L = 2$, the achievable rate is higher than for $L = 3, L = 4, L = 5$ with the same reflection elements $N = 150$. The phenomenon is because adding more RIS on different walls of a room can lead to phase shift cancellation interference, which weakens the achievable rate. However, when $N \leq 120$, the achievable rate of double-RIS ($L = 2$) is lower

than $L \geq 3$. The phenomenon also indicates that adding the appropriate number of RIS and placing them decentralized does improve the achievable rate.

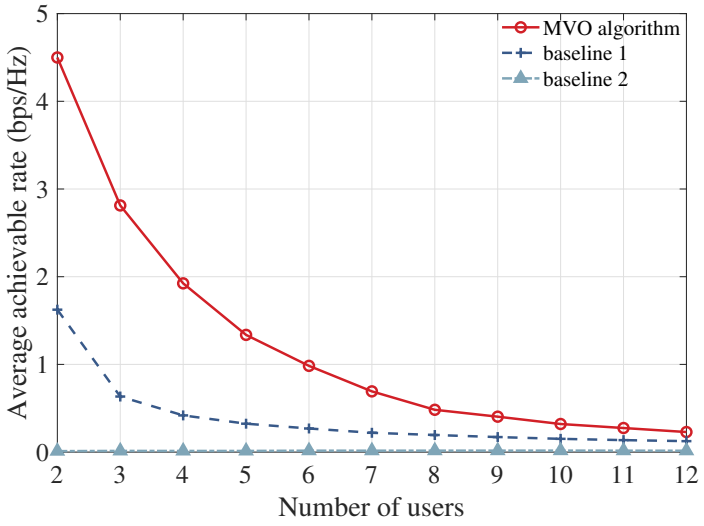

Fig. 2.5 The average achievable rate versus the number of mobile uers N, where $M = 16$, $C = 2$, $N = 32$, $L = 4$.

The average achievable rate versus the number of users is depicted in Fig.2.5. As can be seen, the achievable rate accomplished by the MVO algorithm and both baselines monotonically decrease as the number of users grows. It's because of the fact that fewer reflecting elements are exploited for a single user with increasing the number of users. Meanwhile, the achievable rate of the system is nearly zero if the RISs are not deployed (baseline 2), which is primarily caused by the poor channel conditions between the AP and the mobile users. In addition, the proposed approach achieves a significantly higher achievable rate than baseline 1, indicating that the proposed algorithm is effective.

2.6 Conclusion

In this paper, we have investigated the multiple users wireless indoor communication system assisted by multi-RIS. The intelligent surfaces are composed of numerous almost passive reflective element arrays with discrete phase shifts. Intending to study the multi-RIS effectiveness for indoor wireless communication, we focused on multi-RIS multi-user scenarios and the achievable rate maximization for optimizing each RIS's reflecting elements by the MVO algorithm. Our simulation results showcased that the proposed approach equipped with intelligent surfaces can efficiently focus signal transmissions to users and improve the achievable rate compared with baseline schemes. In future work, we will consider a multi-

RIS-assisted communication system with multi-hop signal reflection to improve coverage and establish a more intelligent radio environment.

Chapter 3

The Enhancement of Coverage in Multi-RIS-Assisted Outdoor Wireless Communication Networks

3.1 Motivation

The exponential data growth in the internet era with limited spectrum resources has derived a strong desire for future wireless communication speed, quality, and security [19]. To fill this vision, reconfigurable intelligent surfaces (RISs) have emerged as an up-and-coming paradigm for wireless communication, offering significant advantages over traditional solutions like adding base stations (BSs) or relays in many tasks, e.g., improving data transmission, enhancing coverage, reducing energy consumption and system costs [20]. The square metal arrays controlled by a digital microcontroller in an RIS produce different amplitudes and phase shifts on the incident signal, intending to enhance the signal quality at receivers [91]. In the absence of complicated signal processing, coding, and decoding procedures, RISs enable telecom operators to control the whole propagation environment by modeling the objects and regulating the electromagnetic response in a controlled environment.

Recently, RISs integrated with promising technologies because of their characteristics for configuring the wireless propagation environment have been applied in various research fields, including signal strength improvement, interference engineering, signal confidentiality, coverage enhancement, and more [52]. A generic scenario is to change the direction of signal propagation by deploying a RIS to create a virtual line-of-sight (LoS) path from the sender to the receiver [7]. In [107], to improve the quality of service for mobile users in non-orthogonal multiple access (NOMA) communication systems, the authors place a RIS

on a robot, which is beneficial to improve the efficiency of power allocation. In [57] and [59], an RIS is integrated with the mobile edge computing (MEC) paradigm, the security of task offloading is improved, and the device's local computing frequency and transmission power are enhanced. Combining RIS and unmanned aerial vehicle (UAV) technology shows excellent potential for emergency and military communications [45, 63]. RIS is also applied in vehicle-to-everything (V2X) communications to improve the reliability of vehicle networks and decrease the disconnect areas [67] [1].

However, existing studies mainly concentrate on optimizing phase shift vectors of elements to maximize the achievable rate and minimize energy consumption, with limited attention given to coverage enhancement issues. Moreover, traditional cellular networks exist in coverage voids, such as in the shadow areas of tall buildings or dense urban areas, and the signal quality of receivers at the cellular network edge is poor. Nonetheless, RISs are a new paradigm for establishing effective links between BSs and users, enhancing coverage probability and network performance. In a single-BS single-user RIS-assisted wireless communication network [100], the authors analyze the coverage by optimizing the direction and horizontal distance of reflecting elements. A theoretical framework for quantifying coverage is presented in [8]. In [103], the authors optimize the positions and orientations of RISs to enhance coverage in a mmWave network with fixed obstacles. However, the above discussions are merely on single RIS or indoor environments, and the network cost of RIS-assisted wireless communications is not considered.

This paper investigates an outdoor wireless communication scenario characterized by several obstacles, multiple users, diverse RISs, and RISs mounted on the obstacles to enhance coverage probability. We aim to optimize the deployment locations of multiple RISs to maximize the coverage probability while ensuring adherence to the network cost constraint. Specifically, we propose coverage probability calculation methods based on approximate cell decomposition and then present a Rule-based and Branch-and-Bound (B&B) algorithm called R&B to optimize the deployment locations of RISs. The Rule-based approach is presented to obtain feasible solutions for RIS deployment locations, and the B&B method maximizes coverage probability while satisfying the network cost based on the feasible solutions. We perform extensive simulations to estimate the effectiveness of the presented R&B approach, and the results clearly demonstrate its superiority over other benchmark methods.

The primary contributions of this paper can be summarized as follows.

- We propose a problem of multi-RIS deployment for the outdoor wireless communication scenario, where multiple obstacles are generated based on a PPP distribution. The

BSs cooperate with the RISs to effectively enhance coverage probability and decrease the network cost.

- We present methods to quantitatively calculate the coverage probability based on approximate cell decomposition. Meanwhile, the coverage probability is derived in wireless communication networks assisted by RIS.
- We formulate the optimization problem that maximizes the coverage probability while satisfying network cost constraints by optimizing RIS deployment locations on obstacles. To solve this problem, we present a two-stage optimization strategy, R&B. Firstly, the Rule-based method obtains feasible solutions for RIS deployment locations. Secondly, the Branch-and-Bound algorithm is applied to select RIS deployment locations to achieve higher coverage while keeping the network cost as low as possible.
- Simulation results substantiate the superior performance of our proposed method regarding coverage probability and network cost in multi-RIS-assisted outdoor wireless communication networks.

3.2 Related Work

RIS has gained significant attention as a wireless communication technology owing to its thinness, small form factor, high integration, and low cost. Recently, RISs have been applied to various communication scenarios by merging with other technologies. The work in [64] explores the integration of UAV and RIS technology to enhance the throughput of multiple-input multiple-output (MIMO) systems. Specifically, an aerial RIS is mounted on the surface of the UAV to extend the coverage area of the BSs. In [80], the authors address user localization and propose a novel online method for tracking the user's location and angle of arrival (AoA) in RIS-aided MIMO networks. In [62], the authors tackle the challenge of channel estimation in RIS-assisted single-user wireless communication systems by employing discrete phase shifts. Additionally, the issue of media access control (MAC) for multi-user access in RIS-enabled channels presents challenges in [10]. The authors in [11] explore RIS-assisted communications at the MAC layer, including a RIS-assisted single-channel multi-user (SCMU) MAC framework and multichannel multiuser (MCMU) communications. In [67], the authors propose a novel framework to enhance the reliability of V2X communication networks by installing RISs along roadsides. Additionally, [1] integrates RIS with vehicular networks, taking into account the dynamic environment, and RIS is deployed to establish communication links between roadside and disconnected areas.

Most existing works have focused on optimizing the performance of multiple-input single-output (MISO) communication systems with the assistance of RIS. These works concentrate on operating phase shifts of reflective elements when RIS deployment locations are given. For example, the authors in [30] consider user-proportional fairness and propose a spectral efficiency (SE) maximization method based on joint optimization of active and passive beamforming techniques. The work presented in [90] introduces the utilization of RIS in a wireless communication scenario involving a multi-antenna access point (AP) and a single-antenna user. The work aims to minimize the total transmit power by optimizing active beamforming at the AP and the beamforming vectors of reflective elements at the RIS. In [55], the authors maximize the influence of multi-RIS deployment on the average achievable rate in an indoor environment. In [23], the security problem of RIS-aided wireless communication networks is addressed, aiming to enhance legitimate users' secrecy rate by designing phase shifts of reflective elements using related techniques. Moreover, machine learning-based methods are applied to design and optimize elements' phase shifts to improve system performance in [2]. However, the above works mainly focus on optimizing SE, transmission power, secrecy rate, and achievable rate by adjusting the phase shifts of the elements, ignoring multi-RIS deployment and placement locations of RIS.

The RIS placement problem is presented for the three-dimensional scenario considering the RIS height, and the experimental results show that the horizontal deployment position of RIS is closer to the BS side or the user side in [94]. In [32], the authors investigate the impact of common obstacles at the user-BS and user-RIS links on downlink performance, and the goal is to minimize the probability of common obstacles or maximize the coverage area in the downlink. The findings indicate that the user-BS and user-RIS links are more likely to be blocked when the RIS is closer or farther from the BS. It is also observed that using intersections to install RISs significantly reduces the probability of blocked links. The authors in [66] employ optimization techniques to select the optimal placement of an RIS in a millimeter-wave wireless network. The objective is to maximize the end-to-end Signal to Interference plus Noise Ratio (SINR), considering the location of the user and the BS.

Moreover, most work focuses on optimizing coverage in an RIS-assisted indoor wireless environment. For example, the authors investigate that RISs and ultra-dense small-cell BSs can be applied in indoor wireless communication, and the analysis of coverage rate and cost demonstrates that multiple strategies combining RIS and BS achieve the same coverage rate in [47]. In [103], the authors consider the location and orientation optimization problem of multiple RISs for indoor obstacle scenarios for the first time, and a gradient descent approach with initialized weights is proposed to maximize the coverage. In addition, the authors of [43] conduct theoretical analysis to determine the proportion of blind spots

within a specific region. The probability of association between a mobile user and the BS in an RIS-assisted wireless communication system is investigated. The above works have discussed the placement locations of RISs in indoor environments. However, there is limited research on large-scale deployments of RISs in outdoor wireless communication networks. Additionally, these studies ignore the selection of RIS placement locations. Meanwhile, while adhering to network cost constraints, the challenge of maximizing coverage through the optimal deployment of RISs in a multi-RIS multi-obstacle outdoor wireless scenario remains unexplored.

3.3 System Model and Problem Formulation

This section begins by presenting the multi-RIS-assisted outdoor wireless communication scenario, followed by an introduction to the RIS and path loss models. The coverage probability and network cost are also analyzed. Finally, we construct the problem formulation.

3.3.1 Multi-RIS-assisted Wireless Communication Scenario

We consider an urban environment with several single-antenna users, multi-antenna BSs, and obstacles like buildings, billboards, and trees. Obstacles block the direct transmission link between the user and the BS, creating blind spots in specific areas. To ensure the dependability and coverage of the system, we consider the data signal is transmitted to users from the BSs through two types of downlink links. The scenario graph illustrating multi-RIS-assisted coverage enhancement in outdoor wireless communication networks is depicted in Fig. 3.1(a). The graph provides a representation of the real scene, incorporating various elements such as obstacles, multiple users, and BSs. In this scenario, RISs are deployed on obstacles to enhance coverage probability. For example, an obstacle blocks the LoS transmission between the BS and the users, leading to communication blind spots. That is to say, the users can not be covered by the BS. To solve the issue, multiple RIS are installed on the facade of obstacles to establish a virtual transmission link to extend the coverage range. Additionally, the Poisson Point Process (PPP) model, compared to other random distribution models (e.g., two-dimensional Gaussian distribution, uniform distribution), offers a more adaptable approach to representing the distribution of users and BSs in an urban center environment. Therefore, the locations of BSs and users are modeled as two independent homogeneous PPP models. We indicate the locations of BSs as $\Psi_{BS} = \{y_i\} \in \mathbb{R}^2$ with a density of λ_{BS}, and the locations of users as $\Psi_U = \{u_i\} \in \mathbb{R}^2$ with a density of λ_u. Moreover, the obstacles are represented by line boolean models [43]. The locations of the midpoint of

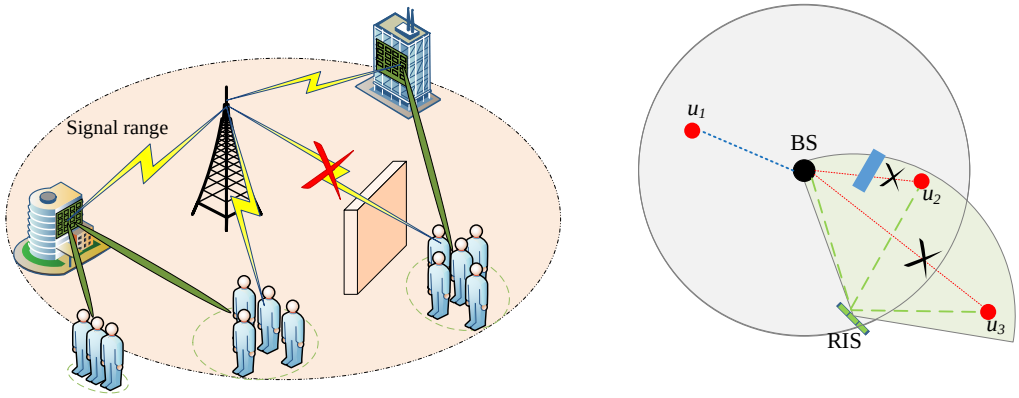

(a) The Scenario Graph (b) The View Graph

Fig. 3.1 The system model of wireless communication networks assisted by multiple RISs. (a) The scenario graph. (b) The view graph.

obstacles are also modeled in the form of $\Psi_{OB} = \{z_i\} \in \mathbb{R}^2$, with a density of λ_{OB}. A subset RISs is denoted $\Psi_{RIS} \subset \Psi_{OB}$, with a density of $\lambda_{RIS} = \mu\lambda_{OB}$, where μ is the proportion of obstacles with RIS installed.

Furthermore, Fig. 3.1(b) provides a view of the system model aided by multiple RISs. This figure is different from the real scene Fig. 3.1(a), offering a more visual comprehension of various aspects, including the signal range of the BS, the coverage of RIS reflection, and the communication links between the BS, RIS, and users. For example, users situated within the signal range (e.g., u_1) can establish communication with the BS. Conversely, if the LoS link is obstructed by obstacles (e.g., u_2) or the user is located beyond the signal range of the BS (e.g., u_3), the establishment of a LoS connection with the BS becomes unfeasible. In such cases, a virtual LoS link can be established with the assistance of an RIS to enhance coverage probability. It should be noted that the signal reflected by the RIS for the first time is considered, and signals reflected for the second or third time are not considered.

To calculate coverage probability, a specific region is divided into multiple cells. If a cell is covered, it is presumed that all users inside the cell are also within the signal range, and vice versa. Therefore, user mobility does not impact the system coverage. We first provide definitions of critical terminologies used throughout the paper to facilitate the discussion of models and algorithms presented in this paper.

Definition 1 *(Direct LoS link). The Direct LoS link can be established to facilitate signal transmission from the BS to the cell when the absence of any obstacles obstructs the path between the cells and the BSs.*

Definition 2 *(Virtual LoS link). The Virtual LoS link can be established via RIS by reflecting signals from the BSs to the specific cells when no obstacles obstruct the path from the BSs to the RISs and from the RISs to the specific cells.*

Definition 3 *(Covered cell). A specific cell is covered when at least one direct LoS or virtual LoS links between the BSs and the specific cells.*

3.3.2 RIS Model

An RIS is a planar surface consisting of M passive reflective elements and an intelligent digital microcontroller, enabling dynamic reconfiguration by adjusting elements coefficients $e^{j\phi_i}$ to manipulate the wireless signals. Each reflecting element is characterized by C different states, having the same amplitude and a phase shift interval of $\Delta\phi = \frac{2\pi}{C}$. Consequently, the phase shift of the nth element is expressed as:

$$\phi_n = \alpha_n e^{j\tau_n \Delta\phi} \tag{3.1}$$

where the amplitude $\alpha_n \in [0,1]$ is a constant for $n = 1,2,\ldots,M$, and $\tau_n \in \{1,\ldots,C\}$. To examine the influence of RIS deployment on coverage, this study focuses on the deployment location of RIS. Therefore, we assume that the amplitude α_n equals 1, and the τ_n values for all RISs are fixed. The phase shifts of all RISs are denoted as $\mathbf{\Phi} = \{\Phi_1, \Phi_2, \ldots, \Phi_L\}$.

In addition, we suppose that the RIS reflecting element M as a random variable with a probability mass function (PMF) denoted as $\mathbb{P}(M = m) = \rho_m$, where m represents the possible values of the RIS reflective element. Meanwhile, the set of all possible values of M is denoted as $\mathscr{M}$. Hence, the union of the set $\Psi_{R,m}$ is defined as Ψ_{RIS} (i.e., $\Psi_{RIS} = \bigcup_{m\in\mathscr{M}} \Psi_{R,m}$), where $\Psi_{R,m}$ indicates the positions of RISs with m elements, with a density of $\lambda_{R,m} = \rho_m \lambda_{RIS} = \rho_m \mu \lambda_{OB}$.

3.3.3 Path Loss Model

Path loss is a critical performance indicator for evaluating wireless communication systems with large-scale RISs. In [43], the analysis of the correlation between the distance, reflecting elements, and the received signal power for the virtual LoS link is presented. Therein, the path loss in RIS-assisted wireless communication networks is determined by various factors, such as the number of reflecting elements M, the distance between the RIS and BS $d_{B,R}$, the distance between the user and RIS $d_{R,U}$, and the path loss exponent α. Specifically, the path loss is inversely proportional to M^2 and proportional to $(d_{R,U} + d_{B,R})^{\alpha}$. Additionally, the received signal power of the direct LoS link is determined by the distance between the user

and the BS, denoted as $d_{B,U}$. Therefore, the path loss of the direct and virtual LoS link can be mathematically expressed as follows.

$$P_L^{B-U} = \frac{1}{\delta_L^{c_i,y}\|y-c_i\|^{-\alpha}} \tag{3.2}$$

$$P_L^{B-R-U} = \frac{1}{\max\limits_{z\in\Psi_{R,m}} \delta_L^{c_i,z}\delta_L^{y,z}\kappa_z^{c_i,y}\left(\|c_i-z\|+|y-z\|\right)^{-\alpha}} \cdot \frac{1}{m^2(1-\delta_L^{c_i,y})} \tag{3.3}$$

where c_i is the location of the ith specific cell, the variable $\delta_L^{c_i,y}$ is set to 1 if a direct LoS link exists between the cell c_i and the BS y, and $\delta_L^{c_i,y} = 0$ otherwise. Similarly, the variable $\kappa_z^{c_i,y}$ is set to 1 when a virtual LoS link can be established between the user situated at c_i and the BS situated at z by the RIS, and otherwise, $\kappa_z^{c_i,y} = 0$. Using the radar distance formula, the path loss P_L^{B-R-U} for a virtual LoS link is expressed as

$$P_L^{B-R-U} = \left(\left(\frac{\lambda}{4\pi}\right)^4 \frac{G_e^i G_e^r}{d_{B,R}^2 d_{R,U}^2}\omega_p\right)^{-1} \tag{3.4}$$

where the wavelength is denoted as λ, G_e^i is the antenna gain of the RIS in incident wave direction, G_e^r is the antenna gain of the RIS in receiving wave direction, and ω_p is the efficiency of the RIS.

We assume that the signal variation obeys Rician fading in space. The fading loss parameters of the ith reflection element from the BS to the RIS and from the RIS to the users are expressed as follows.

$$\begin{aligned} g_i^{B,R} &= \sqrt{\frac{T_1}{1+T_1}}\,\bar{g}_i^{B,R} + \sqrt{\frac{1}{1+T_1}}\,\tilde{g}_i^{B,R} \\ g_i^{R,U} &= \sqrt{\frac{T_2}{1+T_2}}\,\bar{g}_i^{R,U} + \sqrt{\frac{1}{1+T_2}}\,\tilde{g}_i^{R,U} \end{aligned} \tag{3.5}$$

where T_1 and T_2 are the Rician parameters of from the BS to RIS link and from the RIS to user link, $\bar{g}_i^{B,R}$ and $\bar{g}_i^{R,U}$ denote the direct LoS link components, and $\tilde{g}_i^{B,R}$ and $\tilde{g}_i^{R,U}$ express the virtual LoS link components for $i = 1,2,\cdots,M$. Here, $\tilde{g}_i^{B,R}$, $\tilde{g}_i^{R,U} \sim \mathscr{CN}(0,1)$.

The baseband representation of the received signal strength at the destination is expressed by

$$y = \sqrt{p_k}\left[\sqrt{P_L^{B-R-U}}\left(\sum_{i=1}^{M} g_i^{B,R} e^{j\tau_i\Delta\phi} g_i^{R,U}\right)\right]\mathbf{x} + n_k \tag{3.6}$$

where p_k is the transmitted power, $\mathbf{x} \in \mathbb{C}^{M\times 1}$ denotes the transmission signal from the BS to all users, and $n_k \sim \mathscr{CN}(0, \delta^2)$ means Gaussian white noise with variance δ^2.

3.3.4 Coverage Probability Analysis

To enhance the coverage capabilities in multiple RIS-assisted outdoor wireless communication networks, this paper proposes algorithms to calculate the coverage probability quantitatively without RIS and the deployment of RISs. Moreover, the paper derives the coverage probability when deploying large-scale RISs and analyzes the network cost in wireless systems assisted by RIS.

The coverage probability is the ratio of covered cells to all cells in a specific region. However, previous research [47] has predominantly relied on Monte-Carlo simulations to assess coverage in an indoor mmWave wireless system, which is unsuitable for outdoor wireless communication scenarios with multiple obstacles, RISs, and BSs. To address this limitation, we propose Algorithm 2 and Algorithm 3, based on approximate cell decomposition, to calculate the coverage probability without and with RISs, respectively. Additionally, the coverage probability is derived in the multi-RIS-assisted wireless network. Note that we divide the specific region into multiple cells and calculate coverage probability by evaluating whether each cell is covered.

Fig. 3.2 provides examples of calculating coverage probability for outdoor wireless communication networks, without and with RIS deployment, respectively. In Fig. 3.2(a), users u_4 and u_5 are beyond the signal range of the BS, whereas u_2 and u_3 are obstructed by obstacles, and only user u_1 being able to communicate with the BS via the direct LoS link. Moreover, orange denotes the covered cell in the area, while gray represents uncovered cells. As described in Algorithm 2, the BSs and obstacles are generated randomly within a specific region, which is partitioned into $k \times k$ cells. Subsequently, each cell $cell_i$ is traversed to examine for existing obstacles between it and any BS bs_j. If no obstacles are detected, the cell is marked as covered (encoded as 1), and the loop terminates; Otherwise, it is assigned a value of 0. The coverage probability is then calculated based on cell encoding.

For the scenario with multiple RISs, which are strategically placed on obstacles to enhance coverage probability through a virtual LoS link, as depicted in Fig. 3.2(b). In addition, some conditions must be satisfied for the RIS to reflect. Specifically, i) The RIS must be within the signal range of the BS; ii) The cell and BS must be positioned on the same side of the RIS. iii) At least one LoS link between the cell and the RIS is required to exist; iv) At least one LoS link between the RIS and the BS is required to exist; v) The received power must be greater than the threshold P_{th}. For the Algorithm 2, the detailed description is as follows. *Step 1:* Decompose the specific region into $k \times k$ cells; *Step 2:* Identify BSs

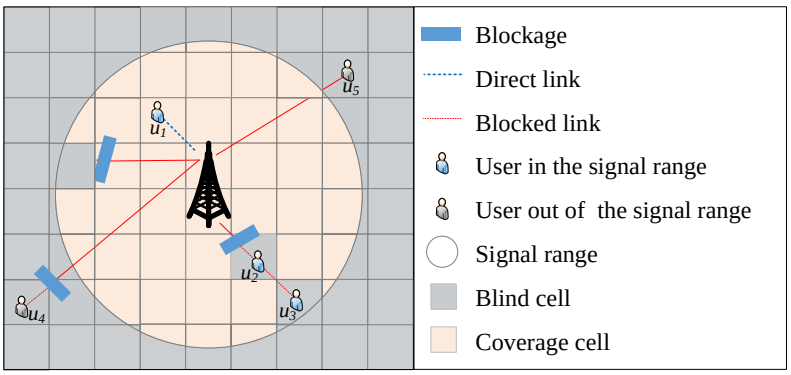

(a) Without RIS

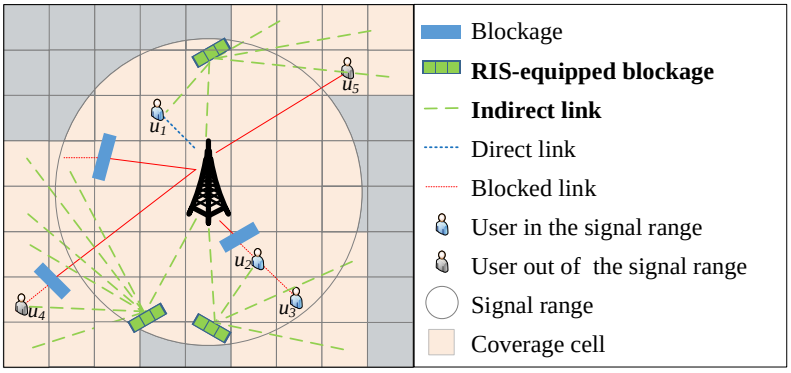

(b) Deployment RIS

Fig. 3.2 Examples of coverage probability calculation. (a) The coverage calculation without RIS. (b) The coverage calculation for deploying RIS.

that can cover the ith cell $cell_i$; *Step 3:* Determine the position of $cell_i$ and bs_j, and find RISs that satisfy the reflection requirements; *Step 4:* If at least one RIS, marked $cell_i$ as covered (encoded as 1); Otherwise, mark it as 0. Iterate over all cells; *Step 5:* Calculate the coverage probability based on all cell encodings. Finally, we obtain the coverage without and with RIS using Algorithms 2 and 3, respectively. Furthermore, we derive the coverage in RIS-aided wireless networks, which can be defined at the bottom of the next page.

Algorithm 2 The Coverage Probability Calculation Algorithm without RIS

Input: Ψ_{BS}, λ_{BS}, Ψ_{OB}, λ_{OB}, R, k

Output: The Coverage Probability without RIS, P_{cov}^{LoS}

Initialization: Generate PPP distributed BSs and obstacles with densities of λ_{BS} and λ_{OB} in the outdoor wireless communication environment, respectively;

Divide the whole outdoor region into $k \times k$ cells;

for $i = 1$ *to* k^2 **do**

  $cell_i \leftarrow$ the ith cell location;

  for $j = 1$ *to* N_{BS} **do**

    $dis_{i,j} \leftarrow$ the distance between $cell_i$ and bs_j;

    if *{*$dis_{i,j} < R$*}* **then**

      if *{No obstacles between* $cell_i$ *and* bs_j*}* **then**

        $cell\_los_i \leftarrow 1$; break;

      else

        $cell\_los_i \leftarrow 0$;

    else

      $cell\_los_i \leftarrow 0$;

The coverage probability $P_{cov}^{LoS} = \frac{sum(cell\_los==1)}{k^2}$.

$$
\begin{aligned}
P_{cov} &= \mathbb{E}\left[\prod_{y\in\Psi_{BS}}\left(\delta_L^{c_i,y} + \left(1-\delta_L^{c_i,y}\right)\times\left(1-\prod_{z\in\Psi_{RIS}}\left(1-\delta_L^{z,c_i}\delta_L^{z,y}\kappa_z^{c_i,y}\right)\right)\right)\right] \\
&\overset{(a)}{=} \mathop{\mathbb{E}}_{\Psi_{BS}}\left[\prod_{y\in\Psi_{BS}}\left(P_{LoS}(\|c,y\|) + P_{NLoS}(\|c,y\|)\times\mathop{\mathbb{E}}_{\Psi_{RIS}}\left[1-\prod_{z\in\Psi_{RIS}}\left(1-f_i\left(\|c,y\|,\|c,z\|,\varphi\right)\right)\right]\right)\right] \\
&\overset{(b)}{=} \exp\left(\lambda_{BS}\int_0^{\infty}\left(P_{LoS}(m) + P_{NLoS}(m)\,P_{cov}^{I}(m)\right)m\mathrm{d}m\right)
\end{aligned}
\tag{3.7}
$$

where (a) assumes that the number of obstacles between the direct LoS link and virtual LoS link in the network is independent, while (b) is the probability generating function (PGFL) using PPP. Moreover, P_{cov}^{I} denotes the probability that at least one RIS can be reflected to establish a virtual LoS link between a specific cell and the BS, given by the following expression.

$$
\begin{aligned}
P_{cov}^{I}(m) &= \mathop{\mathbb{E}}_{\Psi_{RIS}}\left[1-\prod_{z\in\Psi_{RIS}}\left(1-f_i\left(m,\|c,z\|,\varphi\right)\right)\right] \\
&= 1-\exp\left(-\lambda_{RIS}\int_{-\pi}^{\pi}\int_{0}^{\infty} f_i\left(m,n,\varphi\right)\mathrm{d}n\mathrm{d}\varphi\right)
\end{aligned}
\tag{3.8}
$$

where the function $f_i(m,n,\varphi)$ denotes the probability of successfully deploying the RIS to establish an effective virtual LoS link between the typical cell and the BS. Specifically, the function $f_i(m,n,\varphi)$ is determined based on the distances between the BS and the user m, the RIS and the user n, and the angle φ. By calculating this function, we can determine the probability that the RIS will be able to reflect the signal.

Proof. See Appendix 7.1.

Algorithm 3 The Coverage Probability Calculation Algorithm of RIS-assisted Region

Input: Ψ_{BS}, λ_{BS}, Ψ_{OB}, λ_{OB}, μ, R, k

Output: The Coverage Probability with RIS, P_{cov}^{NLoS}

Initialization: Generate PPP distributed of BSs with a density of λ_{BS}, obstacles with a density of λ_{OB}, and a set of RISs with a density of $\lambda_{RIS}=\mu\lambda_{OB}$ for the outdoor RIS-assisted wireless communication environment;

Divide the whole outdoor area into $k\times k$ cells;

for $i=1$ *to* k^2 **do**
  $cell_i \leftarrow$ the ith cell location;
  $bs\_up \leftarrow$ update BSs that can cover $cell_i$;
  for $j=1$ *to* N_{bs_up} **do**
    $bs_j \leftarrow$ the jth BS location;
    for $p=1$ *to* N_{RIS} **do**
      if *{RIS_p satisfies reflection constraints}* **then**
        $cell\_ris_i \leftarrow 1$;
      else
        $cell\_ris_i \leftarrow 0$;

The coverage probability $P_{cov}^{NLoS}=\frac{sum(cell\_ris==1)}{k^2}$.

In outdoor wireless communication systems with multiple RISs, the following conditions must be met to ensure effective signal reflection between a specific cell and the BS:

1. The specific cell should face the side of the obstacle where the RIS is installed.
2. At least one direct LoS link between the specific cell and the RIS is required to exist.

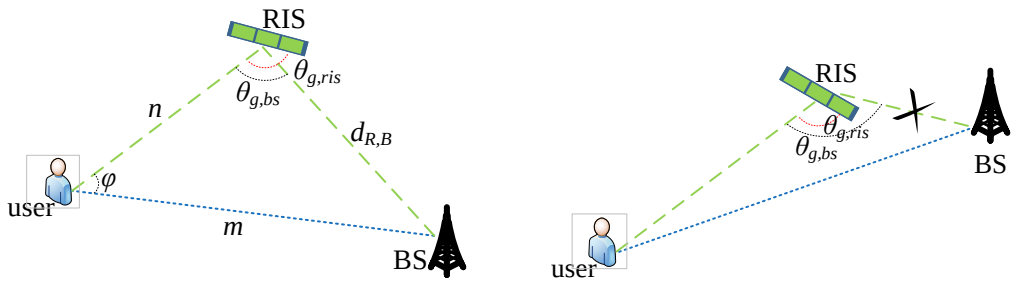

(a) $\theta_{g,ris} \geq \theta_{g,bs}$ (b) $\theta_{g,ris} < \theta_{g,bs}$

Fig. 3.3 The setup for the fourth condition.

3. At least one direct LoS link between the BS and the RIS is required to exist.

4. The specific cell and the BS should be situated on the same side of the obstacle facade equipped with RIS.

The first condition is fulfilled with a probability of $\frac{1}{2}$, as the scenario is two-dimensional. To meet the second condition, the probability of existing a direct LoS link between the specific cell and the RIS at a distance n, with obstacles of length L and density λ_{OB}, is obtained from [43] and is expressed as follows.

$$P_{LoS}(n) = \exp(-\beta n) \tag{3.9}$$

where β is defined as $\frac{2\lambda_{OB}\mathbb{E}[L]}{\pi}$. Likewise, we can determine the probability of a LoS link between the RIS and the BS, satisfying the third condition, by utilizing Eq. (3.10).

$$P_{LoS}(d_{R,B}) = \exp\left(\frac{2\lambda_{OB}\mathbb{E}[L]}{\pi} d_{R,B}\right) \tag{3.10}$$

The fourth condition is satisfied only when $\theta_{g,ris} \geq \theta_{g,bs}$. As displayed in Fig. 3.3 (a), one virtual LoS link communication can be established when the BS and the specific cell are on the same side of the obstacle with RIS. However, if the typical cell and the BS are located on different sides of the RIS (i.e., $\theta_{g,ris} < \theta_{g,bs}$), signal reflection by the RIS is not possible, as shown in Fig. 3.3(b), meaning no virtual LoS link can be established. Therefore, the probability of satisfying the fourth condition can be expressed as:

$$\mathscr{C}(m,n,\varphi) = 1 - \frac{1}{\pi}\cos^{-1}\left(\frac{n - m\cos(\varphi)}{\sqrt{m^2+n^2-2mn\cos(\varphi)}}\right) \tag{3.11}$$

Proof. See Appendix 7.2.

Therefore, the probability of the RIS facilitating a virtual LoS link between the specific cell and the BS through signal reflecting can be given as follows.

$$f_i(m,n,\varphi) = \frac{1}{2} \cdot P_{LoS}(n) \cdot P_{LoS}(d_{R,B}) \cdot \mathscr{C}(m,n,\varphi) \tag{3.12}$$

3.3.5 Network Cost Analysis

The network costs associated with hardware, deployment, operational expenses, etc. For instance, the material costs to manufacture the RIS, the broadband charges for backhauling connections to the BSs, and equipment maintenance expenses. In [9], the authors define equipment costs, which include unit cost, installation time, interest rates, and other factors. Furthermore, the network cost is calculated by multiplying the number of network devices by the quantity of reflecting meta-surfaces by the unit cost of devices. We let ζ_{RIS} represent a RIS device's unit cost, and the RIS network's total cost is expressed as follows.

$$\eta = \lambda_{RIS} M \zeta_{RIS} \tag{3.13}$$

3.3.6 Problem Formulation

We aim to maximize coverage probability while satisfying network cost and other constraints for multi-RIS-assisted outdoor wireless communication networks, where optimization variables are phase shifts of elements and deployment locations of RISs. Note that the coverage in the previous work refers to whether the user is covered. However, this paper determines whether a specific cell is covered. Thus, we formulate the optimization problem as follows.

$$\max_{\mathbf{\Psi}_{RIS},\mathbf{\Phi}} \; P_{cov}(\lambda_{RIS}, M) \tag{3.14}$$

$$\begin{aligned} s.t. & (a)\ \eta < \eta_{th} \\ & (b)\ p_k \geq P_{th} \\ & (c)\ \|y,z\| \leq R, \|y,c\| \leq R \\ & (d)\ \theta_{g,ris} \geq \theta_{g,bs} \\ & (e)\ 0 \leq \phi_n \leq 2\pi \end{aligned} \tag{3.15}$$

where constraint (a) indicates that the network cost is less than the threshold requirement η_{th} for a wireless communication network. As in constraint (b), we constrain the received power to guarantee signal quality efficiently. Constraint (c) requires that both the distance $d_{B,R}$ and the distance $d_{B,U}$ are within the signal range R of the BS. The constraint (d) ensures that the RIS can be reflected signal from BSs. (e) denotes the phase shifts of elements constraint.

3.4 Coverage Probability Maximization Algorithm Design

This section investigates the RIS deployment locations problem concerning coverage probability and network cost. In this paper, we propose an optimal strategy called the R&B algorithm, which consists of two stages. Firstly, we use the Rule-based method to identify feasible solutions in the solution space. Subsequently, we present a Branch-and-Bound (B&B) algorithm to determine the deployment location of RISs installed on obstacles while satisfying the network cost constraint.

3.4.1 Rule-based Algorithm to Obtain Feasible Solutions

The time and space performance of the algorithm is improved by using Rule-based pruning techniques, which avoid unnecessary traversal processes while complying with the principles of accuracy, correctness, and efficiency. In this paper, we utilize viable pruning techniques to remove RISs that do not meet the reflective conditions, as detailed in Section III-D.

This paper investigates the coverage enhancement in an outdoor wireless communication environment with multiple BSs, various RISs, and several obstacles. The RISs are equipped with obstacle facades to enhance coverage and signal quality. Our objective is to maximize the coverage probability while minimizing the network cost by optimizing the placement of RISs. The Rule-based method traverses each RIS, removing it if pruning enhances system performance; Otherwise, it is retained. Therefore, the Rule-based method eliminates RISs that fail to meet reflective conditions. An example is illustrated in Fig. 3.4, ris_1 is pruned since it lies outside the range of BS_1 signal, ris_2 is eliminated as its direct LoS link to BS_2 is blocked, ris_3 is removed since its direct LoS link to the user u_1 is blocked, and ris_4 is clipped since BS_3 and user u_1 are not on the same side. The Rule-based method provides a set of feasible solutions to the problem, which is further optimized by applying the B&B algorithm to determine the deployment locations of RISs.

3.4.2 Branch-and-Bound Algorithm to Optimize RISs Deployment Locations

The Rule-based method determines which obstacles are eligible for RIS installation. The solution space of RIS deployment locations, $\mathbf{\Psi}_{RIS}$, is visualized as a binary tree structure, as depicted in Fig. 3.5. The locations of RIS deployment, i.e., $\mathbf{\Psi}_{RIS} = (ris_1, ris_2, \cdots, ris_L)$, is provided at each node of the tree. At the root node, none of the variables in $\mathbf{\Psi}_{RIS}$ are fixed. Meanwhile, an unfixed variable ris_i at the parent node can be installed on obstacles or not, denoted by 1 and 0, respectively. As shown in Fig. 3.5, this process is repeated on each

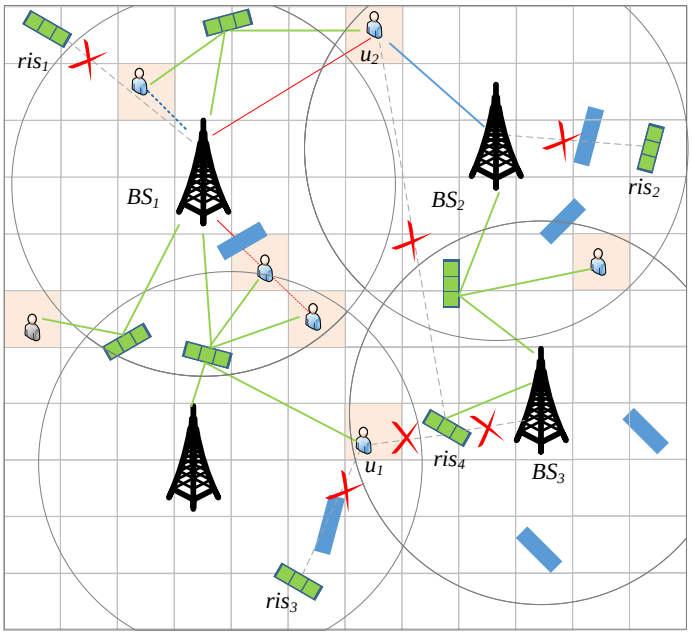

Fig. 3.4 An example of the Rule-based method.

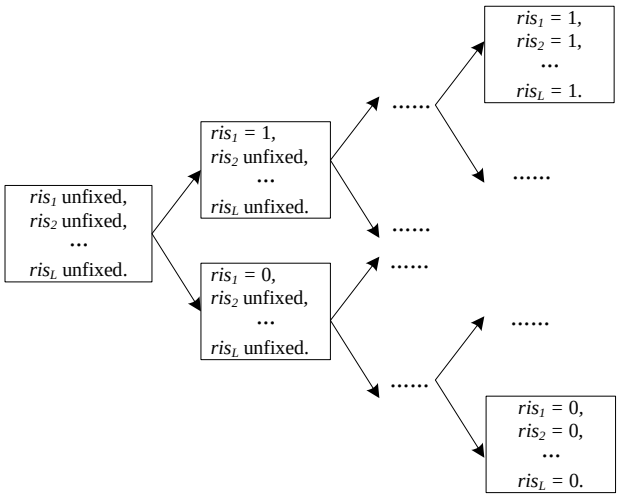

Fig. 3.5 Tree structure of the proposed B&B algorithm.

parent node, branching the parent node into two child nodes. Therefore, the objective is to design an effective algorithm utilizing the tree structure presented in Fig. 3.5 to optimize and resolve the problem stated in (3.14).

The B&B algorithm begins by randomly assigning a feasible solution for ris_i in the solution space, where ris_i can be set to 1 or 0. The objective function provides a lower bound value for the problem (3.14). The search space of problem (3.14) is then recursively

partitioned into smaller subspaces using the tree structure depicted in Fig. 3.5. The search for the optimal solution commences at the tree's root node and proceeds depth-first. At each tree node, the unfixed variable is split into two child nodes by assigning a value of either 0 or 1 to fix the variable. The upper bound value of the coverage probability is compared to the current lower bound value, and the branch corresponding to the analyzed node is either pruned or retained depending on their relationship. The lower bound is updated to the more excellent value of the two when all node variables are fixed, and the lower bound is compared with the node's coverage. The process iterates until all nodes in Fig. 3.5 are visited or pruned. The B&B algorithm aims to optimize the problem of RIS deployment on obstacles and is summarized in Algorithm 4.

Algorithm 4 The RIS Deployment Locations Optimization

Input: Ψ_{BS}, λ_{BS}, Ψ_{OB}, λ_{OB}, μ.

Output: P_{cov}^{lb}, $\mathbf{\Psi}_{RIS}$.

Initialization: Initialize a feasible solution $\mathbf{\Psi}_{RIS}$ for RIS deployment locations problem (3.14) according to the Rule-based method and the coverage probability P_{cov}^{lb} as the lower bound;

while *Not all nodes in Fig. 3.5 have been visited or pruned* **do**
  Calculate the upper bound value P_{cov}^{ub} of the current node;
  if $P_{cov}^{ub} < P_{cov}^{lb}$ **then**
    Pruning the corresponding branch;
  else
    if *Any child node of the current node has not been pruned* **then**
      Moving to any two child nodes; continue;
    else
      Calculating the corresponding coverage probability P_{cov}^{curr};
    if $P_{cov}^{curr} > P_{cov}^{lb}$ **then**
      $P_{cov}^{lb} = P_{cov}^{curr}$;

Proposition 1 *The complexity of the proposed methods of Rule-based and Branch-and-Bound-based (R&B) is* $\mathcal{O}\left(k\lambda_{RIS}\lambda_{BS} + 2^{\lambda_{RIS}}\right)$.

Proof. The computational complexity of the Rule-based method depends on RIS densities λ_{RIS}, BS densities λ_{BS}, and the number of cells k, and is given by $\mathcal{O}(k\lambda_{RIS}\lambda_{BS})$. On the other hand, the computational complexity of the B&B algorithm is given by $\mathcal{O}\left(2^{\lambda_{RIS}}\right)$ in the worst-case scenario. Therefore, the overall computational complexity of the proposed optimization method can be expressed as $\mathcal{O}\left(k\lambda_{RIS}\lambda_{BS} + 2^{\lambda_{RIS}}\right)$.

Note that in practical scenarios, the locations of BS and obstacles typically remain unchanged over extended periods. Once the proposed algorithm determines the RIS placement, it tends to remain static for a considerable duration. Consequently, the algorithm's complexity is of lesser significance for the case. Additionally, if we focus on a smaller specific area, the densities of RIS and BS can be correspondingly reduced, thereby simplifying the complexity of the algorithm. Therefore, in practical RIS placement applications, decreasing the size of the specific region can effectively reduce the complexity of our proposed algorithm.

3.5 Simulation Results

This section conducts extensive simulations to estimate the coverage probability and network cost of large-scale RIS-assisted outdoor wireless communication networks. Specifically, a 2D outdoor scenario with 1 km $\times$ 1 km, frequency of 5GHz, several RISs with different metasurfaces, and multiple obstacles according to the PPP distribution are simulated. Additionally, we set the signal range of the BS, R, to be 300m, and equal power consumption for all cases ($p_k = 1$) to ensure a fair comparison. The simulation symbols are provided in Table 3.1. Three benchmark methods were chosen for comparison in this section.

Table 3.1 Symbols and descriptions

Symbol	Value
D	1 km $\times$1 km
λ_{BS}	[1, 3, 5, 7, 9, 11, 13, 15, 17, 19, 21] /km^2
λ_{OB}	[100, 200, 300, 400, 500, 600, 700] /km^2
μ	[0.1, 0.2, 0.3, 0.4, 0.5, 0.6, 0.7]
R	300 m
G_e^i, G_e^r	5 dbi
ω_p	1
P_{th}	-90 dbm
T	10 dB

3.5.1 Coverage Enhancement for Multi-RIS Deployment

This section aims to exhibit the influence of RIS deployment on the coverage probability and emphasize the significance of BS in RIS-assisted wireless communication scenarios. In Fig. 3.6, we display the coverage probability for different values of RIS density μ in a 1 km $\times$ 1 km with an obstacle density of $400/\text{km}^2$ and a BS density of $10/\text{km}^2$, where

multiple RIS are randomly deployed on the facade of obstacles. Fig. 3.6(a) depicts the scenario with black dots representing the BSs, blue squares for the obstacles, and red for the users. The region is divided into multiple cells to calculate the coverage probability, referring to the proposed method, as shown in Fig. 3.6(b). We use Algorithms 2 and 3 to determine whether a given cell is covered. If it is covered, we mark it in blue; otherwise, we mark it in white. It is not difficult to find that the coverage areas expand as the value of μ increases. Nevertheless, due to the obstacle density and BS locations, some specific cells remain uncovered even with the deployment of RISs, as shown in Fig. 3.6(f). Therefore, the simulation demonstrates that RIS deployment in wireless communication networks improves the coverage probability.

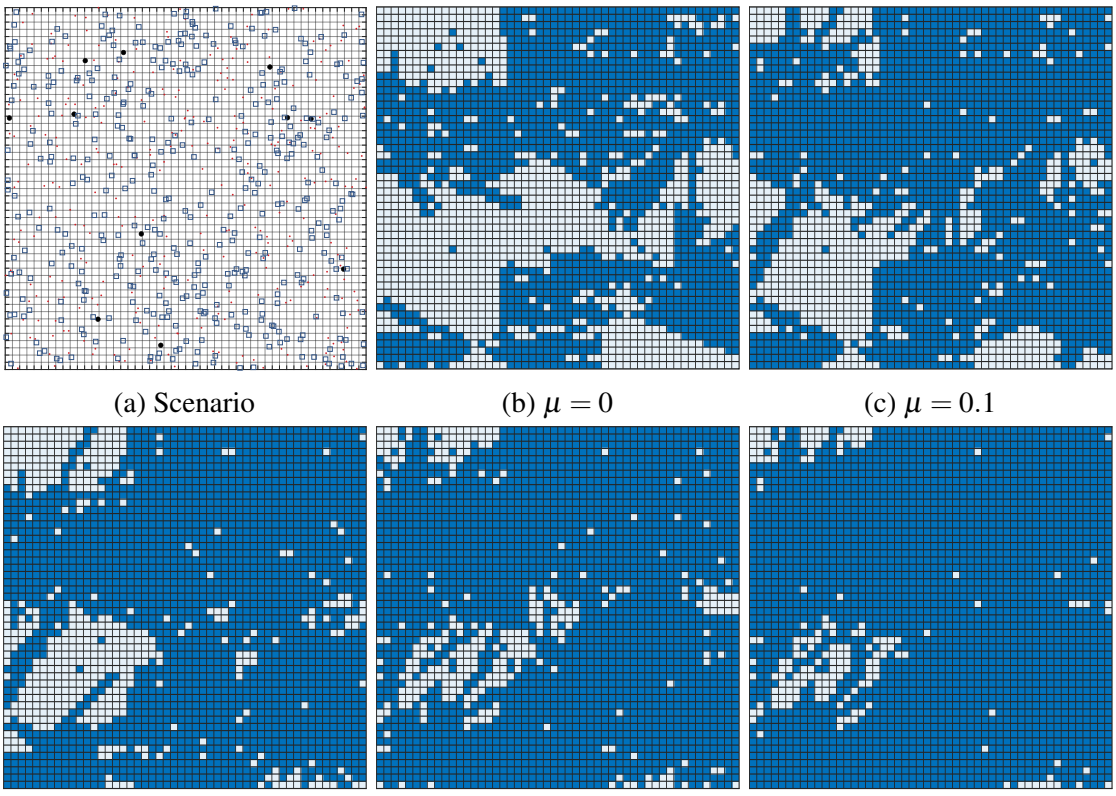

(a) Scenario (b) $\mu = 0$ (c) $\mu = 0.1$

(d) $\mu = 0.2$ (e) $\mu = 0.4$ (f) $\mu = 0.8$

Fig. 3.6 A realization of the coverage regions with the density of BS $\lambda_{BS} = 10/\text{km}^2$, the density of obstacles is $\lambda_{OB} = 400/\text{km}^2$, and the RIS density is $\lambda_{RIS} = \mu\lambda_{OB}$. Fig. 3.6(a) is a scenario diagram. Fig. 3.6(b)-(f) are the coverage diagrams. The μ varies as follows: (a) $\mu = 0$, (b) $\mu = 0$, (c) $\mu = 0.1$, (d) $\mu = 0.2$, (e) $\mu = 0.4$, (f) $\mu = 0.8$.

Fig. 3.7 displays the number of RISs obtained after the pruning discussed in Section IV-A for varying BSs. We can observe that an increase in both the RIS density μ and the number of BSs leads to a rise in the locations for deploying the RISs. This is also demonstrated that

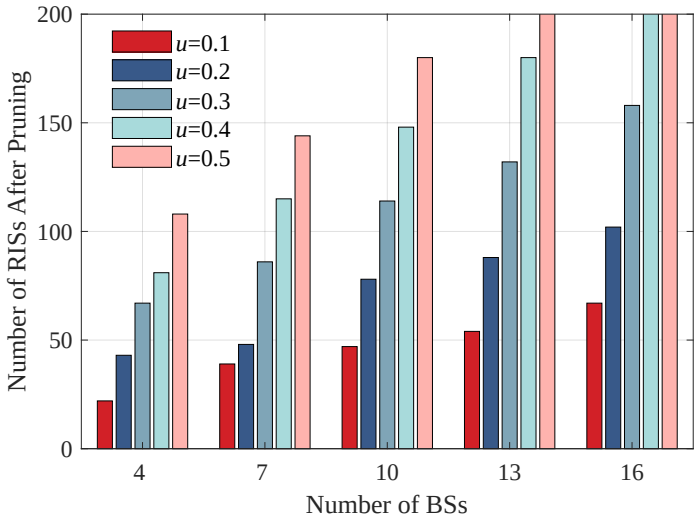

Fig. 3.7 The number of RISs after pruning versus the number of BSs, where $\lambda_{OB} = 700/\text{km}^2$.

BSs play an essential role in RIS-assisted wireless communication systems. However, when the number of BSs is large enough (e.g., $\lambda_{BS} = 16/\text{km}^2$), even if the RIS density is increased, the available RIS deployment locations will not increase linearly due to the presence of multiple obstacles.

3.5.2 Performance Evaluation vs. Number of OBs, BSs, and RISs

This section aims to validate the proposed coverage calculation method and comprehensively evaluate our algorithm through simulations with varying numbers of RISs, OBs, and BSs. Fig. 3.8 presents the coverage probability for different obstacle densities according to the proposed calculation method and theoretical analysis. The coverage probability decreases with an increasing number of obstacles and a decreasing density of RISs. Moreover, the accuracy of the proposed coverage calculation method is confirmed by the theoretical analysis Eq. (3.7).

Fig. 3.9 illustrates the coverage probability and network cost versus different numbers of obstacles and RIS density when BS density is given as $14/\text{km}^2$. As displayed in Fig. 3.9(a), the coverage probability obtained by the R&B algorithm decreases as the number of obstacles increases but increases with the density of RIS. This occurs because increased obstacles result in more direct LoS links being blocked from the BS to the users, leading to lower coverage probability. Conversely, an increase in RIS density leads to a higher number of virtual LoS links between the BS and the users. However, when the obstacle density is low (e.g., $\lambda_{OB} = 100/\text{km}^2$), increasing the RIS density does not significantly increase the

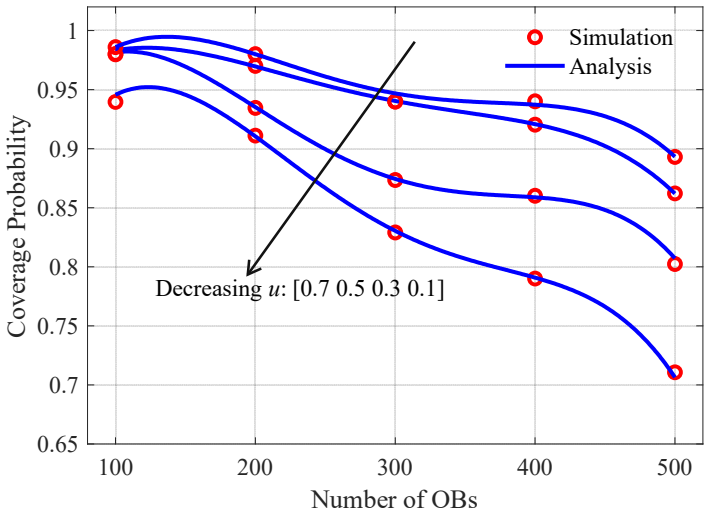

Fig. 3.8 The coverage probability versus the number of OBs, where $\lambda_{BS} = 14/\text{km}^2$.

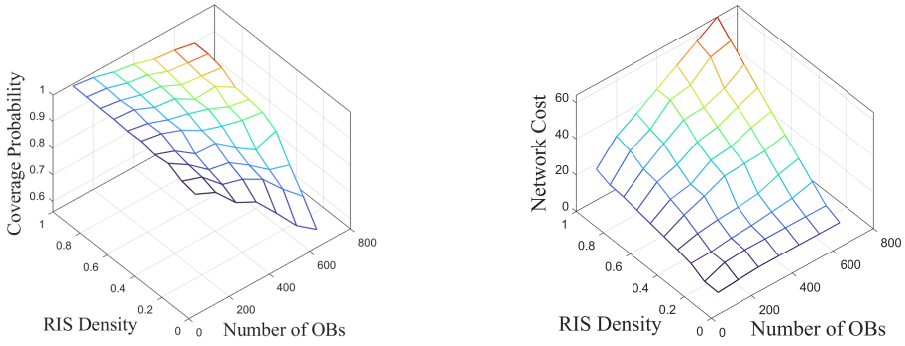

(a) Coverage Probability

(b) Network Cost

Fig. 3.9 The coverage probability and network cost versus the different number of OBs and RIS density for $\lambda_{BS} = 14/\text{km}^2$.

coverage probability. Furthermore, as depicted in Fig. 3.9(b), the network cost rises with increasing obstacles and RIS density.

Fig. 3.10 displays that the coverage probability and network cost grow with the quantity of BSs and RIS density. It can be seen that BSs are essential to RIS-assisted wireless communication systems. When the number of BSs is fixed at 1, increasing the RIS density does not result in a significant increase in coverage probability. This is due to the limited number of BSs reducing the availability of RISs that enable virtual LoS links between the BS and the RIS, as illustrated in Fig. 3.10(a). Additionally, the network cost rises with increased RIS and BS density, as depicted in Fig. 3.10(b).

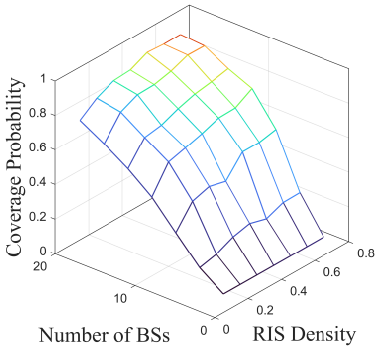

(a) Coverage Probability

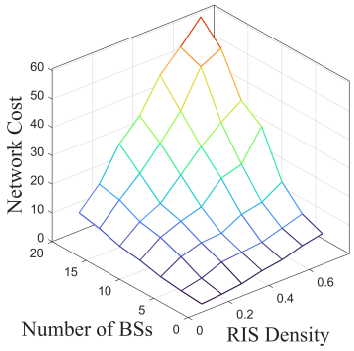

(b) Network Cost

Fig. 3.10 The coverage probability and network cost versus the different number of BS and RIS density for $\lambda_{OB} = 700/\text{km}^2$.

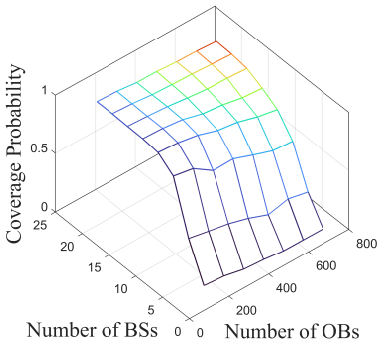

(a) Coverage Probability

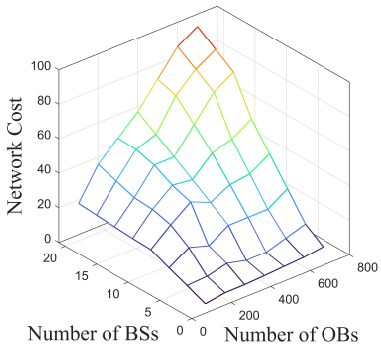

(b) Coverage Probability

Fig. 3.11 The coverage probability and network cost versus the different number of BSs and OBs.

Fig. 3.11 illustrates the coverage probability and network cost against the different number of BSs and obstacles. The coverage probability decreases gradually with an increase in obstacles when the number of BSs is fixed. Conversely, with a fixed number of obstacles, an increase in BSs leads to a rise in the coverage probability. However, the network cost increases with the number of BSs and obstacles. This can be attributed to the need for deploying more RISs as the number of BSs and obstacles increases, leading to higher network costs.

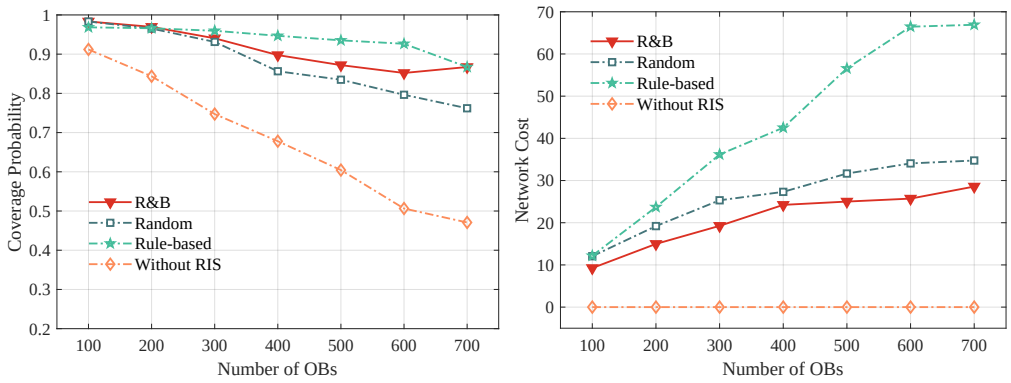

(a) Coverage Probability (b) Network Cost

Fig. 3.12 The coverage probability and network cost versus the number of OBs, where $\lambda_{BS} = 14/\text{km}^2$, $\lambda_{RIS} = 0.5 \cdot \lambda_{OB}/\text{km}^2$.

3.5.3 Comparison Algorithms

This section compares the performance of the proposed scheme with several baseline methods.

- *R&B:* This legend depicted the multi-RIS deployment locations optimization scheme, in which the feasible solutions are obtained by the Rule-based method, and the deployment locations are optimized while considering the network cost by the B&B method.
- *Random:* This legend corresponds to the simplified optimization scheme adopted, whereby deployment locations of RISs are randomly generated, and the feasible solutions space is not optimized.
- *Rule-based:* In the considered multi-RIS-assisted outdoor wireless network, the choice of RIS deployment locations among obstacles is not optimized, only optimizing feasible solutions for RIS.
- *Without RIS:* To verify the potential of deploying multiple RIS in enhancing the coverage and reducing the network cost in the wireless network without RISs.

Fig. 3.12 depicts the coverage probability and network cost for various numbers of obstacles. The four methods exhibit the same trend in coverage probability, with decreases as the number of obstacles increases, as shown in Fig. 3.12(a). Our proposed *R&B* algorithm outperforms the *Random* deployment and *Without RIS* schemes. However, the coverage probability of the *Rule-based* method is superior to our proposed *R&B* algorithm because the *Rule-based* method focuses on coverage probability and does not consider network

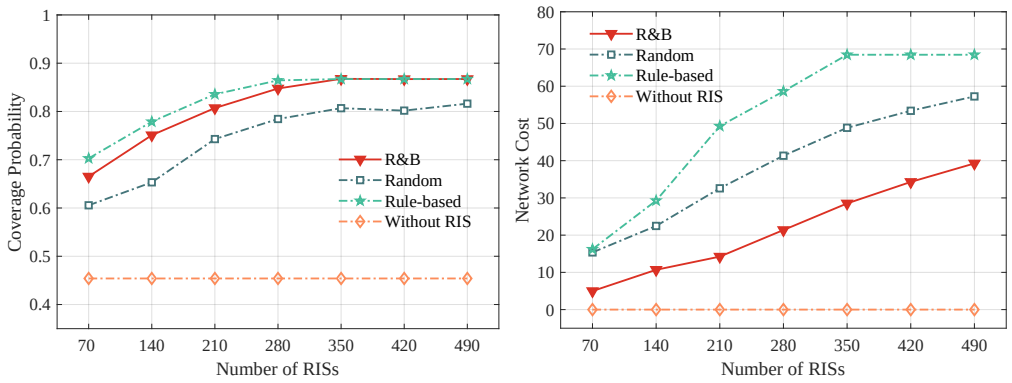

(a) Coverage Probability (b) Network Cost

Fig. 3.13 The coverage probability and network cost versus the number RISs, where $\lambda_{BS} = 14/\text{km}^2$, $\lambda_{OB} = 700/\text{km}^2$.

cost constraints. Specifically, more RIS are deployed in *Rule-based* scheme compared to our proposed *R&B*. In addition, we also observe that as the number of obstacles increases, the *Rule-based* method is gradually at a disadvantage. Certainly, coverage probability typically comes at the expense of network cost, as shown in Fig. 3.12(b). The cost of the *Rule-based* method is relatively high compared to other methods. In addition, the network cost for the scheme without RIS deployment remains 0 regardless of the number of obstacles.

Fig. 3.13 illustrates the coverage probability and network cost against the number of RISs for BS density $\lambda_{BS} = 14/\text{km}^2$ and obstacle density $\lambda_{OB} = 700/\text{km}^2$. Fig. 3.13(a) reveals that coverage probability grows with an increasing number of RISs, except for the *without RIS* case. This is because more virtual LoS links are generated in the outdoor communication network with increasing RISs. However, the scheme *without RIS* deployment yields a coverage probability of 0.454, which remains unchanged as the number of RISs increases. The *Rule-based* method achieves higher coverage probability than *R&B* method because it ignores network cost constraints and deploys more RISs. Meanwhile, when the number of RISs is equal to or greater than 350, the coverage probability for the *Rule-based* scheme reaches a saturation point at 0.867 due to excessive obstacles and non-conforming RISs. Fig. 3.13(b) reveals that the *Rule-based* method incurs higher network cost than other methods. Note that we perform a pruning operation prior to implementing the schemes, resulting in a varying number of RIS for each scheme and consequently, distinct network costs. In conclusion, our proposed *R&B* algorithm achieves a better trade-off between coverage probability and network cost than the other baselines.

3.6 Conclusion

In this paper, we aim to enhance the coverage of outdoor wireless communication networks by deploying large-scale RISs at optimal locations while satisfying network cost constraints. We present quantitative methods based on approximate cell decomposition to calculate coverage probability for RIS-assisted and non-RIS-assisted deployments. Then, we propose the R&B algorithm, which is a Rule-based and Branch-and-Bound-based (B&B) algorithm that optimizes the deployment locations of multiple RIS to maximize coverage probability while satisfying network cost constraints. Extensive simulation results show that the proposed algorithm improves coverage probability by optimizing the deployment locations of RISs. The results also indicate that the R&B algorithm achieves a more excellent trade-off between coverage probability and network cost than other benchmark algorithms.

Chapter 4

The Optimization of Power in Multi-RIS-Assisted Indoor Communication Networks

4.1 Motivation

With the expansion of the Internet of Things (IoT), the number of devices connecting via base stations (BSs) and access points (APs) in 5G and future wireless networks is anticipated to reach 70 billion by 2025 [25], and the data rate will need to be increased by 1,000 times to serve numerous connected devices [99]. However, obtaining higher data rates by simply scaling up transmit power or increasing the number of BS is unrealistic, which leads to problems in energy management, greenhouse gas emissions, higher costs, etc. In addition, it is critical for operators (e.g., saving on electricity bills) and terminal users (e.g., prolonging battery life), thus stimulating a great deal of concerns in power consumption research in academia and industry. Several energy-saving solutions have been recently proposed to achieve a green and sustainable wireless network environment [3], ranging from energy-efficient hardware design [72] and green energy [35] to intelligent resource allocation scheduling [108] and signal processing techniques [22].

To satisfy the higher data rate demands of IoT devices, traditional strategies, including deploying additional BSs and relays, are commonly employed to enhance the performance of wireless communication systems. However, the network costs associated with hardware, deployment, maintenance and operation, and energy consumption are excessively high [9]. Moreover, renewable energy, like wind and solar power for various communication systems, has been the focus of the current research works [44, 95, 33, 24]. Nonetheless, the reliability

of wind and solar energy is heavily dependent on weather conditions and remains inaccessible in many regions. In contrast, Reconfigurable Intelligent surface (RIS), recognized for its promising cost-efficiency and energy-efficient characteristics, consists of a digital controller and an array of passive meta-elements capable of dynamically adjusting phase shifts in response to incident electromagnetic waves [71]. Specifically, RIS is employed to enhance wireless communication links by manipulating the direction, phase shifts, and amplitude of electromagnetic waves, resulting in mitigating signal attenuation, reducing interference, enhancing coverage, and augmenting the signal strength at desired locations.

Recent studies have focused on optimizing the parameters of RIS to achieve various communication objectives [76, 108, 103, 41, 97]. For example, a novel interference nulling method assisted by RIS is proposed in [40] to maximize the K Degrees-of-Freedom (DoF) in the k-user interference channel, employing an alternative optimization algorithm. Channel estimation of RIS-assisted wireless communication systems [18] poses a significant challenge due to the extensive array of passive reflective elements in RIS. In [70], a more realistic indoor scenario is proposed, incorporating a human mobility model to optimize the deployment locations of multiple RISs and enhance coverage. The authors of [56] investigate the transmission data rate for VR users in an indoor wireless communication environment. This study involves the deployment of multiple RIS and joint optimization of the passive beamforming at RIS and the power allocation at users. In [34], the authors explore the physical layer security of RIS-aided wireless networks, where confidential messages are transmitted to an authorized user amidst the threat of a malevolent eavesdropper via a RIS-assisted None- link.

Note that the aforementioned works on RIS-assisted wireless communication systems are aimed at solving challenges such as interference, coverage, achievable rate, and security. However, few studies have focused on power consumption issues in RIS-assisted wireless networks. The modeling and implementation of power consumption for RIS, as proposed in [84], hold great significance in fostering sustainability and green practices within wireless networks. Additionally, the authors in [108] introduce a pioneering framework with double-faced active (DFA) RIS in downlink wireless communication systems. This framework aims to mitigate power consumption through a real-time online strategy, leveraging the principles of Lyapunov control theory. The authors of [79] utilize RIS and Rate Splitting Multiple Access (RSMA) technologies in a multicellular communication system to enhance energy efficiency by jointly optimizing the BS beamforming, RIS phase shifts, and user rate allocation vectors. However, the above studies primarily concentrate on single RIS-assisted wireless networks, ignoring the influence of IoT device status and the association

relationships between multiple RIS and several IoT devices on power consumption and system performance.

This paper investigates power optimization for large indoor wireless communication systems aided by RIS. By exploring the relationships between IoT devices and RISs and optimizing the phase shifts of multiple RISs, we aim to increase the number of IoT devices covered and simultaneously decrease the system's power consumption. The main contributions of the paper are summarized as follows.

- We first explore the power minimization problem in large indoor environments assisted by multiple RISs. In contrast to the existing works [88, 5], this study can simultaneously reduce system power consumption and improve device coverage rate.
- Based on the scenario outlined above, we aim to analyze the association relationships between multiple RISs and several IoT devices with the objective of extending coverage and reducing complexity. Enlightened by heuristic theory, we introduce a novel optimization strategy called the Hybrid Optimization Strategy (AHOS), which dynamically adjusts association relationships to maximize coverage rate.
- Furthermore, we minimize the power consumption of the whole wireless system by optimizing the phase shifts for multiple RISs while considering the status of devices when the association strategy is determined. Additionally, we transform the objective functions into a more tractable form to solve it.
- Extensive simulation results verify the efficiency of the proposed RIS-assisted large indoor wireless communication networks in reducing system power consumption while enhancing coverage for IoT devices. Moreover, numerical results also demonstrate the significance of RIS in achieving coverage with minimal power consumption.

4.2 Related Work

Most previous work on RIS has primarily concentrated on integrating with various technologies to enhance coverage, improve location accuracy, and boost security. In [103], RISs deployed on indoor wall millimeter-wave (mmWave) systems are utilized to establish virtual communication links between the Access Point (AP) and users. Therein, positions and orientations of RISs are jointly optimized using gradient descent with weights to maximize coverage. In [101], the passive indoor localization framework for multiple users, leveraging the degrees of freedom, has been proposed. Furthermore, traditional RIS and Absorptive RIS

(ARIS) with reflection and absorption coefficient phases have been considered to enhance the physical layer security of wireless communication systems [41, 82].

Despite the considerable attention given to RIS-assisted wireless communication systems, relatively limited research has focused on power consumption issues. In [85], the authors analyze the static and dynamic power consumption model of two types of RIS (i.e., varactor-diode RIS and PIN-diode RIS) in the real-world scenarios, exploring the quantitative relationships between power consumption and PIN-diode RIS. Energy efficiency for multiple users in RIS-assisted Multiple Input Single Output (MISO) wireless communication systems is examined in [37]. In [108], a novel Double-Faced-Active (DFA)-RIS framework is given to achieve full-space coverage. The authors focus on jointly optimizing data flows at the Media Access Control (MAC) layer and the RIS beamforming at the physical layer to reduce long-term power consumption and ensure queue stability. In [79], the authors utilize the RSMA technology and RIS to enhance the performance of edge cellular networks, aiming to maximize energy efficiency through joint optimization of beamforming vectors at BS, phase shifts at RIS, and rate allocation matrices at users.

Despite the previous discussion on RIS power consumption and energy efficiency, the mentioned studies fail to demonstrate the influence of multiple RIS deployments. Some work has been made to consider this issue, such as the authors of [5] deploy RIS on multiple Unmanned Aerial Vehicle (UAV) to enhance the average achievable rate and energy efficiency by optimizing the phase shifts of elements, deployment positions of RISs, and power control of the communication system. However, to the best of our knowledge, there is a gap in research regarding the joint optimization of association relationships between RISs and IoT devices, as well as phase shifts of reflective elements in indoor scenarios, aiming at maximizing coverage and minimizing power consumption.

4.3 System Model and Problem Formulation

4.3.1 System Model

In this paper, we consider the indoor downlink wireless communication system assisted by multiple RISs, where a BS equipped with N_b antennas serves several single-antenna IoT devices, as shown in Fig. 4.1. An RIS with N reflective elements and a micro-digital controller is deployed in the environment to enhance the system's coverage and communication performance. Specifically, The propagation direction of the signal is reconfigured by adjusting the phase shift of reflective elements. The LoS path between BS and IoT devices may be obstructed by obstacles in the complex indoor scenario, resulting in blind spot areas.

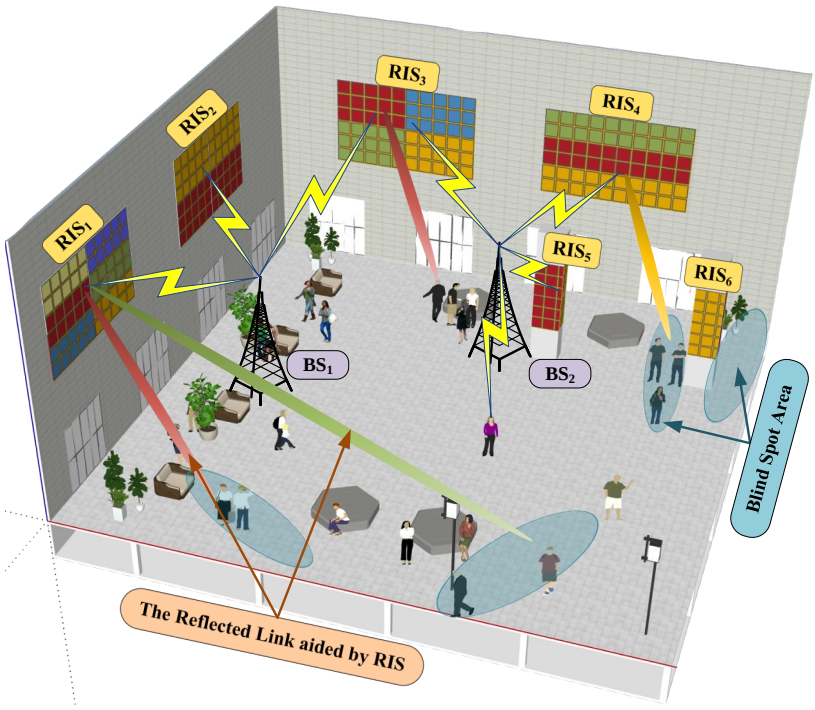

Fig. 4.1 System model.

To ensure effective communication, RISs are installed on the facade of obstacles or walls to establish the virtual LoS link. Note that a large RIS is partitioned into multiple smaller RISs units to serve different devices, with the goal of improving the coverage rate and reducing complexity. We denote the set of RISs as $\mathscr{R} = \{1,\ldots,r,\ldots,|R|\}$, the set of devices as $\mathscr{K} = \{1,\ldots,k,\ldots,|K|\}$, the set of BSs as $\mathscr{B} = \{1,\ldots,b,\ldots,|B|\}$, and the set of obstacles as $\mathscr{OB} = \{1,\ldots,ob,\ldots,|OB|\}$. The coordinates of the RIS, device, BS, and obstacle are represented as $\mathbf{\Psi}_r = \{x_r, y_r\}\ \forall r \in \mathscr{R}$, $\mathbf{\Psi}_k = \{x_k, y_k\}\ \forall k \in \mathscr{K}$, $\mathbf{\Psi}_b = \{x_b, y_b\}\ \forall b \in \mathscr{B}$, and $\mathbf{\Psi}_{ob} = \{x_{ob}, y_{ob}\}\ \forall ob \in \mathscr{OB}$, respectively.

It is worth noting that, in this paper, we make the assumption that only a subset of the devices is active status, denoted as $\mathscr{A}_a$, otherwise $\mathscr{A}_i$. Specifically, we utilize a boolean value to indicate the activity status of the k-th device as follows.

$$a_k = \begin{cases} 1, & \textit{if k-th device is active} \\ 0, & \textit{Otherwise} \end{cases}, \forall k \in \mathscr{K}, \tag{4.1}$$

where collection of active devices is $\mathscr{A}_a = \{k | a_k = 1, k \in \mathscr{K}\}$ and status collections of all devices is $\mathscr{A} = \mathscr{A}_a \cup \mathscr{A}_i$.

4.3.2 Signal Model

In the downlink RIS-assisted wireless communication system, two propagation paths are modeled. One is the direct channel between the BS and devices, and the other is the indirect channel assisted by RIS, which is transmitted to RIS by the BS and then reflected to the devices. Thus, the signal transmitted by the n-th element of the r-th RIS is expressed as

$$y_{r,n} = \phi_{r,n}\left(x_{r,n} + v_{r,n}\right), \tag{4.2}$$

where $\phi_{r,n} \triangleq e^{j\theta_{r,n}}$ denotes the phase shifts for the n-th element of the r-th RIS, $x_{r,n}$ is the incident signal transmitted by BS, and the $v_{r,n}$ represents the thermal noise originating from hardware circuits. Therefore, the reflection signal of r-th RIS is given by

$$\mathbf{y}_r = \mathbf{\Phi}_r\left(\mathbf{x} + \mathbf{v}\right), \tag{4.3}$$

where $\mathbf{\Phi}_r \triangleq diag\left(\boldsymbol{\phi}_r\right) \in \mathbb{C}^{N\times N}$, $\boldsymbol{\phi}_r \triangleq \left[e^{j\theta_{r,1}}, \ldots, e^{j\theta_{r,n}}, \ldots, e^{j\theta_{r,N}}\right]$ denotes the phase shift vector of the r-th RIS, and the $\mathbf{v} \sim \mathscr{CN}(0, \delta_v^2\mathbf{I}_N)$ means the thermal noise. Moreover, $\mathbf{x}$ is equal to $\sum_{k=1}^{K}\mathbf{t}_k\tau_k$ represents the transmit signal at BS. Here, $\tau_k \sim \mathscr{CN}(0,1)$ denotes the information symbol transmitted to the k-th device, and the $\mathbf{t}_k \in \mathbb{C}^{N_b\times 1}$ represents the transmission beamformer at the BS.

In the downlink wireless communication system, the signal received from BS may be obstructed by obstacles. In this case, the BS utilizes virtual LoS links with the assistance of RIS for data transmission. There, the signal received by the k-th device can be expressed as

$$y_k = \sum_{b=1}^{B}\sum_{r=1}^{R}\left(\mathbf{h}_{b,k}\mathbf{x} + \mathbf{H}_{r,k}\mathbf{\Phi}_r\mathbf{G}_{b,r}\mathbf{x}a_k + \mathbf{H}_{r,k}\mathbf{\Phi}_r\mathbf{v}a_k\right) + n_k, \tag{4.4}$$

where B and R denote the number of BS and RIS, respectively. And $\mathbf{x}$ represents the transmission signal at BSs. The channel vectors, which include from the b-th BS to k-th device, from the b-th BS to the r-th RIS, and from the r-th RIS to the k device, are denoted as $\mathbf{h}_{b,k} \in \mathbb{C}^{1\times N_b}$, $\mathbf{G}_{b,r} \in \mathbb{C}^{N\times N_b}$, and $\mathbf{H}_{r,k} \in \mathbb{C}^{1\times N}$, respectively. Additionally, the $n_k \sim \mathscr{CN}(0, \delta_k^2\mathbf{I}_N)$ means the additive Gaussian white noise, a_k indicates the status of k-th device. For simplicity, we consider the case of one BS, and the formula is rewritten as

$$y_k = \sum_{r=1}^{R}\left(\mathbf{h}_k\mathbf{x} + \mathbf{H}_{r,k}\mathbf{\Phi}_r\mathbf{G}_r\mathbf{x}a_k + \mathbf{H}_{r,k}\mathbf{\Phi}_r\mathbf{v}a_k\right) + n_k, \tag{4.5}$$

The SINR of the k-th device is given by

$$\mathrm{SINR}_k(\mathbf{T},\boldsymbol{\Phi}) = \sum_{r=1}^{R} \frac{|\mathbf{g}_k \mathbf{t}_k|^2}{\sum_{j\neq k} |\mathbf{g}_k \mathbf{t}_j|^2 + \delta_v^2 \|\boldsymbol{\Phi}_r \mathbf{H}_{r,k} a_k\|^2 + \delta_k^2}, \tag{4.6}$$

where $\mathbf{T} \triangleq [\mathbf{t}_1, \ldots, \mathbf{t}_k]$ and $\mathbf{g}_k \triangleq \mathbf{h}_k + \mathbf{H}_{r,k}\boldsymbol{\Phi}_r \mathbf{G}_r a_k$. Therefore, the rate of k-th device is obtained as

$$R_k(\mathbf{T},\boldsymbol{\Phi}) = \log_2(1 + \mathrm{SINR}_k(\mathbf{T},\boldsymbol{\Phi})). \tag{4.7}$$

4.3.3 Path Loss and Number of Elements Model

Path loss represents a critical performance metric in conventional wireless communication systems and is proportional to the propagation distance. However, RISs can manipulate the propagation direction by controlling signal reflection, enabling the signal to reach the intended destination and reducing multipath propagation in RIS-assisted wireless communication networks [43]. Therefore, signal attenuation can be mitigated even over extended distances with the assistance of RISs, leading to enhanced communication quality. Specifically, in reference to [27], the power of the received signal via the NLoS path is given by $N^2\left(dis_{b,r} + dis_{r,k}\right)^{-\omega}$, where N represents the number of elements for each RIS, $dis_{b,r}$ corresponds to the distance between the b-th BS and the r-th RIS, $dis_{r,k}$ denotes the distance between the r-th RIS and the k-th device, and ω signifies the path loss exponent. In contrast, the power of the received signal via the LoS link is expressed as ${dis_{b,k}}^{-\omega}$, where $dis_{b,k}$ denotes the distance between the b-th BS and the k-th device.

In this paper, we assume that the number of reflective elements N is fixed for all the RIS. However, an RIS shares reflective elements with different devices, and the elements of each RIS are distributed evenly with $\lfloor \frac{|N|}{|N_r|} \rfloor$, where N_r is the number of the devices associated with the r-th RIS. Furthermore, we use a boolean to indicate the association relationship between the devices and the RISs as follows.

$$\alpha_{ij} = \begin{cases} 1, & \textit{if the i-th RIS associated with the j-th device} \\ 0, & \textit{Otherwise} \end{cases}. \tag{4.8}$$

Therefore, the number of devices associated with a specific RIS r is expressed as $|N_r| = \sum_{k=1}^{K} \alpha_{rk}$.

4.3.4 Communication Region and Coverage Rate

In a complex indoor environment with multiple obstacles and IoT devices, coverage is a significant metric to guarantee the establishment of effective communication links between BSs and devices. The coverage rate is defined as the ratio of covered devices to all devices. For the i-th RIS, the communication region is

$$A_r\left(dis^i_{b,ris_i}, \varphi^i_b, \varphi^i_k\right) = \frac{N\lambda^2\sqrt{P_{c,BS}G_bG_kG_{ris}\left(\varphi^i_b\right)G_{ris}\left(\varphi^i_k\right)}}{(4\pi)^2 dis^i_{b,ris_i}\sqrt{P^u_{th}}}, \tag{4.9}$$

where,

$$G_{ris}(\varphi) = 2(2p+1)cos^{2p}(\varphi), \varphi \in \left(-\frac{\pi}{2}, \frac{\pi}{2}\right), \tag{4.10}$$

where dis^i_{b,ris_i} represents the distance between the i-th RIS and the BS, while φ^i_b and φ^i_k stand for the incident angle from the b-th BS to the i-th RIS and the reflection angle from the i-th RIS to the k-th device, respectively. Moreover, $P_{c,BS}$ signifies the transmission power, G_b is the antenna gain of the BS, and G_k denotes the antenna gain of devices. Additionally, $G_{ris}(\varphi)$ describes the radiation pattern of the RIS reflective element for the angle φ. To facilitate the analysis in the subsequent sections, the communication range of the i-th RIS is defined as a semicircle, with the coverage radius expressed as

$$\begin{aligned}\hat{A}_r\left(dis^i_{b,ris_i}, \varphi^i_b\right) &= \sum_{\varphi^i_k} \max A_r\left(dis^i_{b,ris_i}, \varphi^i_b, \varphi^i_k\right) \\ &= \mathscr{T}\frac{G_{ris}\left(\varphi^i_b\right)}{dis^i_{b,ris_i}},\end{aligned} \tag{4.11}$$

where,

$$\mathscr{T} = \frac{N\lambda^2\sqrt{P_{c,BS}G_bG_kG_{ris}(0)}}{(4\pi)^2\sqrt{P^u_{th}}}. \tag{4.12}$$

It should be noted that the power received by users exceeds the threshold P^u_{th}, and the communication range of i-th RIS falls below the $\hat{A}_r$. Drawing from this analysis, the coverage probability is delineated in Algorithm 5. Specifically, devices are capable of establishing effective communication with BSs via LoS links and virtual LoS links. In the case of LoS links, there must be no obstacles between i-th device and at least one BS, and the distance between i-th device and any BS should be within D. For the virtual LoS link, some conditions must be satisfied, such as the absence of obstacles between i-th device and j-th RIS, the distance between i-th device and j-th RIS is inside $\hat{A}_j$, the distance between j-th RIS and at least one BS is less than D, and the i-th device and at least one BS are on the same side.

Algorithm 5 The Coverage Probability Rate

Input: $\mathbf{\Psi}_r$, $\mathbf{\Psi}_k$, $\mathbf{\Psi}_b$, $\mathscr{R}$, $\mathscr{K}$, $\mathscr{B}$

Output: The Coverage Rate P_{cov}, the association relationship $\mathbf{\Lambda}$

Initialization: Generate PPP distributed of BSs, obstacle, RISs, and devices;

for $i = 1$ *to* $|\mathscr{K}|$ **do**
  $\mathbf{\Psi}_i \leftarrow$ the i-th device location;
  for $j = 1$ *to* $|\mathscr{R}|$ **do**
    $\mathbf{\Psi}_r \leftarrow$ the j-th RIS location;
    if *{no obstacles between i-th device and j-th RIS} && {the distance between i-th device and j-th RIS is less than* $\hat{A}_j$*} && {the distance between j-th RIS and at least one BS is less than D}* **then**
      $dev_i \leftarrow 1$;
    else if *{no obstacles between i-th device and at least one BS} && {the distance between i-th device and any BS is less than D}* **then**
      $dev_i \leftarrow 1$;
    else
      $dev_i \leftarrow 0$;

The coverage rate $P_{cov} = \frac{sum(dev_i==1)}{|\mathscr{K}|}$.

4.3.5 Power Consumption Model

The energy consumption of the BS is given by

$$P_{BS}(\mathbf{T}) = \zeta_{BS} \sum_{k=1}^{K} \|\mathbf{t}_k\|_2^2 + P_{c,BS}, \tag{4.13}$$

where ζ_{BS} is the inverse of energy efficiency of BS, and $P_{c,BS}$ denotes the fixed power required for controlling signal. Similarly, the energy consumption of the RISs is expressed as

$$\begin{aligned} P_{RIS}(\mathbf{T}, \mathbf{\Phi}) &= \zeta_{RIS} a_k \left[\sum_{k=1}^{K} \sum_{r=1}^{R} \|\mathbf{\Phi}_r \mathbf{G} \mathbf{t}_k\|_2^2 + \delta_v^2 \|\mathbf{\Phi}_r\|_F^2 \right] \\ &\quad + \sum_{k=1}^{K} \sum_{r=1}^{R} a_k \alpha_{rk} \lfloor \frac{|N|}{|N_r|} \rfloor P_{c,RIS}, \end{aligned} \tag{4.14}$$

where ζ_{RIS} denotes the inverse of the energy efficiency of the RIS, $\lfloor \frac{|N|}{|N_r|} \rfloor$ represents the number of elements associated with the r-th RIS, and $P_{c,RIS}$ is the power consumption of the

switch and control circuits. Additionally, the energy consumed by devices is given by

$$P_{device} = \sum_{k=1}^{K} a_k \begin{cases} P_{c,k}^{a}, & a_k = 1 \\ P_{c,k}^{in}, & a_k = 0 \end{cases}, \tag{4.15}$$

where $P_{c,k}^{a}$ and $P_{c,k}^{in}$ is the energy consumption of k-th device with active status and inactive status, respectively. Therefore, the total consumption of the whole system is expressed as

$$P_{total}\left(\mathbf{T}, \mathbf{\Phi}\right) = P_{BS}\left(\mathbf{T}\right) + P_{RIS}\left(\mathbf{T}, \mathbf{\Phi}\right) + P_{device}. \tag{4.16}$$

4.3.6 Problem Formulation

Our primary objective is the joint optimization of transmission beamforming at BS and phase shifts at RISs to minimize the power consumption of the entire system while ensuring maximum coverage rate. Additionally, we examine the association relationship between the RISs and the devices. Note that we focus on studying RIS applied in wireless communication systems, enabling the transmission beamforming at BS to be fixed and only optimizing the phase shifts of RISs. To address this, we first explore the association relationship between the RISs and the devices by maximizing the coverage rate. Subsequently, we optimize the phase shifts of multiple RISs to minimize power consumption while taking into account the active status of devices and coverage rate constraints. Thus, maximizing the coverage rate is formulated as

$$\max_{\mathbf{\Lambda}} \quad \sum_{k \in \mathscr{K}} P_{cov} \tag{4.17}$$

$$s.t. \quad p_k \geq P_{th}^{u}, \tag{4.17a}$$

$$\|\Psi_b, \Psi_k\| \leq D, b \in \mathscr{B}, k \in \mathscr{K}, \tag{4.17b}$$

$$\|\Psi_b, \Psi_r\| \leq D, \|\Psi_r, \Psi_k\| \leq \hat{A}_r, r \in \mathscr{R}, \tag{4.17c}$$

where

$$\mathbf{\Lambda} = \begin{pmatrix} \alpha_{11} & \alpha_{12} & \cdots & \alpha_{1k} \\ \alpha_{21} & \alpha_{22} & \cdots & \alpha_{2k} \\ \vdots & \vdots & \vdots & \vdots \\ \alpha_{r1} & \alpha_{r2} & \cdots & \alpha_{rk} \end{pmatrix}, \tag{4.18}$$

where $\mathbf{\Lambda}$ denotes the sets of the association relationships between $|R|$ RISs and $|K|$ devices. Furthermore, (4.17a) guarantees the received signal quality, (4.17b) and (4.17c) ensure to establish effective communication links.

After determining the association relationships between the RISs and the devices, the next is to optimize the phase shifts of the multiple RIS to minimize power consumption while considering the status of the device. Some works are proposed to conduct activity detection of devices [93]. Therefore, the optimization problem is formulated as

$$\min_{\boldsymbol{T},\boldsymbol{\Phi}} \quad P_{total} \tag{4.19}$$

$$s.t. \quad \sum_{k=1}^{K} \|\mathbf{t}_k\|_2^2 \leq P_{BS}^{th}, \tag{4.19a}$$

$$\sum_{k=1}^{K}\sum_{r=1}^{R} a_k \|\boldsymbol{\Phi}_r \mathbf{G}\mathbf{t}_k\|_2^2 + a_k \delta_v^2 \|\boldsymbol{\Phi}_{\boldsymbol{r}}\|_F^2 \leq P_{RIS}^{th}, \tag{4.19b}$$

$$a_k \in \{0,1\}, k \in \mathscr{K}, \tag{4.19c}$$

$$\phi_n \triangleq \left\{ \exp\left(\frac{j2\pi m}{2^c}\right) \right\}_{m=0}^{m=2^{c-1}}, c \in \mathbb{N}^*, \tag{4.19d}$$

$$P_{cov} \geq P_{cov}^{th}, \tag{4.19e}$$

where P_{BS}^{th} and P_{RIS}^{th} refer to the transmission power threshold at the BS and RIS, respectively. Additionally, (4.19a) and (4.19b) represent the constraints on power consumption at BS and RIS, while (4.19c) corresponds to the status of devices. Eq. (4.19d) defines the phase shifts of elements, where m is the phase shift index, and c represents the phase resolution in bits. Moreover, (4.19e) denotes the constraint on coverage rate.

4.4 Solution to Power Minimization Problem

In this section, we explore power minimization by investigating the association relationship between RIS and the device and optimizing the beamforming vectors at RIS elements.

4.4.1 Coverage-Based Association Strategy Design

We aim to explore the association relationship between multiple RISs and several devices to seek the optimal allocation of reflective elements, resulting in coverage maximization. To resolve the issue, the *Adaptive Hybrid Optimization Strategy* (AHOS), which consists of the *Dynamic Exploration Strategy* (DES) and *Pathfinding Optimization Strategy* (POS), is proposed. The AHOS demonstrates excellent adaptability and reliability in addressing complex problems, offering enhanced robustness, superior global search capability, and faster convergence rates compared to alternative methods. Specifically, DES is leveraged

to seek optimal solutions in the solution space, while the POS optimizes the search path towards the global optimum through the solution space by systematically avoiding previously encountered pitfalls.

Dynamic Exploration Strategy

The strategy facilitates a comprehensive exploration of the solution space by employing a stochastic process akin to metal cooling. In this study, DES is employed to conduct a comprehensive and diverse exploration aimed at identifying the optimal association relationships between RISs and devices. The details of the DES are shown in Algorithm 6. Note that T_0 and T_e are the initial and termination temperatures, respectively. Moreover, L denotes the maximum number of iterations, ν is the cooling parameters, and pop represents the number of solutions in the population.

Algorithm 6 Dynamic Exploration Strategy

1: **Initialization:** T_0, T_e, L, ν, f_{th}.
2: $T \leftarrow T_0$;
3: $s^* \leftarrow$ Initialization a solution;
4: $f(s^*) \leftarrow$ Calculate fitness value of solution s^*;
5: **while** $T < T_e$ && $iter < L$ **do**
6: **if** $f(s^*) \geq f_{th}$ **then**
7: Accept the solution s^*, and then clone, crossover, mutation;
8: **else**
9: Accept the solution s^* according to Eq. (4.20);
10: **end if**
11: Update the population **S**;
12: **for** $i = 1 : pop$ **do**
13: **if** $f(s_i) > f(s^*)$ **then**
14: $s^* \leftarrow s_i, f(s^*) \leftarrow f(s_i)$;
15: **end if**
16: **end for**
17: $T = \nu * T$, $iter = iter + 1$;
18: **end while**
19: **return** the optimal solution and fitness value $s^*, f(s^*)$.

To enhance the quality of the initial solution, we first filter the available RIS collections for each IoT device. The initialization solution encoding (in line 3) is $s^* \triangleq \left[d_1, d_2, \cdots, d_{|k|}\right], k \in \mathscr{K}$, where $d_{|k|}$ is an integer value indicating the RIS associate with the k-th device. The key steps (lines $6-10$) in the Algorithm 6 encourage population diversity to a certain extent. Specifically, we preserve the high-quality solutions while increasing the population

diversity through the clone, crossover, and mutation operations. Moreover, the probability P of accepting the original solution is designed as follows.

$$P = \begin{cases} 1, & f(s_i) \geq f_{th} \\ \exp\left(-\frac{f(s_i)-f_{th}}{T}\right), & f(s_i) < f_{th} \end{cases}, \tag{4.20}$$

where T is the current temperature, and $f(s_i)$ represents the fitness value of the current solution s_i, while f_{th} corresponds to the threshold of the fitness value. The current solution is retained if the fitness value is greater than the threshold f_{th}. Conversely, a random number ρ is generated if $P > \rho$, there is still a probability that the inferior solution may be subjected to crossover and mutation operations and be included in the new population. Furthermore, the probability of accepting an inferior solution diminishes as the temperature T decreases.

Additionally, the temperature update function (line 17) significantly impacts the number of iterations and the algorithm's accuracy. Therefore, an appropriately designed temperature update function can efficiently explore solution space and multiple neighborhoods to achieve a satisfactory solution. In the DES algorithm, a rapid decrease in temperature may cause the algorithm to converge to local optima readily. Conversely, a slow temperature decrease, while increasing the chances of the algorithm to seek the optimal solution, can result in sluggish convergence, leading to excessive search processes. In this paper, the temperature update function is given by

$$T(k+1) = \nu * T(k), \tag{4.21}$$

where ν is the cooling parameter. In this paper, we consider the characteristics of the temperature update function and employ an oscillatory cooling parameter method. This approach involves adjusting factors to maintain the cooling parameters within a reasonable range, thereby ensuring the controlled temperature reduction rate and the search space. The improved cooling parameter is expressed as

$$\nu = \begin{cases} -\tau_1 e^{-\frac{c*i}{L}} \sin|\frac{c*i}{L}\pi| + \omega_1, & i = 0,1,c\ldots,\frac{L}{c} \\ -\tau_2 e^{-\frac{c*i}{L}} \sin|\frac{c*i}{L}\pi| + \omega_2, & i = \frac{L}{c}+1,\frac{L}{c}+2,\cdots,L \end{cases}, \tag{4.22}$$

where L is the total number of iterations in the algorithm, and c denotes the oscillation period. Eq. (4.22) is expressed as the case when c equals 2. Additionally, τ_1 and τ_2 denote the oscillation amplitude, and ω_1 and ω_2 represent the modulation factors.

Pathfinding Optimization Strategy

The strategy explores the solution space that voids revisiting previously traversed or prohibited areas. It highlights the intelligent maneuvering capabilities in finding optimal solutions. The implementation processes are as shown in Algorithm 7. Specifically, the maximum number of iterations L_{max} and the history solution set H are initialized (line 1). The set H ensures that the algorithm avoids revisiting the same local optima within a specified iteration. Once the algorithm reaches the iteration limit, the H releases these solutions, enabling them to re-enter the search process. Throughout iterations, denoted as $iter$, until it reaches a maximum limit L_{max}, neighbors of the solution s^* are conducted, and a new solution s' is selected. Subsequently, an evaluation is made to determine whether s^* is updated and added to H. Finally, the optimal solution and its corresponding fitness value are obtained. Note that the neighborhood function refers to generating the set of solutions from the current solution in various manners, guaranteeing the algorithm's quest for a superior solution while influencing computational efficiency. In this paper, an uncovered device is found, and RIS encoding for the device is generated randomly to construct the neighbors of the solution.

Algorithm 7 Pathfinding Optimization Strategy.

1: **Initialization:** L_{max}, H.
2: **while** $iter < L_{max}$ **do**
3: Construct neighbors of solution s^* using neighborhood function and select a new solution s';
4: **if** $f(s') > f(s^*)$ **then**
5: $s^* \leftarrow s'$;
6: $f(s^*) \leftarrow f(s')$;
7: **else**
8: $s^* \leftarrow$ the suboptimal solution s not present in the H;
9: $f(s^*) \leftarrow f(s)$;
10: **end if**
11: update the H;
12: $iter = iter + 1$;
13: **end while**
14: **return** the optimal solution and fitness value $s^*, f(s^*)$.

Adaptive Hybrid Optimization Strategy

The AHOS method summarizes the coverage rate maximization issue for several IoT devices in multi-RIS-assisted wireless communication systems, where association relationships $\mathbf{\Lambda}$ are optimized by DES and POS methods.

4.4.2 Phase-Based Power Consumption Optimization Design

In the framework of a multi-RIS-assisted wireless communication system, the total power encompasses the consumption by BSs, RISs, and devices. However, this paper specifically investigates the impacts of RIS power consumption on the system while maintaining constant beamforming vectors at BSs. Therefore, the Eq. (4.16) is reformulated as follows.

$$\min_{\mathbf{\Phi}} \quad 1 \tag{4.23}$$

$$s.t. \quad \sum_{k=1}^{K}\sum_{r=1}^{R} a_k \|\mathbf{\Phi}_r \mathbf{G}\mathbf{t}_k\|_2^2 + a_k \delta_v^2 \|\mathbf{\Phi}_{\boldsymbol{r}}\|_F^2 \leq P_{RIS}^{th}, \tag{4.23a}$$

$$\phi_n \triangleq \left\{ \exp\left(\frac{j2\pi m}{2^c}\right) \right\}_{m=0}^{m=2^{c-1}}, c \in \mathbb{N}^*. \tag{4.23b}$$

To further solve the problem, we relax the ϕ_n constraint, the Eq. (4.23) is rewritten as

$$\min_{\mathbf{\Phi}} \quad \sum_{k=1}^{K}\sum_{r=1}^{R} a_k \|\mathbf{\Phi}_r \mathbf{G}\mathbf{t}_k\|_2^2 + a_k \delta_v^2 \|\mathbf{\Phi}_{\boldsymbol{r}}\|_F^2 \tag{4.24}$$

$$s.t. \quad 0 \leq \phi_n \leq 2\pi, n \in N. \tag{4.24a}$$

The optimization techniques, including the interior point method, Newton method, and heuristic algorithms, can easily solve the problem. Notably, the `fmincon` function in MATLAB emerges as a practical tool for this purpose. Note that the phase shifts $\mathbf{\Phi}$ are continuous variables of $[0, 2\pi]$ in Eq. (4.24a). To discretize the solution based on the feasible phase shift solution of Eq. (4.19d), we set $\phi_n = 0$ when the phase shift solution of Eq. (4.24a) lies in the range $\frac{3\pi}{2} \leq \phi_n < 2\pi$ and $0 \leq \phi_n < \frac{\pi}{2}$. Similarly, our proposed algorithm for elements with 2-bit can be extended to phase shift values in any finite state.

4.5 Numerical Experiments

This section performs extensive simulations to validate the effectiveness of the proposed model and algorithm. Specifically, we simulate a large 2D indoor scenario with 200 m $\times$ 200 m, operating at a frequency of 5GHz. In this scenario, multiple RISs are positioned on the facade of obstacles, and a variety of IoT devices and BS are simulated based on the PPP distribution. The symbols used in the simulations are detailed in Table 4.1.

Table 4.1 Symbols and descriptions

Symbol	Value
Antenna of BS N_b	2
Reflective elements N	300
The number of RISs R	20
The number of IoT devices K	30
The number of BSs B	2
The number of obstacles OB	40
Antenna gain of BS G_b	10 dBm
Antenna gain of device G_k	0 dBm
Received power threshold P_{th}^{u}	-90 dBm
Signal range of BS D	100 m
Inverse of energy efficiency of BS ζ_{BS}	1.2
Inverse of energy efficiency of RIS ζ_{RIS}	1.2
Fixed power required at BS $P_{c,BS}$	7 W
Fixed power required at RIS $P_{c,RIS}$	0.072 W
Power consumption of active device $P_{c,k}^{a}$	10 dBm
Power consumption of inactive device $P_{c,k}^{in}$	1 dBm
Coverage rate threshold P_{cov}^{th}	0.75
Ratio of inactive devices ϖ_{in}	0.4

4.5.1 Coverage Rate Performance

Change of cooling parameter

In the simulation, we vary the oscillation period c values to examine the impact of cooling parameters ν on algorithm performance. Specifically, we set the oscillation amplitude as $\tau_1 = 0.3, \tau_2 = 0.5, \tau_3 = \tau_4 = 1$, and the modulation factors are fixed at $\omega_1 = \omega_2 = \omega_3 = \omega_4 = 0.95$ for different c values. Fig. 4.2 illustrates the changes in the cooling parameter ν and the convergence of coverage rate. As depicted in Fig. 4.2 (a), the cooling parameter ν varies between 0.75 and 0.95 for different oscillations c. Additionally, as shown in Fig. 4.2 (b), the algorithm exhibits superior global optimization capabilities and the ability to escape local optima, converging effectively when $c = 4$. Therefore, we adopt the oscillation period of $c = 4$ for subsequent simulations.

Association relationships between RISs and devices

This section investigates five cases to explore the relationship between RISs and IoT devices in a large indoor wireless communication environment with 200 m $\times$ 200 m. In *Case I*, there are 2 BSs, 30 IoT devices, 20 RISs with 300 elements, and 40 obstacles. *Case II* increases

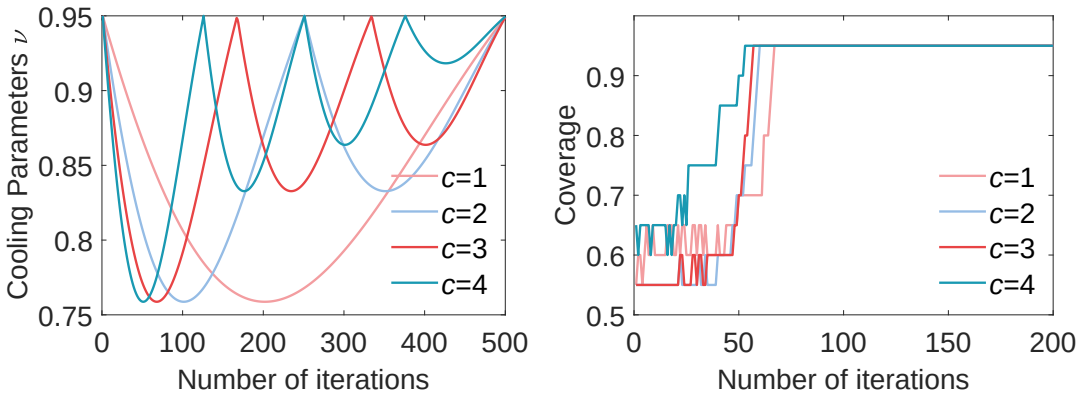

(a) Improved cooling parameter (b) Coverage convergence

Fig. 4.2 Improved cooling parameter ν and coverage convergence of coverage for different oscillation period c.

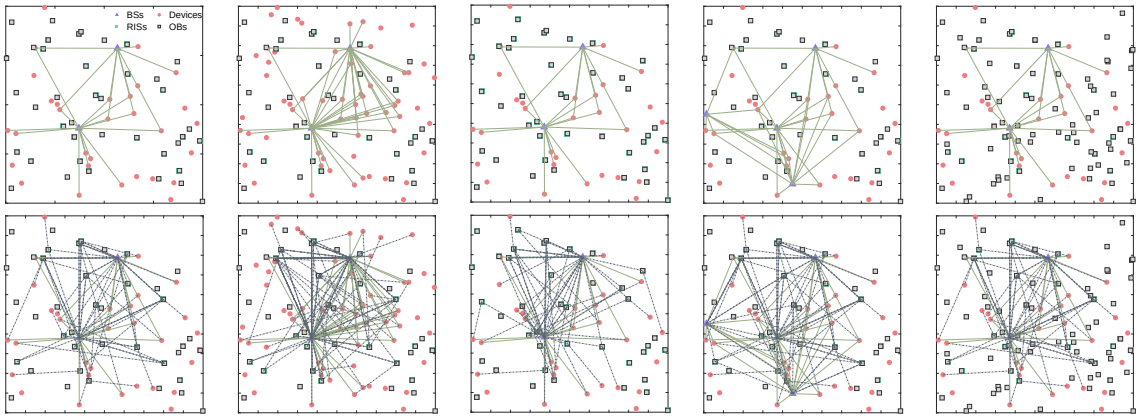

(a) Case I (b) Case II (c) Case III (d) Case IV (e) Case V

Fig. 4.3 The association relationships between RISs and IoT devices for different cases in indoor wireless communication environment with 200 m $\times$ 200 m. (a) Case I: $B = 2, K = 30, R = 20, OB = 40$; (b) Case II: $B = 2, K = 60, R = 20, OB = 40$; (c) Case III: $B = 2, K = 30, R = 40, OB = 40$;(d) Case IV: $B = 4, K = 30, R = 20, OB = 40$; (e) Case V: $B = 2, K = 30, R = 20, OB = 80$.

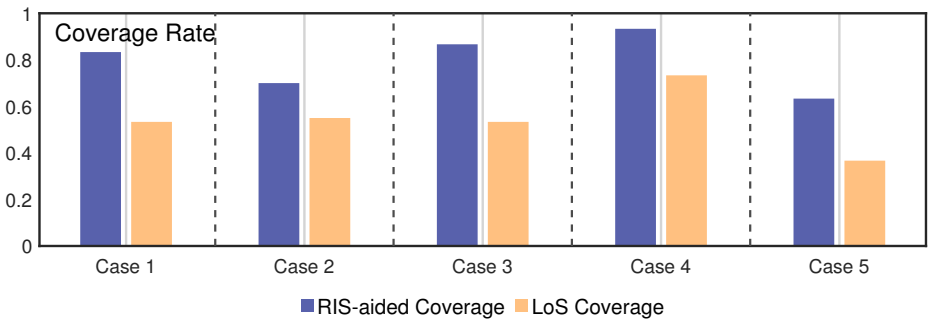

Fig. 4.4 The coverage rate of LoS and RIS-aided for different cases.

the number of devices to 60, *case III* increases the number of RISs to 40, *case IV* increases the number of BSs to 4, and *case V* increases the number of obstacles to 80. To save power consumption, the RIS elements associated with inactive devices are in the *off* state.

Fig. 4.3 displays the relationships between RISs and IoT devices for different cases, where purple triangles represent the BSs, red circles denote the IoT devices, gray squares indicate the obstacles and green squares depict the RISs positioned on the facade of the obstacles. Moreover, solid lines indicate existing LoS links between BSs and IoT devices, while dotted lines represent existing virtual LoS links from BSs to RISs and from RISs to devices. The optimal association relationships, determined by maximizing the coverage rate using the proposed AHOS method, are given in Fig 4.3. It is observed that LoS and virtual LoS links increase with the number of IoT devices and BSs while decreasing with a rise in the number of obstacles. To assess the effectiveness of deploying RISs, we compare LoS coverage with RIS-aided coverage, as shown in Fig. 4.4. It is observed that the coverage rate increases with the number of RISs and BSs and decreases with the number of obstacles and IoT devices. This phenomenon primarily occurs due to the increased presence of BSs and RISs, which aids in establishing more LoS and virtual LoS links, consequently extending coverage to more devices.

4.5.2 Performance evaluation for different deployment strategy

This section aims to explore the performance of various deployment strategies, namely Strategy I with 2 BSs and 20 RISs, Strategy II with 4 BSs and 10 RISs, Strategy III with only 5 BSs, Strategy IV with 5 BSs and 10 RISs, and Strategy V with only 6 BSs. We jointly assess coverage rate and power consumption to determine the most power-efficient deployment strategy.

As illustrated in Fig. 4.5, the coverage rate of different deployment strategies show similar values, there is a significant disparity in power consumption. Specifically, Strategy V exhibits the highest coverage rate of 0.9, followed by Strategy IV with a coverage rate of 0.8667, and the lowest coverage rate is observed in Strategy III with 0.8. Strategy I and Strategy II have a coverage rate of 0.8333. However, Strategy I and Strategy II have the same coverage rate, but Strategy I has the lower power consumption than Strategy II. Conversely, Strategy V experiences the highest power consumption. Therefore, a deployment strategy with an appropriate number of BSs and RISs is critical to achieve a better trade-off between coverage rate and power consumption.

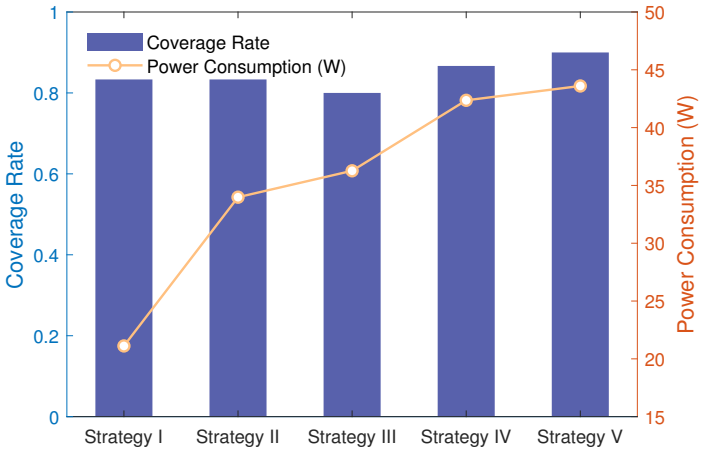

Fig. 4.5 The coverage rate and power consumption for various deployment strategies.

4.5.3 Comparison Algorithms

This section compares the performance of the proposed scheme with several baseline methods.

- *Proposed Method:* This legend depicts the optimization of the association between multiple RIS and several IoT devices and then aims to minimize power consumption. The AHOS method is utilized to determine feasible association relationships, followed by power optimization using the relaxation transformative method.
- *No-RIS:* To verify the potential of deploying multiple RIS in enhancing the coverage rate in the wireless communication network at lower power consumption without RISs.
- *4-RIS:* In the considered multi-RISs multi-devices indoor wireless communication system, deploying more RISs compared to this scheme enhances the coverage rate at the expense of less power consumption.
- *Phase-1:* This legend corresponds to the simplified optimization scheme adopted, whereby deployment phase shifts of RISs are fixed with 1 while satisfying the coverage rate requirement.
- *Random-Association:* In the considered wireless communication system, the association relationships between RISs and IoT devices and phase shifts are not optimized.

Fig. 4.6 depicts the coverage rate and power consumption for varying numbers of RIS elements, with parameters set to $B = 2$, $K = 30$, $R = 20$, $OB = 40$, $\varpi_{in} = 0.4$, and $p_{BS}^{th} = 7$. The schemes *Proposed Method* and *Phase-1* exhibit a gradual increase in coverage rate as the number of elements rises. This phenomenon stems from the increased

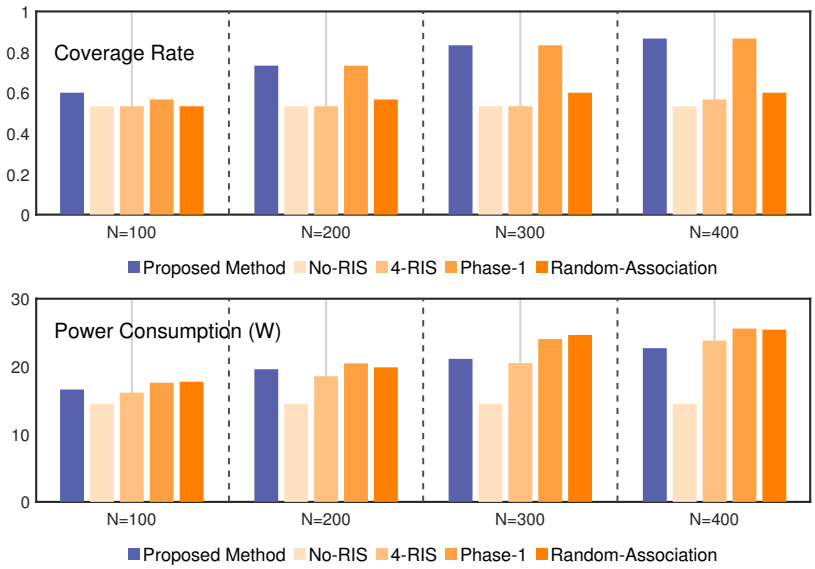

Fig. 4.6 The coverage rate and power consumption *vs.* the number of elements, where $N = 100, N = 200, N = 300$, and $N = 400$, respectively.

allocation of elements to IoT devices, thereby extending the coverage area. Furthermore, the association relationships are optimized to maximize the coverage. The coverage rate for the *Random-Association* scheme marginally increases with the number of elements, while the *No-RIS* and *4-RIS* schemes show negligible changes. Notably, the *Proposed Method* outperforms other simplified schemes in coverage rate. Regarding power consumption, both *Phase-1* and *Random-Association* schemes exhibit an increase with the number of elements. The power consumption for the *No-RIS* scheme remains constant at 14.5 W, while *4-RIS* method shows a slight increase due to the passive characteristic of elements. Therefore, optimizing power consumption is critical when deploying large-scale RISs networks in the environment.

The Fig. 4.7 illustrates the coverage rate and power consumption for different number of devices, where $B = 2$, $R = 20$, $N = 300$, $OB = 40$, $\varpi_{in} = 0.4$, and $p_{BS}^{th} = 7$. It can be observed that all schemes exhibit a similar trend, i.e., the coverage rate decreases as the number of devices increases. This decrease is particularly notable for the *Proposed Method* and *Phase-1* schemes, reaching 1 and 0.628 when the number of devices $K = 10$ and $K = 70$, respectively. This trend occurs because an increased number of devices results in more blind spot areas. Concurrently, power consumption rises with the number of IoT devices. Specifically, the power consumption of the *Phase-1* and *Random-Association* schemes exceeds that of *Proposed Method*, while *No-RIS* exhibits the lowest power consumption, followed by *4-RIS*. Therefore, the *Proposed Method* demonstrates superior coverage rate

and power consumption performance compared to other methods for different numbers of IoT devices.

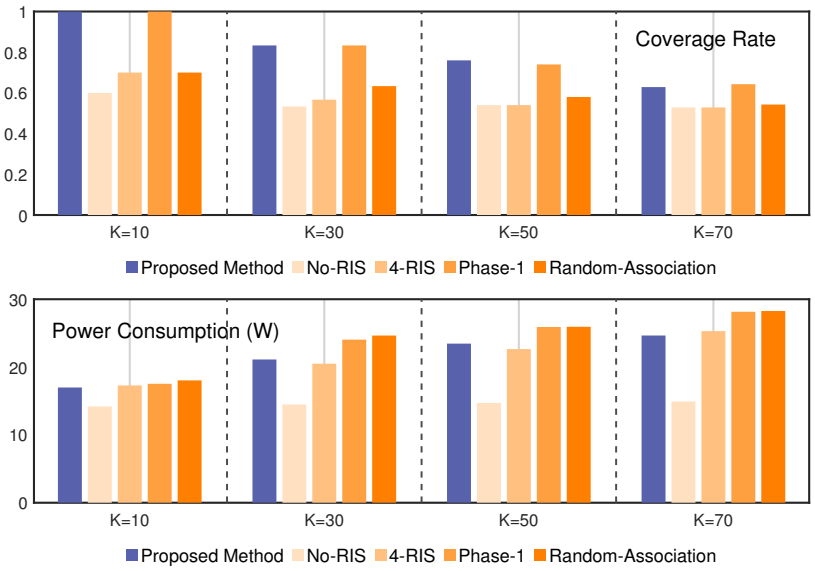

Fig. 4.7 The coverage rate and power consumption *vs.* the number of devices, where $K = 10, K = 30, K = 50$, and $K = 70$, respectively.

Fig. 4.8 displays the coverage rate and power consumption versus the number of obstacles. It is evident that the coverage rate gradually decreases with an increasing number of obstacles. This decline can be attributed to the obstruction of LoS links between BSs and devices by the obstacles. In particular, the positive influence of RIS on coverage is enhanced in areas with dense obstacles (e.g., the number of obstacles equals 80). The *Proposed Method* achieves the highest coverage rate with the lowest possible power consumption. Moreover, the power consumption of all schemes shows little change with the number of obstacles.

Fig. 4.9 plots the coverage rate and power consumption for various numbers of RIS in an indoor wireless communication system. We can observe that increasing the number of RIS enhances the coverage rate for all schemes, with the exception of the *No-RIS* and *4-RIS*. This enhancement is attributed to the increased virtual LoS links between BSs and devices, resulting in expanded coverage. However, it's noteworthy that increasing the number of RIS may not always result in increased coverage in specific environments, owing to the presence of obstacles and locations of BSs. Furthermore, the *Proposed Method* outperforms other schemes on coverage rate. Additionally, the power consumption of all schemes generally increases with the number of RIS, except for the schemes *No-RIS* and *4-RIS*. Overall, the *Proposed Method* achieves a superior balance between coverage rate and power consumption.

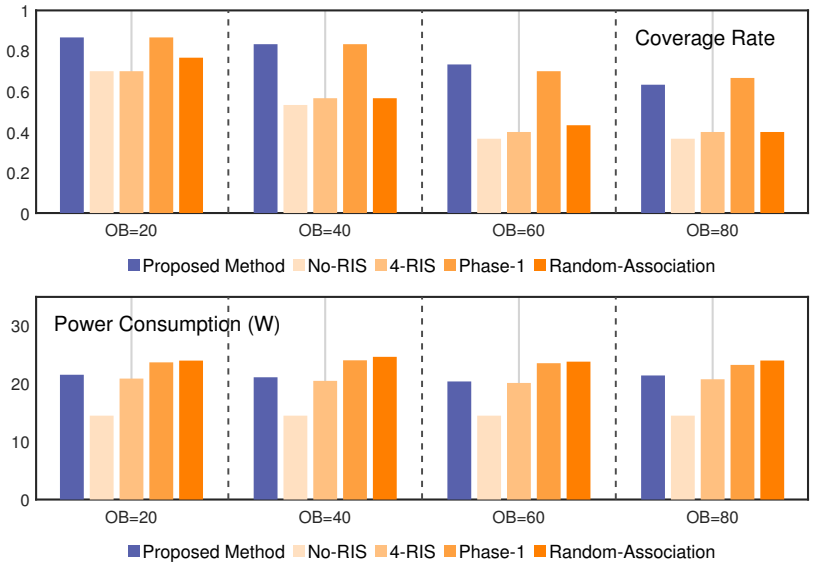

Fig. 4.8 The coverage rate and power consumption *vs.* the number of obstacles, where $OB = 20, OB = 40, OB = 60$, and $OB = 80$, respectively.

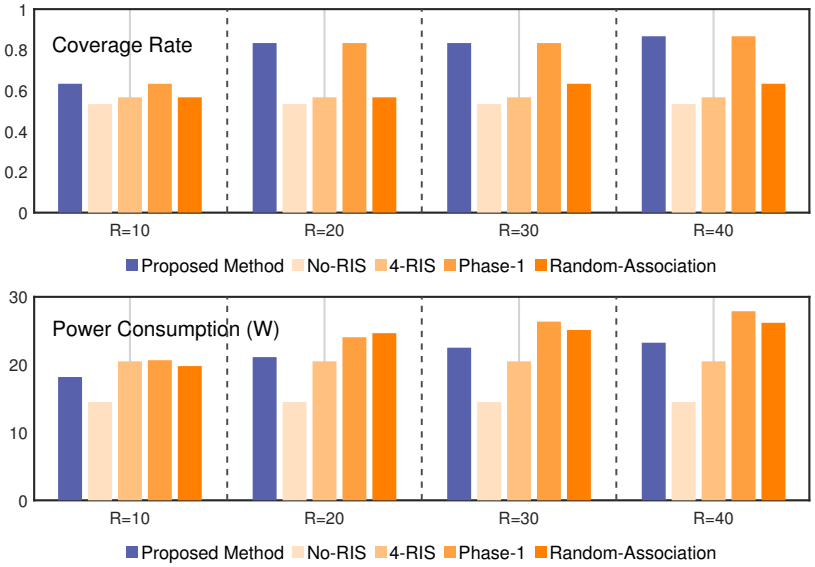

Fig. 4.9 The coverage rate and power consumption *vs.* the number of obstacles, where $R = 10, R = 20, R = 30$, and $R = 40$, respectively.

4.6 Conclusion

In this paper, we discuss an optimization problem of the association strategy between RISs and IoT devices and phase shifts to reduce power consumption while satisfying the coverage rate. The proposed algorithm AHOS is based on a heuristic strategy to maximize the coverage rate, which depends on the association relationships between RISs and devices. The phase shifts are optimized by employing the relaxation transformative method to minimize power consumption. The simulation results also demonstrate that the proposed algorithm can reduce the power consumption of the system while satisfying coverage constraints compared to other schemes.

Chapter 5

QoE Optimization for VR Services in Multi-RIS-Assisted Terahertz Wireless Networks

5.1 Motivation

Virtual reality (VR) is a rapidly evolving technology that holds the potential to reform various industries, including games, entertainment, education, and healthcare. A highly immersive experience enables users to interact with the digital world more naturally and intuitively [65]. However, providing seamless and immersive user experiences presents several challenges, such as ensuring real-time interaction, providing reliable connectivity for mobile VR users, and mitigating dizziness in VR environments [86].

To tackle the challenges associated with VR services, integrating mobile edge computing (MEC) and Terahertz (THz) networks has been identified as a promising solution, enabling a more seamless and natural interaction between the real world and the virtual elements. MEC provides real-time data processing and low-latency communication to enhance the rendering process [87]. Moreover, THz wireless networks offer high bandwidth and data rates, which track hand and body movements more effectively. However, the wireless signal in the THz frequency range is subject to severe attenuation due to factors such as absorption, reflection, and scattering from obstacles. In particular, signal attenuation is even more pronounced when the signal travels through dense or complex environments, such as urban areas or forests. Meanwhile, a similar situation prevails in the indoor environment with complicated obstacles, and line-of-sight (LoS) communication links will be obstructed by walls, furniture, etc. The

LoS link refers to a wireless communication scenario where there is a direct and unobstructed line-of-sight between the AP and VR users.

As two crucial components for enhancing signal quality and coverage, relays and reconfigurable intelligent surfaces (RISs) are employed in THz communication systems to solve wireless signal attenuation caused by obstacles and path loss [100]. However, relays are characterized by high energy consumption, substantial cost, and difficult deployment [27]. On the contrary, RISs offer a more energy-efficient and cost-effective solution for THz wireless networks [8, 58]. RISs possess the capability to control the transmission of electromagnetic waves, exhibiting the promise to remodel the architecture and performance of THz wireless network systems and reduce the Bit Error Rate (BER), which is the number of bit errors occurring in a communication system relative to the total number of bits transmitted. An RIS is a meta-surface composed of multiple electronically controllable reflective elements that can manipulate electromagnetic waves by adjusting their amplitude and phase shift [39]. RIS deployed in wireless networks can establish multiple reliable LoS links by operating phase shifts of elements to provide communications from AP to users located in a blind area [43, 55].

To ensure a high-quality user experience in VR services, addressing interaction delay is crucial, encompassing rendering delay, uplink transmission delay, and downlink transmission delay [106]. Prolonged interaction delay cause dizziness and discomfort for VR users, diminishing the overall QoE. Alleviating the computational burden on head-mounted display (HMD) devices in VR services and enhancing rendering capability, an effective approach is to utilize of high-speed computing units. In this regard, MEC has been recognized as a viable approach to offload resource-intensive VR video tasks from HMD devices to edge servers [51]. Through the mitigation of the computational burden on HMD devices in VR services, MEC can significantly reduce rendering delay and minimize interaction delay, thus delivering a smoother and more immersive user experience in VR [48].

To fill the aforementioned research gaps, this paper aims to optimize the QoE for multiple users in the indoor environment with multi-RIS-assisted THz wireless VR communication systems. To achieve this, the following questions must be solved:

1. How to design and implement the QoE maximization algorithm in a multi-RIS-assisted VR wireless network?

2. How to quantify the QoE from objective and subjective perspectives?

3. How to model the uplink and downlink transmissions channel in multi-RIS-assisted VR Terahertz networks?

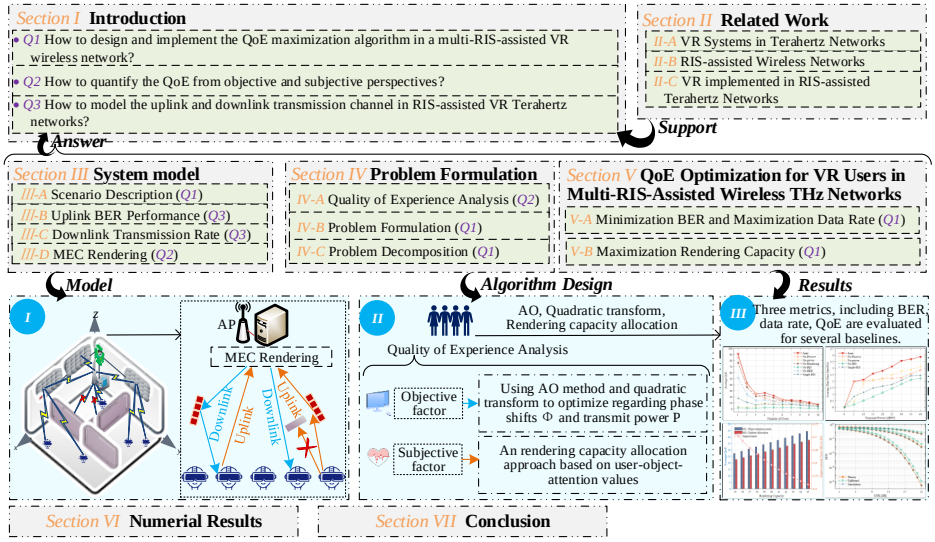

Fig. 5.1 Structure and contributions of this paper. Part I introduces the scenario and system model, which includes uplink BER, downlink transmission rate, and MEC rendering. Part II presents the problem formulation and algorithm design. Part III demonstrates our proposed approach performance versus several simplified schemes regarding average data rate and QoE.

In this paper, our investigation focuses on VR systems in the THz networks, RIS-assisted wireless networks, and VR implemented in RIS-assisted THz networks, as depicted in Fig. 5.1. Furthermore, the integration of VR and RIS is vital for enhancing the VR user experience, given the tremendous potential of both technologies. From the perspective of VR users, achieving optimal objective performance and subjective experience is crucial. To address this, we propose an alternative optimization (AO) algorithm that simultaneously optimizes the phase shifts of reflective elements at the RIS side and the transmission power allocation for users, while considering rendering capability based on user-object-attention values. The primary contributions of this paper can be summarized as follows.

- We propose a multi-RIS-assisted THz wireless network to service multiple VR users in indoor environments. Our proposed network considers several key performances, including uplink BER, rendering capability, downlink data transmission rate, and QoE.
- We focus on maximizing users' QoE in multi-RIS-assisted THz wireless networks by jointly optimizing passive beamforming vectors at the RISs, the transmission power among VR users, and the rendering capability allocation among virtual objects.
- We propose a two-stage optimization workflow: minimization of uplink BER and maximization of downlink data transmission rate in stage-1, and maximization of

rendering capacity in stage-2. The two sub-problems are solved by transforming objective functions into a more tractable form, an AO algorithm, and a rendering capacity allocation algorithm based on user-object-attention values.

- To verify the feasibility of the proposed multi-RIS-assisted THz wireless VR network system, extensive simulations are conducted. The simulation results analyze the impact of crucial parameters, including the number of RIS, reflective elements, the total transmit power, and rendering capability, on the downlink transmission rate, the uplink BER, and QoE.

5.2 Related Work

This section presents a concise overview of the existing literature on VR systems in THz wireless networks, RIS-assisted wireless networks, and VR employed in RIS-assisted wireless THz systems.

1) VR Systems in Wireless THz Networks: In [49, 14, 15, 42, 109, 17], the downlink data transmission rate, delay, and reliability of the XR systems in the wireless THz networks were investigated. In [49], the authors introduced a MEC-assisted wireless VR system, which employed the RNN approach to predict the Field of View (FoV) for each VR user in a real-time manner. Additionally, the rendering data was offloaded from the VR device to the MEC for processing, and the DRL method was employed to optimize the long-term QoE for the VR user. In [14], the delay and reliability of VR services in THz cellular networks were explored, and the end-to-end (E2E) delay expression was derived to demonstrate that VR services achieve higher reliability and data rate by providing high bandwidth and balancing the proximity of the user to the small base station (SBS). In [15], a real-time ruin-aware performance analysis method was proposed to detect the peak age of information (PAoI) in Augmented Reality (AR) over THz networks, overcoming the channel uncertainty. In [42], the concept of PAoI was applied to analyze the downlink data transmission rate in an indoor small-cell THz network, and SBS was modeled as M/M/1 and M/G/1 queues, where the former was responsible for data processing, and the latter was utilized for storing and transmitting data. In [109], the authors proposed a low-latency VR system assisted by UAV-BS, where the VR data was processed either at the UAV-BS or at the users before transmission, and an iterative algorithm with low complexity was introduced to minimize the maximum communication and computation delays for all VR users. In [17], a two-tandem queue method was applied to derive the expression and probability distribution function (PDF) of the E2E delay and reliability in THz networks, which showed that increasing the bandwidth in indoor areas improves the reliability of the VR user's experience. However,

the works mentioned above primarily concentrated on the theoretical investigation of the delay, reliability, and downlink data rate of VR services in THz networks while ignoring the deployment of RIS and the subjective feelings of users.

2) RIS-Assisted Wireless Networks: In [81, 38, 59, 105, 26, 75], the achievable data rate, the BER, and coverage probability of RIS-assisted wireless networks were studied. Specifically, in [81], the impact of RIS-assisted wireless networks on BER was analyzed. In [38], through jointly optimizing the active beamforming vectors at the BS side and the passive beamforming vectors at the single RIS side to maximize the data transmission rate of multiple users in RIS-assisted wireless network systems, and a deep reinforcement learning (DRL) method with standard formulation, low complexity, and robustness was proposed to solve this issue. [59] studied the integration of RIS and MEC for wireless communication networks and jointly optimized the passive beamforming of RIS, downlink transmission power, task offloading from IoT devices to MEC server, the local computing frequency of devices to maximize the total computing bits of the system. In [105] and [26], a double-RIS-assisted MIMO communication system with multiple hops between BS and users was analyzed, where an AO algorithm was proposed to optimize the cooperative passive beamforming to maximize-minimum the data rate. In [75], the challenge of aligning users in real-world millimeter wave environments operating RIS was addressed, and a feasible solution was proposed by deploying multiple distributed RIS to increase the probability of user reflection. And a stochastic geometry-based method was also introduced to further enhance the coverage rate. A novel projected gradient method (PGM) in [69] was presented to optimize the data transmission rate for RIS-assisted MIMO wireless communication systems. However, in [81, 38, 59, 105, 26, 75], the authors mainly concentrated on optimizing the data transmission rate, the uplink BER, the coverage probability by jointly optimizing passive and active beamforming vectors in single-RIS-assisted wireless systems, with little consideration given to multiple RIS deployed in VR scenarios.

3) VR employed in RIS-assisted Wireless THz networks: In [16], a risk-aware framework was proposed to ensure reliability and real-time performance of the system, and the association problem between RIS and VR users was addressed through Lyapunov optimization, which transformed it into a weighted linear function. Additionally, a Recurrent Neural Network (RNN) was proposed to resolve this issue. [50] presented a THz wireless VR network assisted by RIS that aims to optimize the long-term QoE and satisfy the interaction latency requirements. To achieve this, the deep learning (DL) method was employed to predict VR users' viewpoints, positions, and status, while optimizing the phase shifts of reflective elements. However, the authors of [16] and [50] mainly focused on downlink delay

and the association between users and RIS while neglecting the subjective experience of VR users, the uplink BER, and rendering capacity allocation.

5.3 System Model

5.3.1 Scenario Description

Fig. 5.2 illustrates an indoor VR scenario for providing virtual games, meetings, and travel. To satisfy the requirements of low latency and high data rate, we focus on deploying multiple RISs at the wall to assist the indoor wireless communication between one AP and multiple VR users. Specifically, during the downlink transmission, the AP transmits various types of data (graphics, sound, and visual) to the VR device via RISs, enabling immersive visual, auditory, and interactive experiences. During the uplink transmission, the VR device transmits data (position, posture, and abnormal information) to the AP assisted by RISs, providing feedback on user interaction, status, and other relevant information [31]. Each RIS consists of N reflective elements. One AP with M antennas is associated with a rich-resource edge computing server and several single-antenna VR users. An intelligent digital controller connects the RIS for operating phase shifts and communicates with MEC via a wired link. Let $\mathscr{K} = \{1,2,\ldots,K\}$, $\mathscr{L} = \{1,2,\ldots,L\}$, and $\mathscr{N} = \{1,2,\ldots,N\}$ indicate the collections of VR users, RISs, and reflective elements, respectively. The LoS link between the AP and VR user can be established without obstacles. On the contrary, NLoS communications between the AP and the VR user are established by RIS. The NLoS refers to a wireless communication scenario with no direct LoS between the AP and the VR user. Due to the significant attenuation caused by path loss and indoor obstacles in THz wireless networks, only the signal reflected from the RIS for the first time is considered, and multiple signal reflections are ignored [89]. Furthermore, we assume that users are fixed in a 3D space, and the RISs are fixed on the wall. However, it should be noted that the proposed method can also be applied for long-term QoE evaluation.

5.3.2 Uplink BER Performance

In VR services, some user-related data (i.e., location, motion, and sound) are transmitted to edge servers through uplinks. Due to the mobility of VR users and the presence of indoor obstacles, users can be located in either LoS or NLoS areas. LoS and NLoS areas denote regions where communication with the BS is established through LoS and NLoS links, respectively. To ensure the reliability of uplink transmission and the comfort of user experience, we consider two uplink transmission modes: a LoS link and a NLoS link

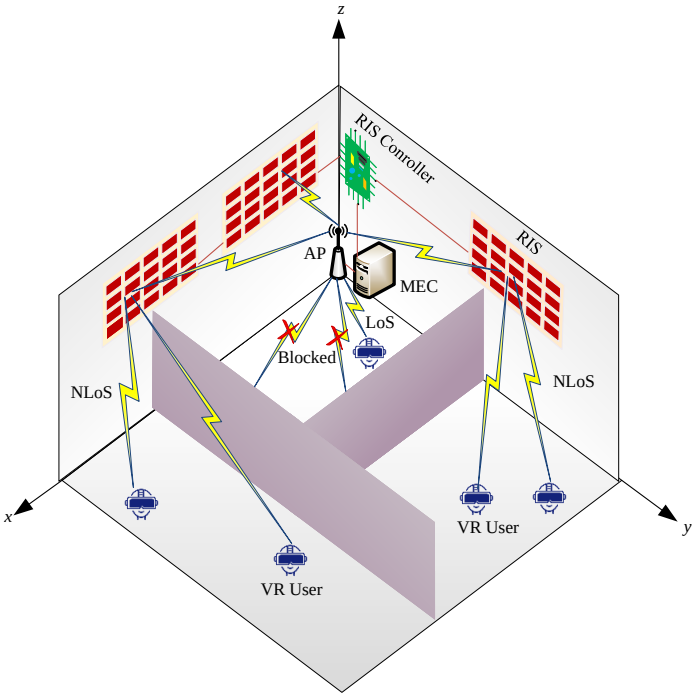

Fig. 5.2 Multi-RIS-assisted THz wireless VR system in the indoor environment.

equipped with RIS. Considering the limited coverage of a single RIS, we deploy multiple RISs to enhance the reliability and stability of the uplink transmission. To account for different signal reception scenarios, VR users in the LoS area receive signals from both LoS and multiple NLoS links. In contrast, users in the NLoS area receive signals solely from the NLoS links. The signal transmitted by the kth user in both uplink modes can be represented as

$$\begin{aligned} y_k^{up} &= \sum_{l=1}^{L} \mathbf{u}_k \left(\mathbf{G}_l^{up} \mathbf{\Phi}_l^{up} \mathbf{H}_{k,l}^{up} + \mathbf{h}_k^{up} \right) x_k^{up} \\ &\quad + \sum_{l=1}^{L} \sum_{i=1, i\neq k}^{K} \mathbf{u}_k \left(\mathbf{G}_l^{up} \mathbf{\Phi}_l^{up} \mathbf{H}_{i,l}^{up} + \mathbf{h}_i^{up} \right) x_i^{up} \\ &\quad + \mathbf{n}_k^{up} \end{aligned} \tag{5.1}$$

where L denotes the number of RIS, and $x_k^{up} \sim \mathscr{CN}(0,1)$ means the transmission data symbol. The channel gain vectors between the AP and the lth RIS, between the lth RIS and the kth VR user, and between the kth VR user and the AP are denoted as $\mathbf{G}_l^{up} \in \mathbb{C}^{M\times N}$, $\mathbf{H}_{k,l}^{up} \in \mathbb{C}^{N\times 1}$, and $\mathbf{h}_k^{up} \in \mathbb{C}^{M\times 1}$, respectively. $\mathbf{u}_k \in \mathbb{C}^{1\times M}$ denotes the beamforming matrix at the kth user, which is equal to $\frac{\mathbf{G}_l^{up} \mathbf{\Phi}_l^{up} \mathbf{H}_{k,l}^{up} + \mathbf{h}_k^{up}}{\left\| \mathbf{G}_l^{up} \mathbf{\Phi}_l^{up} \mathbf{H}_{k,l}^{up} + \mathbf{h}_k^{up} \right\|}$ and satisfies $\mathbb{E}\left[|\mathbf{u}_k|^2 \right] = p_k$. And

$\mathbf{n}_k^{up} \sim \mathscr{CN}(0, N_0)$ means the additive Gaussian white noise, where N_0 is the total noise power, and $\mathbf{\Phi}_l^{up} \triangleq \text{diag}\{\Theta_1^{up}, \Theta_2^{up}, \ldots, \Theta_N^{up}\}, \in \mathbb{C}^{N\times N}$, denotes a diagonal matrix. Here, $\Theta_n^{up} \in \mathscr{C} \triangleq \left\{\exp\left(\frac{j2\pi m}{2^c}\right)\right\}_{m=0}^{m=2^{c-1}}$ represents the set of available phase shift values for the reflective elements, where m is the phase shift index and c denotes the phase resolution in bits [37]. Moreover, $\sum_{l=1}^{L}\sum_{i=1,i\neq k}^{K}\mathbf{u}_k\left(\mathbf{G}_l^{up}\mathbf{\Phi}_l^{up}\mathbf{H}_{i,l}^{up} + \mathbf{h}_i^{up}\right)x_i^{up}$ represents the interference caused by other VR users through both LoS and multiple NLoS transmission.

The Signal-to-Interference-plus-Noise Ratio (SINR) represents the ratio of the desired signal power to the combined interference and noise power, the SINR of kth VR user for the uplink transmission is given by

$$R_k^{up} = \log_2\left|\mathbf{I} + \frac{\sum_{l=1}^{L} p_k\left|\mathbf{u}_k\left(\mathbf{G}_l^{up}\mathbf{\Phi}_l^{up}\mathbf{H}_{k,l}^{up} + \mathbf{h}_k^{up}\right)\right|^2}{\mathbf{I}_k^{up} + N_0\mathbf{I}_M}\right| \tag{5.2}$$

where $\mathbf{I}_M$ is the identity matrix, and

$$\mathbf{I}_k^{up} = \sum_{l=1}^{L}\sum_{i=1,i\neq k}^{K} p_i\left|\mathbf{u}_k\left(\mathbf{G}_l^{up}\mathbf{\Phi}_l^{up}\mathbf{H}_{i,l}^{up} + \mathbf{h}_i^{up}\right)\right|^2 \tag{5.3}$$

The uplink transmission rate of VR users is affected by LoS and multiple NLoS links, as indicated by (5.2). However, in the presence of an obstacle between the VR user and the AP, the uplink communication is solely affected by the NLoS links, resulting in $\mathbf{h}_k^{up}\mathbf{u}_k = 0$. Path loss is a performance indicator for evaluating wireless communication systems assisted by RIS [78]. The path loss is proportional to the distance d_{UR} from the VR user to RIS, the distance d_{RA} from the RIS to the AP, which is denoted as $(d_{UR} + d_{RA})^2$. The path loss from the kth VR user to AP assisted by lth RIS, denoted as P_{loss}^l, can be expressed using the radar distance formula as follows

$$P_{loss}^l = \left(\left(\frac{\lambda}{4\pi}\right)^4 \frac{G_e^i G_e^r}{d_{UR}^2 d_{RA}^2}\omega_p\right)^{-1} \tag{5.4}$$

where the efficiency of the RIS is denoted by ω_p, and λ represents wavelength. G_e^i and G_e^r denote the antenna gain of the RIS in the incident wave direction and the antenna gain of the RIS in the receiving wave direction, respectively. In this paper, RIS consists of multiple passive reflective elements, and ω_p is assumed 1. In the case of slow and flat Rician fading

channels, the baseband signal at the AP is expressed as

$$R_k^{up} = \sqrt{p_k}\left(\sum_{l=1}^{L}\sqrt{P_{loss}^{l}}\left(\sum_{i=1}^{N} h_{l,i}^{UR} e^{j\phi_{l,i}} h_{l,i}^{RA}\right)\right) x_k^{up} + \mathbf{n}_k^{up} \tag{5.5}$$

where $\phi_{l,i}$ represents the phase shifts induced by ith reflective element of lth RIS. The channel are modeled as $h_{l,i}^{UR} = \alpha_{l,i} e^{-j\theta_{l,i}}$ and $h_{l,i}^{RA} = \beta_{l,i} e^{-j\varphi_{l,i}}$, representing the transmission from the VR user to the ith element of the lth RIS, and from ith element of lth RIS to the AP, respectively. Here, $l = 1,2,\ldots,L$ and $i = 1,2,\ldots,N$. Additionally, $\alpha_{l,i}$, $\beta_{l,i}$ denote the channel amplitudes of ith element of lth RIS, while $\theta_{l,i}$ and $\varphi_{l,i}$ represent the channel phase shifts from the VR user to the ith element of lth RIS and from ith element of lth RIS to the AP, respectively. Therefore, (5.5) can be expressed as

$$R_k^{up} = \sqrt{p_k}\left(\sum_{l=1}^{L}\sqrt{P_{loss}^{l}}\left(\sum_{i=1}^{N} \alpha_{l,i}\beta_{l,i} e^{j\Delta\Phi_{l,i}^{up}}\right)\right) x_k^{up} + \mathbf{n}_k^{up} \tag{5.6}$$

where $\Delta\Phi_{l,i}^{up} = \phi_{l,i} - \theta_{l,i} - \varphi_{l,i}$ represents the phase difference term. Therefore, the instantaneous SINR at the AP is expressed as

$$R_k^{up} = \frac{\left|\sum_{l=1}^{L}\sqrt{P_{loss}^{l}}\left(\sum_{i=1}^{N}\alpha_{l,i}\beta_{l,i}e^{j\Delta\Phi_{l,i}^{up}}\right)\right|^2 p_k}{N_0} \tag{5.7}$$

Here, the instantaneous SINR at the AP is maximization with the phase shift satisfying $\Delta\Phi_{1,i}^{up} = \Delta\Phi_{2,i}^{up} = \ldots = \Delta\Phi_{l,i}^{up} = 0, i \in \mathcal{N}$, and the following expression can be derived

$$R_{k,max}^{up} = \frac{\left|\sum_{l=1}^{L}\sqrt{P_{loss}^{l}}\left(\sum_{i=1}^{N}\alpha_{l,i}\beta_{l,i}\right)\right|^2 p_k}{N_0} = \frac{A^2 p_k}{N_0} \tag{5.8}$$

Note that $\alpha_{l,i}$ and $\beta_{l,i}$ are independent of each other, and each follows a Rician distribution. The variable A represents the sum of the variables N, which is assumed to be large enough (i.e., $N \gg 1$) for A to follow a Gaussian distribution with the following mean and variance.

$$E[A] = \frac{\left(\sum_{l=1}^{L} N_l\sqrt{P_{loss}^{l}}\right)\pi}{4(K+1)}\left(L_{1/2}\left(-\frac{K^2}{K+1}\right)\right)^2 \tag{5.9}$$

$$VAR[A] = \left(\sum_{l=1}^{L} N_l P_{loss}^{l}\right)\left(1 - \frac{\pi^2\left(L_{1/2}\left(-\frac{K^2}{K+1}\right)\right)^4}{16(K+1)^2}\right) \tag{5.10}$$

where the Laguerre polynomials of degree 1/2, denoted as $L^2_{1/2}(x)$, N_l represents the number of elements for lth RIS. The Rician factor K is used to calculate the moment generating function (MGF) of $R^{up}_{k,max}$, which follows a non-central chi-square distribution with one degree of freedom. The MGF is expressed in (5.11) as shown at the bottom of the next page. Where s is the moment of the MGF, and we consider the generic BER expression of for binary phase shift keying (BPSK) signaling, the average uplink BER can be obtained as

$$M_{R^{up}_{k,max}}(s) = \frac{\exp\left(\frac{\frac{s\sum_{l=1}^{L} N_l P^l_{loss}\pi^2 L^4_{1/2}\left(-K^2/(K+1)\right)p_k}{16(K+1)^2N_0}}{1-\frac{s\sum_{l=1}^{L} N_l P^l_{loss}\left(16(K+1)^2-\pi^2 L^4_{1/2}\left(-K^2/(K+1)\right)\right)p_k}{8(K+1)^2N_0}}\right)}{\sqrt{1-\frac{s\sum_{l=1}^{L} N_l P^l_{loss}\left(16(K+1)^2-\pi^2 L^4_{1/2}\left(-K^2/(K+1)\right)\right)p_k}{8(K+1)^2N_0}}} \tag{5.11}$$

$$P^k_e = \frac{1}{\pi}\int_0^{\frac{\pi}{2}} M_{R^{up}_{k,max}}\left(-\frac{sin(\frac{\pi}{2})}{sin^2\xi}\right)\mathrm{d}\xi \tag{5.12}$$

It is assumed that each RIS consists of N reflective elements and path loss from the VR user to the AP are approximately equal with P_{loss} (i.e., $P^1_{loss}, P^2_{loss}, \ldots, P^l_{loss} = P_{loss}, l \in \mathscr{L}$), the upper bound for the average BER with BPSK can be expressed as

$$P^k_e \leq \frac{\exp\left(\frac{-\frac{L^2N^2P_{loss}\pi^2L^4_{1/2}\left(-k^2/(K+1)\right)p_k}{16(K+1)^2N_0}}{1+\frac{LNP_{loss}\left(16(K+1)^2-\pi^2L^4_{1/2}\left(-k^2/(K+1)\right)\right)p_k}{8(K+1)^2N_0}}\right)}{2\sqrt{1+\frac{LNP_{loss}\left(16(K+1)^2-\pi^2L^4_{1/2}\left(-k^2/(K+1)\right)\right)p_k}{8(K+1)^2N_0}}} \tag{5.13}$$

The simultaneous transmission for a multiple RIS-assisted wireless system is provided as

$$P_e \propto \exp\left(-\frac{L^2N^2P_{loss}\pi^2L^4_{1/2}\left(-K^2/(K+1)\right)p_k}{16(K+1)^2N_0}\right) \tag{5.14}$$

where LN denotes the total number of reflective elements when the number of RIS equals L. From (5.14), it is not difficult to find that the BER is inversely proportional to L and N, which allows for more flexibility in designing limited indoor wireless communication environments that deploy multiple RIS. In other words, compared to deploying a single RIS in an indoor

environment, multiple RISs can achieve better performance and are more suitable for indoor scenarios.

5.3.3 Downlink Transmission Rate

In an indoor downlink wireless communication environment, VR users receiving data from the AP may be hindered by obstructions or other taller VR users. For VR users blocked by obstacles, the AP transmits data through the NLoS links assisted by RISs, while other VR users receive transmission data directly from the AP through the LoS link. In this paper, let sets $\mathscr{U}_{LoS} = \{u_1^{LoS}, u_2^{LoS}, \ldots, u_p^{LoS}\}$ and $\mathscr{U}_{NLoS} = \{u_1^{NLoS}, u_2^{NLoS}, \ldots, u_q^{NLoS}\}$ denote the VR user collections in LoS area and NLoS area, respectively. The signal received by the qth VR user in the LoS collections can be expressed as follows.

$$\begin{aligned} y_p^{LoS} &= x_p^{LoS}\mathbf{h}_p^d\mathbf{u}_p^{LoS} \\ &\quad + \sum_{i\neq p, i\in\mathscr{U}_{LoS}} x_i^{LoS}\mathbf{h}_p^d\mathbf{u}_i^{LoS} \\ &\quad + \sum_{j\in\mathscr{U}_{NLoS}} x_j^{NLoS}\mathbf{h}_p^d\mathbf{u}_j^{NLoS} + \mathbf{n}_p \end{aligned} \tag{5.15}$$

where $\mathbf{n}_p \sim \mathscr{CN}(0, \delta^2\mathbf{I}_M)$ means the additive Gaussian white noise, the transmission data symbol at the pth user in the LoS collections and the jth user in the NLoS collections are represented by x_p^{LoS} and x_j^{NLoS}, which follows a Gaussian distribution (i.e., $x_p^{LoS}, x_j^{NLoS} \sim \mathscr{CN}(0,1)$). Meanwhile, $\mathbf{h}_p^d \in \mathbb{C}^{1\times M}$ represent the channel gain vectors between AP and the pth VR user. In (5.15), $\mathbf{u}_p^{LoS}$ is equal to $\frac{\mathbf{h}_p^d}{\|\mathbf{h}_p^d\|}$, $\mathbf{u}_p^{LoS}$ and $\mathbf{u}_j^{NLoS} \in \mathbb{C}^{M\times 1}$ are the beamforming matrixes of the pth user in LoS collections and the jth user in NLoS collections, respectively. And $\sum_{i\neq p, i\in\mathscr{U}_{LoS}} x_i^{LoS}\mathbf{h}_p^d\mathbf{u}_i^{LoS}$ and $\sum_{j\in\mathscr{U}_{NLoS}} x_j^{NLoS}\mathbf{h}_p^d\mathbf{u}_j^{NLoS}$ are the interference from the AP. The data transmission rate between AP and the pth user located in LoS collections is given

$$R_p^{LoS} = \log_2\left(1 + \frac{p_p\left|\mathbf{h}_p^d\mathbf{u}_p^{LoS}\right|^2}{\mathbf{I}_p^{LoS} + \delta^2}\right) \tag{5.16}$$

where

$$I_p^{LoS} = \sum_{i\in\mathscr{U}_{LoS}, i\neq p} p_i\left|\mathbf{h}_p^d\mathbf{u}_i^{LoS}\right|^2 + \sum_{j\in\mathscr{U}_{NLoS}} p_j\left|\mathbf{h}_p^d\mathbf{u}_j^{NLoS}\right|^2 \tag{5.17}$$

The received signal in downlink transmission for qth VR user in the NLoS collection is denoted as

$$\begin{aligned} y_q^{NLoS} &= \sum_{l=1}^{L} x_q^{NLoS} \mathbf{H}_{q,l}^d \mathbf{\Phi}_l^d \mathbf{G}_l^d \mathbf{u}_q^{NLoS} \\ &+ \sum_{j\neq q, j\in\mathscr{U}_{NLoS}} \sum_{l=1}^{L} x_j^{NLoS} \mathbf{H}_{q,l}^d \mathbf{\Phi}_l^d \mathbf{G}_l^d \mathbf{u}_j^{NLoS} \\ &+ \mathbf{n}_q \end{aligned} \tag{5.18}$$

where $x_q^{NLoS} \sim \mathscr{CN}(0,1)$ is the transmission data symbol at the qth user in NLoS area, $\mathbf{H}_{q,l}^d \in \mathbb{C}^{1\times N}$ denotes the channel gain between the lth RIS and qth VR user, $\mathbf{G}_l^d \in \mathbb{C}^{N\times M}$ denotes the channel gain between the lth RIS and AP, $\mathbf{u}_q^{NLoS} \in \mathbb{C}^{M\times 1}$ is the beamforming matrix at the qth user, which is equal to $\frac{\mathbf{H}_{q,l}^d \mathbf{\Phi}_l^d \mathbf{G}_l^d}{\left\|\mathbf{H}_{q,l}^d \mathbf{\Phi}_l^d \mathbf{G}_l^d\right\|}$, $\mathbf{n}_q \sim \mathscr{CN}(0, \delta^2 \mathbf{I}_M)$ means the additive Gaussian white noise. And $\mathbf{\Phi}_l^d \triangleq \text{diag}\{\Theta_1^d, \Theta_2^d, \ldots, \Theta_N^d\}, \in \mathbb{C}^{N\times N}$ denotes a diagonal matrix. In addition, $\sum_{j\neq q, j\in\mathscr{U}_{NLoS}} \sum_{l=1}^{L} x_j^{NLoS} \mathbf{H}_{q,l}^d \mathbf{\Phi}_l^d \mathbf{G}_l^d \mathbf{u}_j^{NLoS}$ denotes the interference resulting from the multiple RIS deployment. Then, the downlink transmission rate at the qth user in the NLoS collections can be expressed as follows.

$$R_q^{NLoS} = \log_2 \left(1 + \frac{\sum_{l=1}^{L} p_q \left| \mathbf{H}_{q,l}^d \mathbf{\Phi}_l^d \mathbf{G}_l^d \mathbf{u}_q^{NLoS} \right|^2}{\mathbf{I}_q^{NLoS} + \delta^2} \right) \tag{5.19}$$

where

$$\mathbf{I}_q^{NLoS} = \sum_{i\neq q, i\in\mathscr{U}_{NLoS}} \sum_{l=1}^{L} p_i \left| \mathbf{H}_{q,l}^d \mathbf{\Phi}_l^d \mathbf{G}_l^d \mathbf{u}_i^{NLoS} \right|^2 \tag{5.20}$$

Note that the downlink transmission rate at the kth user can be represented as $R_k^{LoS} + R_k^{NLoS}$ if the VR users are situated in the LoS area. Conversely, in the NLoS area, the downlink transmission rate is denoted by R_k^{NLoS}.

5.3.4 MEC Rendering

3D rendering, the process of generating images using models, plays a considerably significant role in VR scenes. In traditional VR, all viewpoints are rendered at full resolution in the HMD to provide stereoscopic vision for both the left and right eye. However, this approach results in increased workload and additional processing when switching between rendering states [104]. Various approaches have been proposed to tackle this shortcoming, including those based on the Graphics processing unit (GPU) as described in [73]. Nevertheless, the

utilization of new rendering hardware in the HMD devices has resulted in issues related to excessive workload and overheating. One potential solution is to employ remote rendering techniques, as proposed in [60]. Resource-intensive rendering tasks in VR are offloaded to edge servers with rich resources for execution. In this paper, we propose a rendering resource allocation algorithm that leverages user-object-attention values, obtained from the attention-aware dataset [29], to enhance rendering capabilities and optimize computing resources. The process of obtaining the user-object-attention dataset involves image data preprocessing, virtual object segmentation labels, scene grouping, and attention value calculation. We find that users demonstrate varying attention values towards different virtual objects during the VR service experience. Objects that capture higher attention values, indicated by longer eyeball fixation times, are allocated more rendering resources.

5.4 Problem Formulation and Decomposition

5.4.1 Quality of Experience Analysis

In VR services, three meaningful feelings, namely the feeling of presence (i.e., resolution, frame rate, refresh rate), the feeling of interaction (i.e., tracking sensor, operation delay, response time), and the feeling of pleasure (i.e., cybersickness, scenery, sensory mismatch), are key service indicators associated with VR performance. An important insight is that VR services are predominantly user-oriented, prompting the exploration of designing user-centric VR systems [29]. The BER and downlink data rate are objective performance indicators impacting the interaction between virtual elements and the natural world in VR services. Meanwhile, VR users' subjective experience is a considerably important indicator [28]. Therefore, this paper focuses on three key performance indicators to formulate the QoE in VR systems, i.e., the uplink BER P_e^k, the downlink data transmission rate R_k, and the user's subjective experience S_k.

As objective performance indicators, the uplink BER and downlink data transmission rate affect the interaction between the virtual elements and the natural world. Meanwhile, users' subjective experience becomes the primary performance indicator in VR services. Unlike traditional ultra-reliable and low-latency communications (URLLC), the focus shifts to users' subjective perceptions. Therefore, this paper investigates users' subjective perceptions determined by the rendering quality. Let $I_{k,n}^r$ denote the rendering capability of kth user for nth virtual object, and N_{ob} corresponds to the count of virtual objects observed by the user within a single service screen. The subjective feeling of the kth user in the VR service can be represented as a function consisting of $I_{k,n}^r$ and N_{ob}. To effectively reflect the user's

subjective experience within the VR service, the Weber-Fechner Law is employed to deduce the subjective feelings of the user. Thus, the subjective experience of kth user can be formulated as [53]

$$\mathrm{d}S_k = \sum_{n=1}^{N_{ob}} Q_{k,n} \frac{\mathrm{d}I_{k,n}^r}{I_{k,n}^r} \tag{5.21}$$

where $Q_{k,n}$ represents the attention value of kth user for the nth virtual object in the screen, which is a constant determined by the user's subjective feelings and attention mechanism [29]. To solve the (5.21), the subjective service experience of kth user as given

$$S_k = \sum_{n=1}^{N_{ob}} Q_{k,n} \ln\left(\frac{I_{k,n}^r}{I_{th}^r}\right) \tag{5.22}$$

where I_{th}^r is the rendering capacity threshold of kth user for virtual objects. The correlation between the objective network performance indicators and the subjective feeling for kth user can be established as follows.

$$QoE_k = \left(1 - \mathscr{F}_1(P_e^k)\right) \mathscr{F}_2(R_k) S_k \tag{5.23}$$

where $\mathscr{F}_1(\cdot)$ and $\mathscr{F}_2(\cdot)$ denotes the normalization method, which is equal to $\mathscr{F}_1(x) = \frac{x-\bar{x}}{\sqrt{(x-\bar{x})^2/(k-1)}}$ and $\mathscr{F}(x) = \frac{x-x_{\min}}{x_{\max}-x_{\min}}$, respectively. From (5.23), it is evident that higher transmission rates, lower BER, and a comfortable subjective experience lead to an improved QoE for VR users.

5.4.2 Problem Formulation

In this paper, we aim to improve QoE for VR users in RIS-assisted wireless communication THz network. Specifically, the QoE is maximized by jointly optimizing the passive beamforming vectors at uplink/downlink transmission, the transmit power allocation for users, and rendering capacity allocation among all the virtual objects. Therefore, the problem of joint

optimization QoE can be formulated as follows

$$\textbf{(P0)} \max_{\mathbf{P},\mathbf{\Phi},\mathbf{\Phi_1},\mathbf{I}} \quad \sum_{k\in\mathscr{K}} QoE_k \tag{5.24}$$

$$s.t. \quad \mathrm{Tr}\left[\sum_{l=1}^{L}\left(\mathbf{g}_l^{+}\mathbf{P}\left(\mathbf{g}_l^{+}\right)^H\right)\right] \leq P, \tag{5.24a}$$

$$\Theta_n = \left\{1, e^{j2^{1-c}\pi}, \ldots, e^{j2\pi(2^c-1)/2^c}\right\}, c = 1,2,\cdots \tag{5.24b}$$

$$I_{k,n}^r \geq I_{th}^r,\ k \in \mathscr{K}, \tag{5.24c}$$

$$\sum_{k=1}^{K}\sum_{n=1}^{N_{ob}} I_{k,n}^r \leq I_{all}^r, \tag{5.24d}$$

$$T_{up} + T_{render} + T_{down} < T_{th}. \tag{5.24e}$$

where $\mathbf{P},\mathbf{\Phi},\mathbf{\Phi_1}$, and $\mathbf{I}$ refer to the collections of $p_k, e^{j\phi_j^{down}}, e^{j\phi_j^{up}}$, and $I_{k,n}^r$, respectively. Moreover, $\mathbf{P} \triangleq \{p_1, p_2, \ldots, p_k\}^H$ denotes the transmission power allocation for users, $\mathbf{g}_l$ is equal to $\mathbf{H}_l^d\mathbf{\Phi}_l^d\mathbf{G}_l^d + \mathbf{h}^d$, P is the transmission power constraint, and $P > 0$. (5.24a) and (5.24b) denote the constraints of transmission power at the AP and passive beamforming at RISs, respectively. (5.24c), (5.24d), and (5.24e) represent the constraints of rendering capacity, rendering capacity allocation for the virtual object, and interaction latency, respectively. Note that user mobility has little impact on system performance since we can re-optimize the phase shifts, transmission power, rendering capacity allocation, etc., to maximize QoE when the users are in motion.

5.4.3 Problem Decomposition

It is not easy to directly solve the non-convex optimization problem **(P0)** because the transmit power, passive beamforming, the time of rendering, and the time of downlink transmission are coupled. In the VR wireless THz system assisted by RIS, the QoE optimization is divided into two successive stages associated with each other according to constraint (5.24e). Note that the uplink transmission latency is negligible due to smaller data. Thus, the constraint (5.24e) is rewritten as $T_{render} + T_{down} < T_{th}$. In the first stage, the uplink BER and downlink transmission rate are optimized, and the corresponding constraints are (5.24a) and (5.24b). In the second stage, the rendering resource is optimized, and the corresponding constraints are (5.24c) and (5.24d). In contrast to other approaches, our proposed method quantifies the QoE among VR users from objective and subjective perspectives while jointly optimizing multiple variables to enhance the performance of the system. Corresponding to the two stages, the non-convex problem **(P0)** is divided into two sub-problems, namely minimizing

the uplink BER P_e^k while maximizing the data transmission rate R_k in stage-I and maximizing the rendering capability allocation $I_{k,n}^r$ in stage-II.

Problem 1: *Minimization BER and maximization data transmission rate of Stage-I*

$$\textbf{(P1)} \quad \max_{\mathbf{P},\mathbf{\Phi},\mathbf{\Phi_1}} \quad \sum_{k\in\mathscr{K}} \left(1-\mathscr{F}_1\left(P_e^k\right)\right)\mathscr{F}_2\left(R_k\right) \tag{5.25}$$

$$s.t. \quad (5.24a), (5.24b) \tag{5.25a}$$

Problem 2: *Maximization rendering capacity allocation of Stage-II*

$$\textbf{(P2)} \quad \max_{\mathbf{I}} \quad \sum_{k\in\mathscr{K}} S_k \tag{5.26}$$

$$s.t. \quad (5.24c), (5.24d) \tag{5.26a}$$

Note that minimizing P_e^k, that is, maximizing $(1-P_e^k)$ in problem **(P1)**. The two optimization problems are solved in Section V, so that problem **(P0)** is also successfully solved.

5.5 QoE Optimization for VR Users in Multi-RIS-Assisted Wireless THz Networks

5.5.1 Minimization BER and Maximization Data Rate at Stage-I

This section presents an optimization scheme to address the problem **(P1)**. With $\mathscr{F}_2(R_k)$ given in problem **(P1)**, $1-\mathscr{F}_1\left(P_e^k\right)$ is a linear programming problem that can be easily solved, and the solution is omitted here. RIS deployment has a greater impact on downlink transmission than uplink, and optimizing the phase shift $\mathbf{\Phi}_1$ is neglected in the uplink. Therefore, $\mathscr{F}_2(R_k)$ is determined by the coupling of $\mathbf{P}$ and $\mathbf{\Phi}$, and the corresponding constraints are (4.17a) and (4.17b). Thus, we concentrate on solving the following problem.

$$\textbf{(P3)} \quad \max_{\mathbf{P},\mathbf{\Phi}} \sum_{k\in\mathscr{K}} R_k = \sum_{k\in\mathscr{K}} \left(R_k^{LoS}+R_k^{NLoS}\right) \tag{5.27}$$

$$s.t. \quad (4.17a), (4.17b). \tag{5.27a}$$

The problem **(P3)** still is a non-convex, which can be solved by an AO method. In doing so, we assume $\mathbf{\Phi}$ is given and solve $\mathbf{P}$ to optimize the objective function in **(P3)**. Then $\mathbf{P}$ is fixed, find the optimal $\mathbf{\Phi}$ to maximize the data transmission rate. This process is repeated until the objective function is converged. For simplicity, in this paper, the phase resolution in bits c is set to 1 (i.e., the phase shifts are either 0 or π), and the amplitude is equal to 1.

1) Optimization regarding $\mathbf{\Phi}$*:* When transmit power allocation matrix $\mathbf{P}$ is given, the problem **(P3)** is reformulated as

$$\textbf{(P4)} \max_{\mathbf{\Phi}} \quad \log_2\left(1+\frac{\sum_{l=1}^{L}\left|\left(\mathbf{H}_{k,l}\mathbf{\Phi}_l\mathbf{G}_l+\mathbf{h}_k\right)\mathbf{u}_k\right|^2}{\mathbf{I}_k+\delta^2}\right) \tag{5.28}$$

$$s.t. \quad \mathrm{Tr}\left[\sum_{l=1}^{L}\left[\mathbf{g}^{+}\mathbf{P}\left(\mathbf{g}^{+}\right)^H\right]\right]\leq P, \tag{5.28a}$$

$$\phi_n\in\{0,\pi\}, n\in\mathscr{N}. \tag{5.28b}$$

where ϕ_n denotes the phase shifts of reflective elements. Furthermore, we have assumed that the phase shift bits for RIS elements c is equal to 1, i.e., $\mathbf{\Phi}=\{1,-1\}$, and $\phi_n\in\{0,\pi\}$. To solve the problem **(P4)**, we relax the constraint on phase shifts ϕ_n and implement a quadratic transform [74]. Then, **(P4)** can be reformulated as

$$\textbf{(P5)} \max_{\mathbf{\Phi},\mathbf{y_1}} \quad f_1(\mathbf{\Phi},\boldsymbol{y}_1) \tag{5.29}$$

$$s.t. \quad \text{(5.28a), (5.28b).} \tag{5.29a}$$

$$y_{1,k}\in\mathbb{R}, k\in\mathscr{K}. \tag{5.29b}$$

where variable $\mathbf{y_1}$ is an auxiliary vector with $y_{1,k}$. The new objective function $f_1(\mathbf{\Phi},\boldsymbol{y}_1)$ can be given by

$$\begin{aligned} f_1(\mathbf{\Phi},\boldsymbol{y}_1)=&\sum_k\log_2\left(1+2Re\left\{y_{1,k}^H A_{m,k}\right\}\right.\\ &\left.-y_{1,k}^H\left(\delta^2\mathbf{I}+\sum_{k_1\neq k}\left(A_{m,k_1}{A_{m,k_1}}^H\right)\right)y_{1,k}\right) \end{aligned} \tag{5.30}$$

where

$$A_{m,k}=\mathbf{H}_{ml}\mathbf{\Phi}_l\mathbf{G}_{lk}+\mathbf{h}_{mk} \tag{5.31}$$

The problem **(P5)** is convex when the auxiliary vector $\mathbf{y_1}$ is given. The optimal $y_{1,k}$ for fixed $\mathbf{\Phi}$ is given

$$y_{1,k}^*=\left(\delta^2\mathbf{I}+\sum_{k_1\neq k}A_{m,k_1}{A_{m,k_1}}^H\right)^{-1}A_{m,k} \tag{5.32}$$

Then, it is found that optimizing $\mathbf{\Phi}$ for given $\mathbf{y_1}$ is a convex problem, which can be resolved by convex optimization solvers. As shown in Algorithm 8, the phase shifts of all reflective elements are obtained through continuous iterative optimization. Note that ϕ_n will be generated at interval $[0,2\pi]$. However, the feasible solutions of constraint (5.29a) are discrete

sets before relaxation. To discretize the solution according to the phase shift feasible solution of (5.28b) in **(P4)**, we set $\phi_n = 0$ for problem **(P4)** when the phase shift solution of **(P5)** is $\frac{3\pi}{2} \leq \phi_n < 2\pi$ and $0 \leq \phi_n < \frac{\pi}{2}$. In similarity, the solution for problem **(P4)** is set to $\phi_n = \pi$ when the solution for **(P5)** is $\frac{\pi}{2} \leq \phi_n < \frac{3\pi}{2}$. In the same way, our proposed algorithm for elements with 2-bit can be generalized to the phase shift values in any finite state.

Algorithm 8 Fractional Problem for Phase Shifts Optimization.

1: **Initialization: $\mathbf{\Phi}$**
2: **while** the function f_1 in (5.30) not converged **do**
3: Update $\mathbf{y_1}$ according to (5.32).
4: Update $\mathbf{\Phi}$ in (5.29) for given $\mathbf{y_1}$.
5: **end while**

2) Optimization regarding $\mathbf{P}$*:* With phase shift values $\mathbf{\Phi}$ given, the problem **(P3)** is reformulated as (5.33), shown at the bottom of next page.

$$\textbf{(P6)} \quad \max_{\mathbf{P}} \quad \sum_{k\in\mathscr{K}} \mathscr{F}(R_k) = \sum_{k\in\mathscr{K}} \left(R_k^{LoS} + R_k^{NLoS}\right)$$
$$= \sum_{k\in\mathscr{K}} \log_2\left(1 + \frac{p_k \left|\mathbf{h}_k^{LoS}\mathbf{u}_k^{LoS}\right|^2}{\mathbf{I}_k^{LoS} + \delta^2}\right) + \log_2\left(1 + \frac{\sum_{l=1}^{L} p_k \left|\mathbf{H}_{k,l}\mathbf{\Phi}_l\mathbf{G}_l\mathbf{u}_k^{NLoS}\right|^2}{\mathbf{I}_k^{NLoS} + \delta^2}\right) \tag{5.33}$$

$$s.t. \quad \text{(5.28a)}. \tag{5.33a}$$

From (5.33), it is not difficult to find that the transmission mode differs for VR users located in different locations. In this paper, the problem **(P6)** is maximized, i.e., $R_k^{NLoS} + R_k^{LoS}$ is maximized when the users are located in the LoS area. Otherwise, R_k^{NLoS} is optimized. In addition, **(P6)** is composed of fractional forms of SINR, and each term has a logarithmic function, which is non-decreasing and concave. Therefore, **(P6)** is concave-convex fractional programming problems, i.e., the numerator, denominator, and constraint of the fraction are concave function, convex function, and convex sets. To address this, we apply a quadratic transform [74] to a concave-convex problem and reformulate the problem as

$$\textbf{(P7)} \quad \min_{\mathbf{P},\mathbf{y_2}} \quad f_2(\mathbf{P},\mathbf{y_2}) \tag{5.34}$$

$$s.t. \quad 0 \leq p_k \leq P, \tag{5.34a}$$

$$y_{2,k} \in \mathbb{R}, k \in \mathscr{K}. \tag{5.34b}$$

where $\mathbf{y_2}$ is the set of $y_{2,k}, k \in \mathscr{K}$. The new objective $f_2(\mathbf{P}, \mathbf{y_2})$ can be expressed as

$$f_2(\mathbf{P}, \mathbf{y_2}) = \sum_{k \in \mathscr{K}} \log_2 \left(1 + 2y_{2,k} \sqrt{\sum_{l=1}^{L} \left| A_{k,l} \mathbf{u}_k \right|^2 p_k} - y_{2,k}^2 \left(\sum_{l=1}^{L} \sum_{j \neq k} \left| A_{k,l} \mathbf{u}_j \right|^2 p_j + \delta^2 \right) \right) \tag{5.35}$$

where

$$A_{k,l} = \mathbf{H}_{k,l} \mathbf{\Phi}_l \mathbf{G}_l + \mathbf{h}_k \tag{5.36}$$

Note that $\mathbf{h}_k \mathbf{u}_k$ equals 0 when the user is located in the NLoS area. According to Algorithm 9, p_k and $y_{2,k}$ are optimized iteratively in an alternative manner. With p_k given, the optimal $y_{2,k}$ is calculated as

$$y_{2,k}^* = \frac{\sqrt{\sum_{l=1}^{L} \left| \left(\mathbf{H}_{k,l} \mathbf{\Phi}_l \mathbf{G}_l + \mathbf{h}_k \right) \mathbf{u}_k \right|^2 p_k}}{\sum_{l=1}^{L} \sum_{j \neq k} \left| \left(\mathbf{H}_{k,l} \mathbf{\Phi}_l \mathbf{G}_l + \mathbf{h}_j \right) \mathbf{u}_j \right|^2 p_j + \delta^2} \tag{5.37}$$

Then, it is observed that optimizing p_k for given $y_{2,k}$ is a convex problem, which can be resolved by convex optimization solvers. As shown in Algorithm 9, where K denotes the number of users and P is equal to $\frac{P}{K} \mathbf{I}_K$. The function finally achieves convergence through continuous iterative optimization, and the transmission power allocation is obtained.

Algorithm 9 Fractional Problem for Power Allocation.

Input:
$P, K, \mathbf{\Phi}$
Output:
$\mathbf{P}_t^*$
Initialization: $\mathbf{P} = \frac{P}{K} \mathbf{I}_K, \mathbf{y}_{2,t} = \mathbf{0}_K, \varepsilon > 0$
for $t = 1, 2, \ldots$ **do**
  $\mathbf{P}_t^* = \arg\max f(\mathbf{P}_t, \mathbf{y}_{2,t-1})$.
  Update $y_{2,t}^*$ according to (5.37).
  if $\| f\left(\mathbf{P}_t^*, \mathbf{y}_{2,t}^*\right) - f\left(\mathbf{P}_{t-1}^*, \mathbf{y}_{2,t-1}^*\right) \| < \varepsilon$ **then**
    return $\mathbf{P}_t^*$.
  end if
end for

3) Optimization sum rate algorithm: Algorithm 10 summarizes the sum rate maximization algorithm for VR users in a multi-RIS-assisted THz network, where the bits of the reflective element is set to 1. $\mathbf{P}$ and $\mathbf{\Phi}$ are alternately optimized until convergence, as discussed above.

Algorithm 10 Sum rate maximization for elements with 1-bit.

Input:
$P, \delta^2, \mathbf{H}, \mathbf{G}, \mathbf{h}, \mathbf{\Phi}$
Output:
$\mathbf{\Phi}$ and $\mathbf{P}$
Initialization: $\mathbf{P}_0 = \frac{P}{K}\mathbf{I}_K, \mathbf{\Phi}_0 = \mathbf{0}_K, and\ \varepsilon > 0.$
for $t = 1, 2, \ldots$ **do**
  Find $\mathbf{\Phi}_t$ solving problem **(P5)** for the fixed $\mathbf{P}_{t-1}$.
  if (5.28a) holds true for $\mathbf{\Phi}_t$ **then**
    Find $\mathbf{P}_t$ solving problem **(P6)** using algorithm 9 for the fixed $\mathbf{\Phi}_t$.
  else
    break and unfeasibility.
  end if
  if $\|\mathbf{\Phi}_t - \mathbf{\Phi}_{t-1}\|^2 < \varepsilon$ and $\|\mathbf{P}_t - \mathbf{P}_{t-1}\|^2 < \varepsilon$ **then**
    return $\mathbf{\Phi}_t$ and $\mathbf{P}_t$
  end if
end for

5.5.2 Maximization Rendering Capacity Allocation at Stage-II

In this section, a rendering capacity allocation scheme is proposed to improve the subjective experience of VR users. The problem **(P2)** is convex, and the Lagrangian method is employed. The optimal rendering capacity allocation of kth user can be denoted as

$$I_{k,n}^{r\,*} = \max\left\{ Q_{k,n}\frac{1}{\kappa^*}, I_{th}^r \right\} \tag{5.38}$$

where κ^* can be obtained from the following formula

$$I_k^r = \sum_{n=1}^{N_{ob}} \max\left\{ Q_{k,n}\frac{1}{\kappa^*}, I_{th}^r \right\} \tag{5.39}$$

Note that the subjective experience is optimized based on user-object-attention values, which reflect the user's attention to objects in virtual scenes (e.g., virtual conferences and games). If the user pays attention to a specific virtual object, i.e., longer gaze time according to eye tracking data, the $Q_{k,n}$ value is higher, and vice versa. Algorithm 11 presents the rendering

capacity allocation scheme derived from the analysis of user-object-attention values. So far, problems **(P1)** and **(P2)** have been successfully solved, leading to the optimization of problem **(P0)**.

Algorithm 11 Rendering capacity allocation with user-object-attention values.

Input:
$I^r_{all}, I^r_{th}, \mathbf{Q} = \{Q_{k,1}, Q_{k,2}, \ldots, Q_{k,N_{ob}}\}$
Output:
$\mathbf{I}^r = \{I^{r\,*}_{k,1}, I^{r\,*}_{k,2}, \ldots, I^{r\,*}_{k,N_{ob}}\}$
Initialization: $j = 1, s_1 = [\,], s_2 = [\,], s_3 = [\,]$, and $I^{r\,*}_{k,n} = Q_{k,n}\frac{1}{\kappa^*}$.
Calculate $\kappa^* = \sum_{n=1}^{N_{ob}} Q_{k,n}/I^r_{all}$, $I^{r\,*}_{k,n} = Q_{k,n}/\kappa^*$ for $\forall n$.
while the minimum of $I^{r\,*}_{k,n} < I^r_{th}$ **do**
  $s_1[j] \leftarrow$ the minimum of $I^{r\,*}_{k,n}$.
  $s_2[j] \leftarrow$ the user-object-attention values corresponding to $s_1[j]$.
  $s_3[j] \leftarrow$ the index corresponding to $s_1[j]$.
  Update $\kappa^* = \sum_{n=1}^{N_{ob}} \left(Q_{k,n} - \sum s_2\right) / \left(I^r_{all} - j \times I^r_{th}\right)$.
  Update $I^{r\,*}_{k,n} = Q_{k,n}/\kappa^*$ for $\forall n$.
  for temp = 1 : j **do**
    $n \leftarrow s_3[temp]_{th}$, $I^{r\,*}_{k,n} = I^r_{th}$.
  end for
  $j = j + 1$.
end while
return the optimal rendering capacity allocation scheme $I^{r\,*}_{k,1}, I^{r\,*}_{k,2}, \ldots, I^{r\,*}_{k,N_{ob}}$.

5.6 Simulation Results

In the multi-RIS-assisted THz wireless VR system considered for indoor scenarios, the QoE performance metrics for multiple users are characterized by the downlink data rate, uplink BER, and rendering capability. Therefore, in this section, we present simulation results that investigate the impact of various system parameters on the QoE performance metrics, including the number of RIS L, the number of reflective elements N, the total transmit power P, the number of VR users K, and the rendering capability $\mathbf{Q}$. To provide a comprehensive evaluation, we compare it with several simplified optimization schemes in addition to the proposed `Joint` optimization method that simultaneously optimizes various parameters.

- `Joint:` This legend depicted the multi-user QoE optimization scheme for the proposed multi-RIS-assisted THz wireless VR system, in which the passive beamforming vectors at the RIS side, the uplink BER, the transmission power allocation for users and the

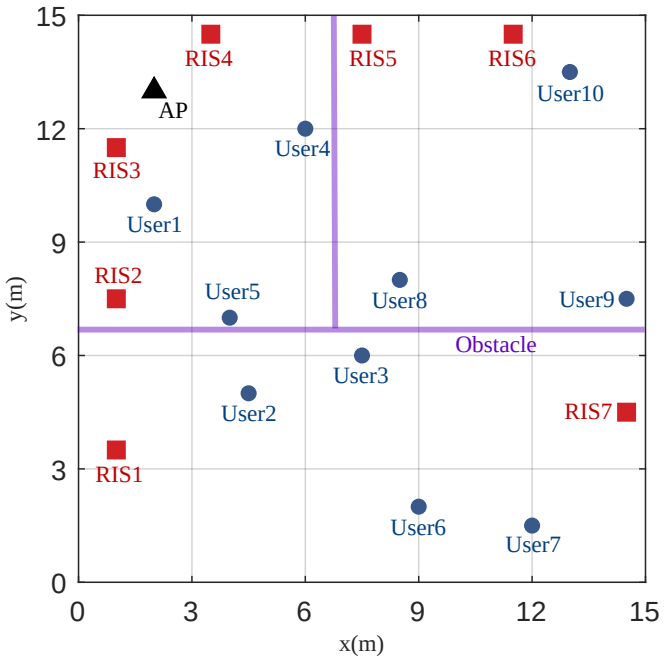

Fig. 5.3 A top view of considered multi-RIS-assisted wireless VR system.

rendering capability allocation for virtual objects are jointly optimized, as described in Section V.

- *No-Passive:* This legend corresponds to the simplified optimization scheme adopted in the multi-RIS-assisted THz wireless VR system, whereby the passive beamforming at the RIS is randomly generated and left unoptimized, while other parameters, such as the uplink BER, power allocation, and rendering capability are jointly optimized.
- *No-power:* In the considered multi-RIS-assisted THz wireless VR system, the transmission power among users is uniformly distributed without optimization, and other parameters are jointly optimized.
- *No-Rendering:* In the considered multi-RIS-assisted THz wireless VR system, the rendering capability allocation among users is uniformly distributed without taking into account user-object-attention values, while other variables are jointly optimized.
- *No-RIS:* To verify the potential of deploying RIS in enhancing the transmission data rate and reducing the BER in the THz wireless VR network, a simplified optimization algorithm is designed. Furthermore, other variables are jointly optimized while ignoring RIS deployment.

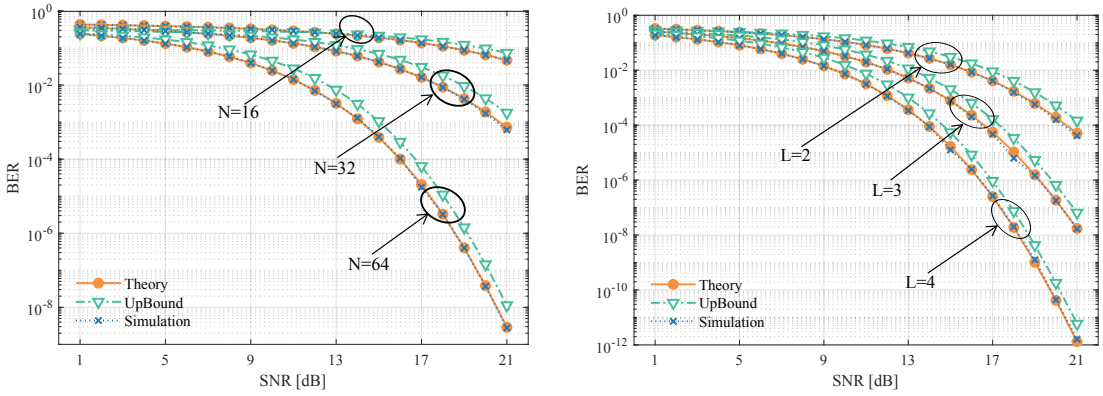

(a) Single RIS (b) Multiple RIS

Fig. 5.4 BER performance of single/multiple RIS-assisted THz wireless VR network. (a) Case of a single RIS with different reflective elements. (b) Case of multiple RIS with same reflective elements $N = 20$.

- *No-BER:* This legend signifies that the optimization of BER is not considered, while the remaining variables are jointly optimized.
- *Single-RIS:* This legend is designed to compare the performance of multi-RIS and single-RIS in the THz wireless VR system. The scheme includes a single RIS with 32 reflective elements, which is the only difference from the *Joint* optimization scheme.

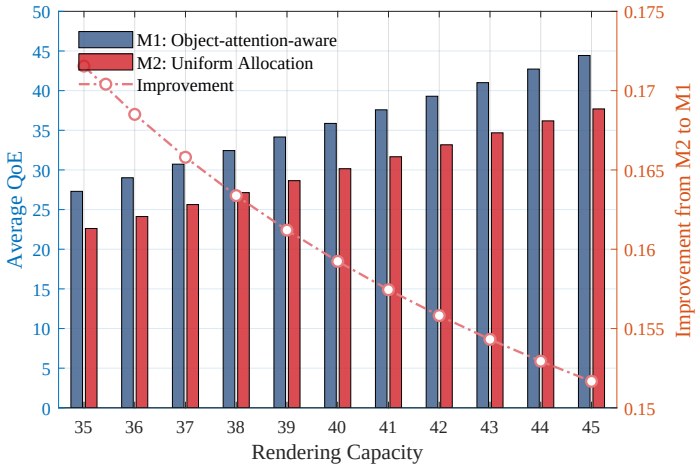

Fig. 5.5 The effect of rendering capacity on the average QoE in the considered multi-RIS-assisted THz wireless VR system.

Unless otherwise noted, the simulation settings are as follows. The user-object-attention data obtained from [29] comprises 1,000 images, encompassing 96 distinct types of objects, with attention values provided by 30 users for each object. For our analysis, we randomly

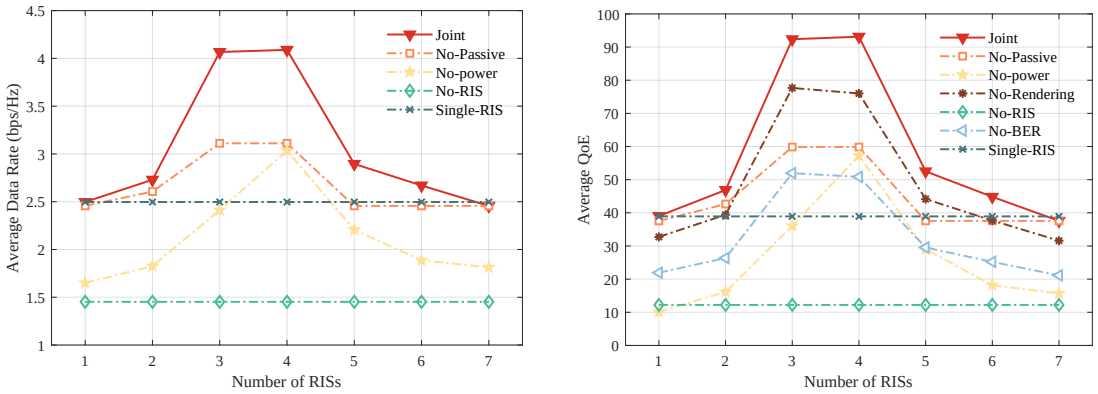

(a) Downlink data rate

(b) Average QoE

Fig. 5.6 The effect of the number of RIS on the downlink data rate from AP to the users and the average QoE among VR users in the considered multi-RIS-assisted THz wireless VR system.

select 10 VR users. Additionally, considering the real-world context, we simulate an indoor office scene with 15m$\times$15m$\times$3m, where the number of VR users $K = 10$, the number of RIS $L = 7$, the reflective elements $N = 32$ and one AP, the top view is shown in Fig. 3. Given the confined nature of the indoor environment, we simulate the AP with 2 antennas ($N_a = 2$) and each RIS with an identical set of reflective elements ($N = 32$). Meanwhile, $\mathscr{U}_{LoS} = \{u_1, u_4, u_6\}$ and $\mathscr{U}_{NLoS} = \{u_2, u_3, u_5, u_7, u_8, u_9, u_{10}\}$ present the VR users located in LoS area and NLoS area due to obstacles, respectively. The total transmit power of AP P is 43dbm, and the white Gaussian noise is equal to -105dbm.

Firstly, we evaluate the effectiveness of RIS in reducing the uplink BER for indoor THz wireless VR systems, where BPSK is employed. Fig. 5.4 shows that all cases exhibit the same trend, whereby BER performance decreases with increasing SNR. Specifically, Fig. 5.4(a) displays a decrease in BER as the number of reflective elements goes up for the case of single RIS with varying reflective elements (i.e., $N = 16, N = 32$, and $N = 64$). Moreover, Fig. 5.4(b) indicates a monotonic decrease in BER as the number of RIS rises for the case of multiple RISs with the same number of elements (i.e., with $N = 20$ given, $L = 2, L = 3$, and $L = 4$).

Fig. 5.5 plots how the average QoE varies with the rendering capacity for two different allocation schemes. Notably, the scheme based on user-object-attention values is superior to the uniform allocation scheme, and the former exhibits a more significant improvement in QoE than the latter scheme as rendering capacity decreases. This observation highlights that an optimization algorithm based on user-object-attention values can enhance the user experience in VR services.

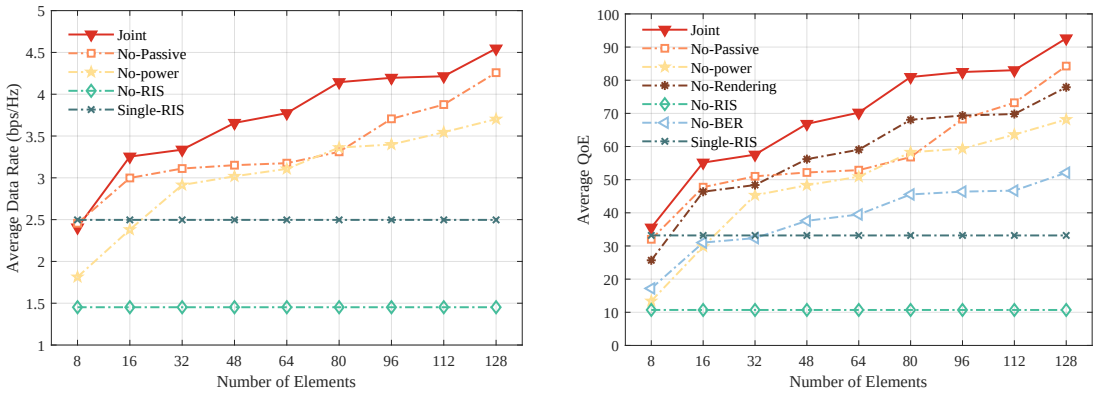

(a) Downlink data rate (b) Average QoE

Fig. 5.7 The effect of the number of reflecting elements on the downlink data rate from AP to the users and the average QoE among VR users in the considered multi-RIS-assisted THz wireless VR system.

Fig. 5.6 depicts the influence of the number of RIS on the downlink data rate from the AP to the users and the average QoE experienced by VR users. From Fig. 5.6(a) and Fig. 5.6(b), it is not difficult to find that the optimization schemes, except for the *No-RIS* and *Single-RIS* schemes, exhibit superior performance when the number of RIS is either 3 or 4. This is due to the fact that an increased number of RISs generate multiple channels, resulting in higher interference between the AP and VR users. This phenomenon indicates that an appropriate number of RIS distributed in an indoor environment can effectively enhance the downlink data rate and the QoE for VR users. Furthermore, it can be observed that the proposed optimization method, *Joint*, achieves the highest downlink data rate from the AP to the VR users and average QoE. This result highlights that joint optimization of the passive beamforming vectors at the RIS, uplink BER, transmission power, and rendering capacity is superior to simplified optimization schemes.

Fig. 5.7 shows how the downlink data transmission rate from the AP to the VR users and the average QoE depend on the number of reflective elements. In Fig. 5.7, the reflective element number N is not constrained to a power of 2, as doing so can result in an excessively large number of elements. For example, setting the reflecting element number $N = 2^{10}$ leads to $N = 1024$, significantly increasing the algorithm's computational complexity. According to Fig. 5.7(a) and Fig. 5.7(b), it is found that the downlink data rate and average QoE go up with an increase in the number of reflective elements for all schemes, except for *No-RIS* and *Single-RIS* cases. Nevertheless, the performance of *No-RIS* and *Single-RIS* schemes remain unchanged as the number of elements goes up, since the former does not incorporate reflective elements, and the latter has a fixed number of reflective elements. This finding indicates that an increase in the number of reflective elements can effectively enhance the

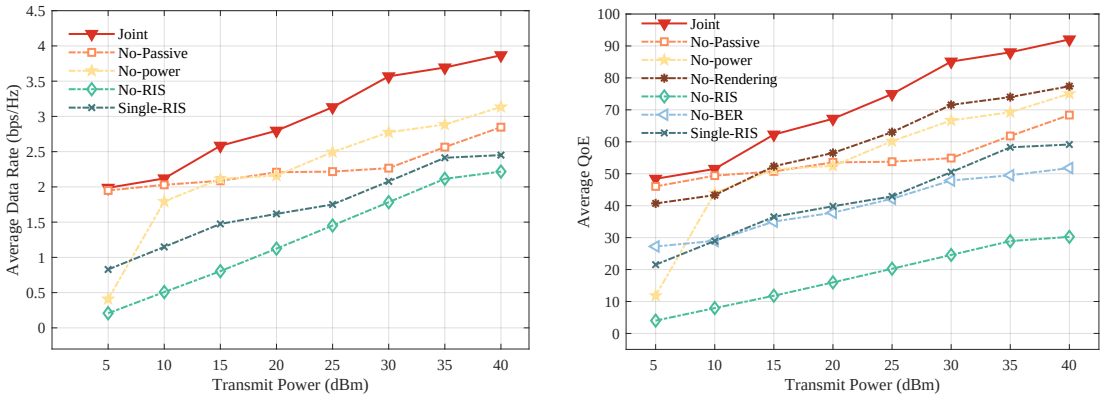

(a) Downlink data rate (b) Average QoE

Fig. 5.8 The effect of the total transmit power on the downlink data rate from AP to the users and the average QoE among VR users in the considered multiple RIS-assisted THz wireless VR system.

system's performance. Furthermore, the *Joint* scheme outperforms the *No-Passive* and *No-Power* schemes in terms of downlink data rate and average QoE, regardless of whether the number of elements is set to 8 or 128. It is noteworthy that when the number of elements is less than 16 (i.e., $N \leq 16$), the *No-Power* scheme performs worse than the *Single-RIS* case. This observation emphasizes the importance of optimizing transmit power to achieve optimal system performance.

Fig. 5.8 illustrates how the total transmit power at the AP affects the downlink data transmission rate from the AP to the users and the average QoE among VR users in a multi-RIS-assisted wireless VR system. Fig. 5.8 shows that increasing the total transmission power contributes to enhancing the downlink data rate from the AP to users and the average QoE for all schemes. This improvement is attributed to the increased signal power received by VR users, resulting in better reception performance. Moreover, the proposed *Joint* optimization scheme outperforms other schemes regarding the downlink data rate and the average QoE. This finding confirms the effectiveness of joint optimization, including passive beamforming at RIS, the uplink BER, the transmission power allocation for VR users, and the rendering capacity allocation among virtual objects.

Fig. 5.9 displays the influence of the number of VR users on the average downlink data rate from the AP to the users and average QoE among users in the considered multi-RIS assisted THz wireless VR system. As shown in Fig. 5.9, it can be seen that the average downlink data rate from AP to users and the QoE for all schemes generally decrease as the number of VR users increases, except for an upward trend observed when K is equal to 4 and 5. This is due to the fact that individual users utilize fewer reflective elements as the number

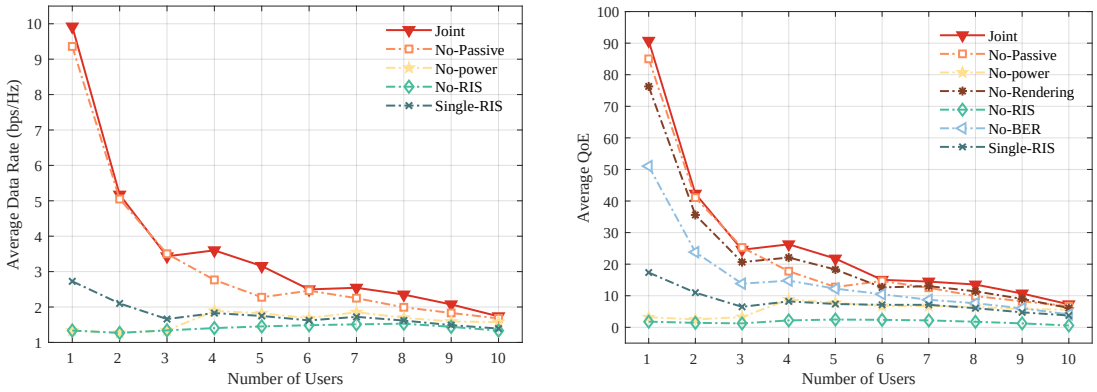

(a) Downlink data rate

(b) Average QoE

Fig. 5.9 The effect of the number of VR users on the downlink data rate from AP to the users and the average QoE among VR users in the considered multiple RIS-assisted THz wireless VR system.

of users increases. However, users u_4 and u_5 are located in LoS area, which includes LoS and NLoS transmission links.

5.7 Conclusion

In this paper, we explore a multi-RIS-assisted THz wireless VR system in the indoor environment and formulate the problem of maximizing QoE for users while ensuring low interaction latency. To tackle the issue, we jointly optimize the passive beamforming at the multiple RIS, the transmission power, and rendering capacity allocation among VR users by objective function conversion and alternative optimization methods. Through simulations, it was demonstrated that increasing the number of reflective elements, the total transmit power, and rendering capacity, can effectively improve the data rate in downlink and the QoE. On the contrary, the performance degrades with increasing VR users. Additionally, deploying an appropriate number of RISs can enhance the data rate and QoE, but excess RISs can be counterproductive in indoor scenarios. To sum up, the proposed multi-RIS-assisted THz wireless VR system is feasible, and the jointly optimized method outperforms other benchmark schemes in terms of QoE.

Chapter 6

Conclusions and Future Directions

In the first task, we focus on multi-RIS multi-user scenarios and the achievable rate maximization for optimizing each RIS's reflecting elements by the MVO algorithm. Our simulation results showcased that the proposed approach equipped with intelligent surfaces can efficiently focus signal transmissions to users and improve the achievable rate compared with baseline schemes. In future work, we will consider a multi-RIS-assisted communication system with multi-hop signal reflection to improve coverage and establish a more intelligent radio environment.

In the second task, we aim to enhance the coverage of outdoor wireless communication networks by deploying large-scale RISs at optimal locations while satisfying network cost constraints. We present quantitative methods based on approximate cell decomposition to calculate coverage probability for RIS-assisted and non-RIS-assisted deployments. Then, we propose the R&B algorithm, which is a Rule-based and Branch-and-Bound-based (B&B) algorithm that optimizes the deployment locations of multiple RIS to maximize coverage probability while satisfying network cost constraints. Extensive simulation results show that the proposed algorithm improves coverage probability by optimizing the deployment locations of RISs. The results also indicate that the R&B algorithm achieves a more excellent trade-off between coverage probability and network cost than other benchmark algorithms. In the future, we will consider a three-dimensional space and user mobility to accurately evaluate the coverage probability.

The third task discusses an optimization problem of the association strategy between RISs and IoT devices and phase shifts to reduce power consumption while satisfying the coverage rate. The proposed algorithm AHOS is based on a heuristic strategy to maximize the coverage rate, which depends on the association relationships between RISs and devices. The phase shifts are optimized by employing the relaxation transformative method to minimize power consumption. The simulation results also demonstrate that the proposed algorithm can

reduce the power consumption of the system while satisfying coverage constraints compared to other schemes. In future work, we will try to design a strategic codebook to achieve a real-time operation for multiple RISs, aiming to respond dynamically to the requests of mobile users.

The last task explores a multi-RIS-assisted THz wireless VR system in the indoor environment and formulate the problem of maximizing QoE for users while ensuring low interaction latency. To tackle the issue, we jointly optimize the passive beamforming at the multiple RIS, the transmission power, and rendering capacity allocation among VR users by objective function conversion and alternative optimization methods. Through simulations, it was demonstrated that increasing the number of reflective elements, the total transmit power, and rendering capacity, can effectively improve the data rate in downlink and the QoE. On the contrary, the performance degrades with increasing VR users. Additionally, deploying an appropriate number of RISs can enhance the data rate and QoE, but excess RISs can be counterproductive in indoor scenarios. To sum up, the proposed multi-RIS-assisted THz wireless VR system is feasible, and the jointly optimized method outperforms other benchmark schemes in terms of QoE.

References

[1] Al-Hilo, A., Samir, M., Elhattab, M., Assi, C., and Sharafeddine, S. (2022). Reconfigurable intelligent surface enabled vehicular communication: Joint user scheduling and passive beamforming. *IEEE Transactions on Vehicular Technology*, 71(3):2333–2345.

[2] Alexandropoulos, G. C., Stylianopoulos, K., Huang, C., Yuen, C., Bennis, M., and Debbah, M. (2022). Pervasive machine learning for smart radio environments enabled by reconfigurable intelligent surfaces. *Proceedings of the IEEE*, 110(9):1494–1525.

[3] Alsharif, M. H., Jahid, A., Kelechi, A. H., and Kannadasan, R. (2023). Green iot: A review and future research directions. *Symmetry*, 15(3):757.

[4] Arun, V. and Balakrishnan, H. (2020). RFocus: Beamforming using thousands of passive antennas. In *17th USENIX symposium on networked systems design and implementation (NSDI 20)*, pages 1047–1061.

[5] Aung, P. S., Park, Y. M., Tun, Y. K., Han, Z., and Hong, C. S. (2023). Energy-efficient communication networks via multiple aerial reconfigurable intelligent surfaces: Drl and optimization approach. *IEEE Transactions on Vehicular Technology*.

[6] Bai, T., Pan, C., Deng, Y., Elkashlan, M., Nallanathan, A., and Hanzo, L. (2020). Latency minimization for intelligent reflecting surface aided mobile edge computing. *IEEE Journal on Selected Areas in Communications*, 38(11):2666–2682.

[7] Basharat, S., Hassan, S. A., Pervaiz, H., Mahmood, A., Ding, Z., and Gidlund, M. (2021). Reconfigurable intelligent surfaces: Potentials, applications, and challenges for 6g wireless networks. *IEEE Wireless Communications*, 28(6):184–191.

[8] Boulogeorgos, A.-A. A. and Alexiou, A. (2021). Coverage analysis of reconfigurable intelligent surface assisted thz wireless systems. *IEEE Open Journal of Vehicular Technology*, 2:94–110.

[9] Bouras, C., Kokkinos, V., and Papazois, A. (2014). Financing and pricing small cells in next-generation mobile networks. In *International Conference on Wired/Wireless Internet Communications*, pages 41–54. Springer.

[10] Cao, X., Yang, B., Huang, C., Yuen, C., Di Renzo, M., Han, Z., Niyato, D., Poor, H. V., and Hanzo, L. (2021a). Ai-assisted mac for reconfigurable intelligent-surface-aided wireless networks: Challenges and opportunities. *IEEE Communications Magazine*, 59(6):21–27.

[11] Cao, X., Yang, B., Zhang, H., Huang, C., Yuen, C., and Han, Z. (2021b). Reconfigurable-intelligent-surface-assisted mac for wireless networks: Protocol design, analysis, and optimization. *IEEE Internet of Things Journal*, 8(18):14171–14186.

[12] Cao, Y. and Lv, T. (2019). Intelligent reflecting surface enhanced resilient design for mec offloading over millimeter wave links. *arXiv preprint arXiv:1912.06361*.

[13] Cao, Y. and Lv, T. (2020). Sum rate maximization for reconfigurable intelligent surface assisted device-to-device communications. *arXiv preprint arXiv:2001.03344*.

[14] Chaccour, C., Amer, R., Zhou, B., and Saad, W. (2019). On the reliability of wireless virtual reality at terahertz (thz) frequencies. In *2019 10th IFIP International Conference on New Technologies, Mobility and Security (NTMS)*, pages 1–5. IEEE.

[15] Chaccour, C. and Saad, W. (2020). On the ruin of age of information in augmented reality over wireless terahertz (thz) networks. In *GLOBECOM 2020-2020 IEEE Global Communications Conference*, pages 1–6. IEEE.

[16] Chaccour, C., Soorki, M. N., Saad, W., Bennis, M., and Popovski, P. (2020). Risk-based optimization of virtual reality over terahertz reconfigurable intelligent surfaces. In *ICC 2020-2020 IEEE International Conference on Communications (ICC)*, pages 1–6. IEEE.

[17] Chaccour, C., Soorki, M. N., Saad, W., Bennis, M., and Popovski, P. (2022). Can terahertz provide high-rate reliable low-latency communications for wireless vr? *IEEE Internet of Things Journal*, 9(12):9712–9729.

[18] Chen, J., Liang, Y.-C., Cheng, H. V., and Yu, W. (2023). Channel estimation for reconfigurable intelligent surface aided multi-user mmwave mimo systems. *IEEE Transactions on Wireless Communications*.

[19] Chen, S., Liang, Y.-C., Sun, S., Kang, S., Cheng, W., and Peng, M. (2020a). Vision, requirements, and technology trend of 6g: How to tackle the challenges of system coverage, capacity, user data-rate and movement speed. *IEEE Wireless Communications*, 27(2):218–228.

[20] Chen, Y., Ai, B., Zhang, H., Niu, Y., Song, L., Han, Z., and Poor, H. V. (2020b). Reconfigurable intelligent surface assisted device-to-device communications. *IEEE Transactions on Wireless Communications*, 20(5):2792–2804.

[21] Cheng, Y., Li, K. H., Liu, Y., Teh, K. C., and Poor, H. V. (2021). Downlink and uplink intelligent reflecting surface aided networks: Noma and oma. *IEEE Transactions on Wireless Communications*, 20(6):3988–4000.

[22] Chepuri, S. P., Shlezinger, N., Liu, F., Alexandropoulos, G. C., Buzzi, S., and Eldar, Y. C. (2023). Integrated sensing and communications with reconfigurable intelligent surfaces: From signal modeling to processing. *IEEE Signal Processing Magazine*, 40(6):41–62.

[23] Cui, M., Zhang, G., and Zhang, R. (2019). Secure wireless communication via intelligent reflecting surface. *IEEE Wireless Communications Letters*, 8(5):1410–1414.

[24] Dai, X., Duo, B., Yuan, X., and Di Renzo, M. (2023). Energy-efficient uav communications in the presence of wind: 3d modeling and trajectory design. *IEEE Transactions on Wireless Communications*.

[25] Das, S. and Mao, E. (2020). The global energy footprint of information and communication technology electronics in connected internet-of-things devices. *Sustainable Energy, Grids and Networks*, 24:100408.

[26] Di, B., Zhang, H., Song, L., Li, Y., Han, Z., and Poor, H. V. (2020). Hybrid beamforming for reconfigurable intelligent surface based multi-user communications: Achievable rates with limited discrete phase shifts. *IEEE Journal on Selected Areas in Communications*, 38(8):1809–1822.

[27] Di Renzo, M., Ntontin, K., Song, J., Danufane, F. H., Qian, X., Lazarakis, F., De Rosny, J., Phan-Huy, D.-T., Simeone, O., Zhang, R., et al. (2020). Reconfigurable intelligent surfaces vs. relaying: Differences, similarities, and performance comparison. *IEEE Open Journal of the Communications Society*, 1:798–807.

[28] Du, H., Liu, J., Niyato, D., Kang, J., Xiong, Z., Zhang, J., and Kim, D. I. (2023). Attention-aware resource allocation and qoe analysis for metaverse xurllc services. *IEEE Journal on Selected Areas in Communications*.

[29] Du, H., Wang, J., Niyato, D., Kang, J., Xiong, Z., Shen, X. S., and Kim, D. I. (2022). Exploring attention-aware network resource allocation for customized metaverse services. *IEEE Network*.

[30] Gao, Y., Yong, C., Xiong, Z., Niyato, D., Xiao, Y., and Zhao, J. (2020). Reconfigurable intelligent surface for miso systems with proportional rate constraints. In *ICC 2020-2020 IEEE International Conference on Communications (ICC)*, pages 1–7. IEEE.

[31] Ge, X., Pan, L., Li, Q., Mao, G., and Tu, S. (2017). Multipath cooperative communications networks for augmented and virtual reality transmission. *IEEE Transactions on Multimedia*, 19(10):2345–2358.

[32] Ghatak, G., Malik, V., Kalamkar, S. S., and Gupta, A. K. (2021). Where to deploy reconfigurable intelligent surfaces in the presence of blockages? In *2021 IEEE 32nd Annual International Symposium on Personal, Indoor and Mobile Radio Communications (PIMRC)*, pages 1419–1424. IEEE.

[33] Guisasola, A., Cortés, A., Cejudo, J., da Silva, A., Losada, M., and Bustamante, P. (2022). Reliable and low-power communications system based on ir-uwb for offshore wind turbines. *Electronics*, 11(4):570.

[34] Guo, H., Yang, Z., Zou, Y., Lyu, B., Jiang, Y., and Hanzo, L. (2022). Joint reconfigurable intelligent surface location and passive beamforming optimization for maximizing the secrecy-rate. *IEEE Transactions on Vehicular Technology*, 72(2):2098–2110.

[35] He, J., Mao, Y., Zhou, Y., Wang, T., and Shi, Y. (2023). Reconfigurable intelligent surfaces empowered green wireless networks with user admission control. *IEEE Transactions on Communications*.

[36] Huang, C., Alexandropoulos, G. C., Yuen, C., and Debbah, M. (2019). Indoor signal focusing with deep learning designed reconfigurable intelligent surfaces. In *2019 IEEE 20th international workshop on signal processing advances in wireless communications (SPAWC)*, pages 1–5. IEEE.

[37] Huang, C., Alexandropoulos, G. C., Zappone, A., Debbah, M., and Yuen, C. (2018). Energy efficient multi-user miso communication using low resolution large intelligent surfaces. In *2018 IEEE Globecom Workshops (GC Wkshps)*, pages 1–6. IEEE.

[38] Huang, C., Mo, R., and Yuen, C. (2020). Reconfigurable intelligent surface assisted multiuser miso systems exploiting deep reinforcement learning. *IEEE Journal on Selected Areas in Communications*, 38(8):1839–1850.

[39] Jian, M., Alexandropoulos, G. C., Basar, E., Huang, C., Liu, R., Liu, Y., and Yuen, C. (2022). Reconfigurable intelligent surfaces for wireless communications: Overview of hardware designs, channel models, and estimation techniques. *Intelligent and Converged Networks*, 3(1):1–32.

[40] Jiang, T. and Yu, W. (2022). Interference nulling using reconfigurable intelligent surface. *IEEE Journal on Selected Areas in Communications*, 40(5):1392–1406.

[41] Khalid, W., Rehman, M. A. U., Van Chien, T., Kaleem, Z., Lee, H., and Yu, H. (2023). Reconfigurable intelligent surface for physical layer security in 6g-iot: Designs, issues, and advances. *IEEE Internet of Things Journal*.

[42] Khorsandmanesh, Y. and Emadi, M. J. (2020). Peak age of information analysis for virtual reality in terahertz communications. In *2020 Iran Workshop on Communication and Information Theory (IWCIT)*, pages 1–6. IEEE.

[43] Kishk, M. A. and Alouini, M.-S. (2020). Exploiting randomly located blockages for large-scale deployment of intelligent surfaces. *IEEE Journal on Selected Areas in Communications*, 39(4):1043–1056.

[44] Lei, W., Wang, Y., Liang, Z., Feng, J., Zhang, W., Fang, J., Chen, Z., and Hou, L. (2023). Asymmetric additive-assisted organic solar cells with much better energy harvesting and wireless communication performance. *Advanced Energy Materials*, 13(40):2301755.

[45] Li, S., Duo, B., Di Renzo, M., Tao, M., and Yuan, X. (2021a). Robust secure uav communications with the aid of reconfigurable intelligent surfaces. *IEEE Transactions on Wireless Communications*, 20(10):6402–6417.

[46] Li, S., Duo, B., Yuan, X., Liang, Y.-C., and Di Renzo, M. (2020). Reconfigurable intelligent surface assisted uav communication: Joint trajectory design and passive beamforming. *IEEE Wireless Communications Letters*, 9(5):716–720.

[47] Li, Z., Hu, H., Zhang, J., and Zhang, J. (2021b). Enhancing indoor mmwave wireless coverage: Small-cell densification or reconfigurable intelligent surfaces deployment? *IEEE Wireless Communications Letters*, 10(11):2547–2551.

[48] Liu, X. and Deng, Y. (2021a). A decoupled learning strategy for mec-enabled wireless virtual reality (vr) network. In *2021 IEEE International Conference on Communications Workshops (ICC Workshops)*, pages 1–6. IEEE.

[49] Liu, X. and Deng, Y. (2021b). Learning-based prediction, rendering and association optimization for mec-enabled wireless virtual reality (vr) networks. *IEEE Transactions on Wireless Communications*, 20(10):6356–6370.

[50] Liu, X., Deng, Y., Han, C., and Di Renzo, M. (2021a). Learning-based prediction, rendering and transmission for interactive virtual reality in ris-assisted terahertz networks. *IEEE Journal on Selected Areas in Communications*, 40(2):710–724.

[51] Liu, Y., Liu, J., Argyriou, A., Wang, L., and Xu, Z. (2021b). Rendering-aware vr video caching over multi-cell mec networks. *IEEE Transactions on Vehicular Technology*, 70(3):2728–2742.

[52] Liu, Y., Liu, X., Mu, X., Hou, T., Xu, J., Di Renzo, M., and Al-Dhahir, N. (2021c). Reconfigurable intelligent surfaces: Principles and opportunities. *IEEE Communications Surveys & Tutorials*, 23(3):1546–1577.

[53] Lubashevsky, I. (2019). Psychophysical laws as reflection of mental space properties. *Physics of Life Reviews*, 31:276–303.

[54] Ma, D., Ding, M., and Hassan, M. (2020). Enhancing cellular communications for uavs via intelligent reflective surface. In *2020 IEEE Wireless Communications and Networking Conference (WCNC)*, pages 1–6. IEEE.

[55] Ma, Y., Ota, K., and Dong, M. (2022). Multi-verse optimizer for multiple reconfigurable intelligent surfaces aided indoor wireless network. In *GLOBECOM 2022-2022 IEEE Global Communications Conference*, pages 6152–6157. IEEE.

[56] Ma, Y., Ota, K., and Dong, M. (2024). Qoe optimization for virtual reality services in multi-ris-assisted terahertz wireless networks. *IEEE Journal on Selected Areas in Communications*.

[57] Mao, S., Liu, L., Zhang, N., Dong, M., Zhao, J., Wu, J., and Leung, V. C. (2022a). Reconfigurable intelligent surface-assisted secure mobile edge computing networks. *IEEE Transactions on Vehicular Technology*.

[58] Mao, S., Liu, L., Zhang, N., Hu, J., Yang, K., Dong, M., and Ota, K. (2022b). Resource scheduling for intelligent reflecting surface-assisted full-duplex wireless-powered communication networks with phase errors. *IEEE Internet of Things Journal*, 10(7):6018–6030.

[59] Mao, S., Zhang, N., Liu, L., Wu, J., Dong, M., Ota, K., Liu, T., and Wu, D. (2021). Computation rate maximization for intelligent reflecting surface enhanced wireless powered mobile edge computing networks. *IEEE Transactions on Vehicular Technology*, 70(10):10820–10831.

[60] Mehrabi, A., Siekkinen, M., Kämäräinen, T., and Yl̈-J̈ski, A. (2021). Multi-tier cloudvr: Leveraging edge computing in remote rendered virtual reality. *ACM Transactions on Multimedia Computing, Communications, and Applications (TOMM)*, 17(2):1–24.

[61] Mirjalili, S., Mirjalili, S. M., and Hatamlou, A. (2016). Multi-verse optimizer: a nature-inspired algorithm for global optimization. *Neural Computing and Applications*, 27(2):495–513.

[62] Multi-User, M. (2020). Channel estimation for ris-empowered multi-user miso wireless communications. *arXiv preprint arXiv:2008.01459*.

[63] Nguyen, K. K., Khosravirad, S. R., Da Costa, D. B., Nguyen, L. D., and Duong, T. Q. (2021). Reconfigurable intelligent surface-assisted multi-uav networks: Efficient resource allocation with deep reinforcement learning. *IEEE Journal of Selected Topics in Signal Processing*, 16(3):358–368.

[64] Nguyen, M.-H. T., Garcia-Palacios, E., Do-Duy, T., Dobre, O. A., and Duong, T. Q. (2022). Uav-aided aerial reconfigurable intelligent surface communications with massive mimo system. *IEEE Transactions on Cognitive Communications and Networking*, 8(4):1828–1838.

[65] Ning, H., Wang, H., Lin, Y., Wang, W., Dhelim, S., Farha, F., Ding, J., and Daneshmand, M. (2021). A survey on metaverse: the state-of-the-art, technologies, applications, and challenges. *arXiv preprint arXiv:2111.09673*.

[66] Ntontin, K., Selimis, D., Boulogeorgos, A.-A. A., Alexandridis, A., Tsolis, A., Vlachodimitropoulos, V., and Lazarakis, F. (2021). Optimal reconfigurable intelligent surface placement in millimeter-wave communications. In *2021 15th European Conference on Antennas and Propagation (EuCAP)*, pages 1–5. IEEE.

[67] Ozcan, Y. U., Ozdemir, O., and Kurt, G. K. (2021). Reconfigurable intelligent surfaces for the connectivity of autonomous vehicles. *IEEE Transactions on Vehicular Technology*, 70(3):2508–2513.

[68] Perović, N. S., Di Renzo, M., and Flanagan, M. F. (2020). Channel capacity optimization using reconfigurable intelligent surfaces in indoor mmwave environments. In *ICC 2020-2020 IEEE International Conference on Communications (ICC)*, pages 1–7. IEEE.

[69] Perović, N. S., Tran, L.-N., Di Renzo, M., and Flanagan, M. F. (2021). Achievable rate optimization for mimo systems with reconfigurable intelligent surfaces. *IEEE Transactions on Wireless Communications*, 20(6):3865–3882.

[70] Qin, H., Liu, Z., and Yang, C. (2022). Indoor mm-wave coverage enhancement: Reconfigurable intelligent surface deployment strategy based on human mobility model. *IEEE Communications Letters*, 26(10):2475–2479.

[71] Rao, J., Zhang, Y., Tang, S., Li, Z., Chiu, C.-Y., and Murch, R. (2023). An active reconfigurable intelligent surface utilizing phase-reconfigurable reflection amplifiers. *IEEE Transactions on Microwave Theory and Techniques*.

[72] Rasilainen, K., Phan, T. D., Berg, M., Pärssinen, A., and Soh, P. J. (2023). Hardware aspects of sub-thz antennas and reconfigurable intelligent surfaces for 6g applications. *IEEE Journal on Selected Areas in Communications*.

[73] Shao, X., Xu, W., Lin, L., and Zhang, F. (2019). A multi-gpu accelerated virtual-reality interaction simulation framework. *Plos one*, 14(4):e0214852.

[74] Shen, K. and Yu, W. (2018). Fractional programming for communication systems—part i: Power control and beamforming. *IEEE Transactions on Signal Processing*, 66(10):2616–2630.

[75] Shi, X., Deng, N., Zhao, N., and Niyato, D. (2022). Coverage enhancement in millimeter-wave cellular networks via distributed irss. *IEEE Transactions on Communications*.

[76] Shu, J., Ota, K., and Dong, M. (2023). Optimizing ris configurations for diverse user requirements via network traffic prediction. In *2023 IEEE 8th International Conference on Smart Cloud (SmartCloud)*, pages 1–6. IEEE.

[77] Shukri, E. S., Al-Sayyed, R., Hudaib, A., and Mirjalili, S. (2021). Enhanced multi-verse optimizer for task scheduling in cloud computing environments. *EXPERT SYSTEMS WITH APPLICATIONS*.

[78] Tang, W., Chen, M. Z., Chen, X., Dai, J. Y., Han, Y., Di Renzo, M., Zeng, Y., Jin, S., Cheng, Q., and Cui, T. J. (2020). Wireless communications with reconfigurable intelligent surface: Path loss modeling and experimental measurement. *IEEE Transactions on Wireless Communications*, 20(1):421–439.

[79] Tang, Z., Zhu, X., Zhu, H., and Xu, H. (2023). Energy efficient optimization algorithm based on reconfigurable intelligent surface and rate splitting multiple access for 6g multicell communication system. *IEEE Internet of Things Journal*.

[80] Teng, B., Yuan, X., Wang, R., and Jin, S. (2022). Bayesian user localization and tracking for reconfigurable intelligent surface aided mimo systems. *IEEE Journal of Selected Topics in Signal Processing*, 16(5):1040–1054.

[81] Thirumavalavan, V. C. and Jayaraman, T. S. (2020). Ber analysis of reconfigurable intelligent surface assisted downlink power domain noma system. In *2020 international conference on COMmunication systems & NETworkS (COMSNETS)*, pages 519–522. IEEE.

[82] Wang, F. and Swindlehurst, A. L. (2023). Applications of absorptive reconfigurable intelligent surfaces in interference mitigation and physical layer security. *IEEE Transactions on Wireless Communications*.

[83] Wang, H., Zhang, Z., Zhu, B., Dang, J., Wu, L., Wang, L., Zhang, K., and Zhang, Y. (2020). Performance of wireless optical communication with reconfigurable intelligent surfaces and random obstacles. *arXiv preprint arXiv:2001.05715*.

[84] Wang, J., Tang, W., Liang, J. C., Zhang, L., Dai, J. Y., Li, X., Jin, S., Cheng, Q., and Cui, T. J. (2022a). Reconfigurable intelligent surface: Power consumption modeling and practical measurement validation. *arXiv preprint arXiv:2211.00323*.

[85] Wang, J., Tang, W., Liang, J. C., Zhang, L., Dai, J. Y., Li, X., Jin, S., Cheng, Q., and Cui, T. J. (2024). Reconfigurable intelligent surface: Power consumption modeling and practical measurement validation. *IEEE Transactions on Communications*.

[86] Wang, Y., Su, Z., Zhang, N., Xing, R., Liu, D., Luan, T. H., and Shen, X. (2022b). A survey on metaverse: Fundamentals, security, and privacy. *IEEE Communications Surveys & Tutorials*.

[87] Wang, Y. and Zhao, J. (2022). Mobile edge computing, metaverse, 6g wireless communications, artificial intelligence, and blockchain: Survey and their convergence. *arXiv preprint arXiv:2209.14147*.

[88] Wu, J., Kim, S., and Shim, B. (2022). Energy-efficient power control and beamforming for reconfigurable intelligent surface-aided uplink iot networks. *IEEE Transactions on Wireless Communications*, 21(12):10162–10176.

[89] Wu, Q. and Zhang, R. (2019a). Beamforming optimization for wireless network aided by intelligent reflecting surface with discrete phase shifts. *IEEE Transactions on Communications*, 68(3):1838–1851.

[90] Wu, Q. and Zhang, R. (2019b). Intelligent reflecting surface enhanced wireless network via joint active and passive beamforming. *IEEE Transactions on Wireless Communications*, 18(11):5394–5409.

[91] Wu, Q. and Zhang, R. (2019c). Towards smart and reconfigurable environment: Intelligent reflecting surface aided wireless network. *IEEE Communications Magazine*, 58(1):106–112.

[92] Wu, Q., Zhang, S., Zheng, B., You, C., and Zhang, R. (2021). Intelligent reflecting surface-aided wireless communications: A tutorial. *IEEE Transactions on Communications*, 69(5):3313–3351.

[93] Xia, S., Shi, Y., Zhou, Y., and Yuan, X. (2021). Reconfigurable intelligent surface for massive connectivity: Joint activity detection and channel estimation. *IEEE Transactions on Signal Processing*, 69:5693–5707.

[94] Xu, B., Zhou, T., Xu, T., and Wang, Y. (2021). Reconfigurable intelligent surface configuration and deployment in three-dimensional scenarios. In *2021 IEEE International Conference on Communications Workshops (ICC Workshops)*, pages 1–6. IEEE.

[95] Yang, G. and Luo, C. (2023). Performance improvement in uav communication systems with uncertain solar energy supply. *IEEE Internet of Things Journal*.

[96] Yang, L., Yang, J., Xie, W., Hasna, M. O., Tsiftsis, T., and Di Renzo, M. (2020). Secrecy performance analysis of ris-aided wireless communication systems. *IEEE Transactions on Vehicular Technology*, 69(10):12296–12300.

[97] Yang, Z., Zhang, H., Zhang, H., Di, B., Dong, M., Yang, L., and Song, L. (2022). Metaslam: Wireless simultaneous localization and mapping using reconfigurable intelligent surfaces. *IEEE Transactions on Wireless Communications*, 22(4):2606–2620.

[98] Yu, X., Xu, D., Sun, Y., Ng, D. W. K., and Schober, R. (2020). Robust and secure wireless communications via intelligent reflecting surfaces. *IEEE Journal on Selected Areas in Communications*, 38(11):2637–2652.

[99] Zappone, A., Sanguinetti, L., Bacci, G., Jorswieck, E., and Debbah, M. (2015). Energy-efficient power control: A look at 5g wireless technologies. *IEEE Transactions on Signal Processing*, 64(7):1668–1683.

[100] Zeng, S., Zhang, H., Di, B., Han, Z., and Song, L. (2020). Reconfigurable intelligent surface (ris) assisted wireless coverage extension: Ris orientation and location optimization. *IEEE Communications Letters*, 25(1):269–273.

[101] Zhang, G., Zhang, D., He, Y., Chen, J., Zhou, F., and Chen, Y. (2023). Passive human localization with the aid of reconfigurable intelligent surface. In *2023 IEEE Wireless Communications and Networking Conference (WCNC)*, pages 1–6. IEEE.

[102] Zhang, H., Zhang, H., Di, B., Bian, K., Han, Z., and Song, L. (2021). Metalocalization: Reconfigurable intelligent surface aided multi-user wireless indoor localization. *IEEE Transactions on Wireless Communications*, 20(12):7743–7757.

[103] Zhang, J. and Blough, D. M. (2022). Optimizing coverage with intelligent surfaces for indoor mmwave networks. In *IEEE INFOCOM 2022-IEEE Conference on Computer Communications*, pages 830–839. IEEE.

[104] Zhang, Y., Jiao, L., Yan, J., and Lin, X. (2019). Dynamic service placement for virtual reality group gaming on mobile edge cloudlets. *IEEE Journal on Selected Areas in Communications*, 37(8):1881–1897.

[105] Zheng, B., You, C., and Zhang, R. (2021). Double-irs assisted multi-user mimo: Cooperative passive beamforming design. *IEEE Transactions on Wireless Communications*, 20(7):4513–4526.

[106] Zheng, G. and Yuan, L. (2023). A review of qoe research progress in metaverse. *Displays*, page 102389.

[107] Zhong, R., Liu, X., Liu, Y., Chen, Y., and Han, Z. (2022). Mobile reconfigurable intelligent surfaces for noma networks: Federated learning approaches. *IEEE Transactions on Wireless Communications*, 21(11):10020–10034.

[108] Zhou, Y., Liu, Y., Wu, Q., Shi, Q., Zhao, J., and Zhao, Y. (2023). Queueing aware power minimization for wireless communication aided by double-faced active ris. *IEEE Transactions on Communications*.

[109] Zhou, Y., Pan, C., Yeoh, P. L., Wang, K., Elkashlan, M., Vucetic, B., and Li, Y. (2020). Communication-and-computing latency minimization for uav-enabled virtual reality delivery systems. *IEEE Transactions on Communications*, 69(3):1723–1735.

Publications

Journals

1. Yuyin Ma, Kaoru Ota, Mianxiong Dong, "QoE Optimization for Virtual Reality Services in Multi-RIS-Assisted Terahertz Wireless Networks," IEEE Journal on Selected Areas in Communications (JSAC), vol. 42, Issue 3, pp 538 - 551, March 2024.

2. Yuyin Ma, Kaoru Ota, Mianxiong Dong, "Multi-RIS Deployment Location Optimization for Coverage Enhancement in Outdoor Wireless Communication Networks," IEEE Transactions on Vehicular Technology (TVT), *In Press*.

Proceeding of International Conference

1. Yuyin Ma, Kaoru Ota, "Multi-verse optimizer for multiple reconfigurable intelligent surfaces aided indoor wireless network," IEEE Global Communications Conference (Globecom), Rio de Janeiro, Brazil, December 4-8, 2022.

Under Review

1. Yuyin Ma, Kaoru Ota, "Optimizing Power with Reconfigurable Intelligent Surfaces for Indoor Communication Networks," IIEEE Transactions on Wireless Communications.

Chapter 7

Appendix

7.1 Proof of Virtual LoS Link Probability

Assuming the user is situated at the origin and the BS is positioned at a distance of m from the user, as shown in Fig. 3.3. RISs can be utilized to establish virtual LoS connections between specific cells and BSs. RIS locations are modeled using an inhomogeneous Poisson point process (PPP) $\Psi_{RIS}^{I|m}$, with the density function $\lambda_I(m,n,\varphi) = \lambda_{RIS} f_i(m,n,\varphi)$. As a result, the probability of establishing at least one virtual LoS link between a specific cell and the BS, located at a distance of m, can be defined as follows.

$$\begin{aligned} P_{cov}^{I}(m) &= \mathbb{P}\left(\mathscr{N}_{\Psi_{RIS}^{I|m}}\left(\mathbb{R}^2\right) > 0\right) \\ &= 1 - \mathbb{P}\left(\mathscr{N}_{\Psi_{RIS}^{I|m}}\left(\mathbb{R}^2\right) = 0\right) \end{aligned} \tag{7.1}$$

where $\mathscr{N}_{\Psi_{RIS}^{I|m}}\left(\mathbb{R}^2\right)$ represents the number of $\Psi_{RIS}^{I|m}$ in area $\mathbb{R}^2$, then

$$\mathbb{P}\left(\mathscr{N}_{\Psi_{RIS}^{I|m}}\left(\mathbb{R}^2\right) = 0\right) = \exp\left(-\int_{\mathbb{R}^2} \lambda_{RIS}(m,n,\varphi)\, d\mathrm{n} d\varphi\right) \tag{7.2}$$

Substituting (7.2) in (7.1) results in the final expression in (3.8).

7.2 Proof of Reflection Probability

As shown in Fig. 3.3, we first derive $d_{R,B}$ using the law of cosines with respect to m, n, and φ, which can be implemented as follows.

$$d_{R,B}^2 = m^2 + n^2 - 2mn\cos(\varphi) \tag{7.3}$$

Similarly, the value of the $\theta_{g,bs}$ can be obtained with respect to m, n, and φ as follows.

$$\begin{aligned} m^2 &= n^2 + d_{R,B}^2 - 2d_{R,B}n\cos(\varphi) \\ &\overset{(7.3)}{=} n^2 + m^2 + n^2 - 2mn\cos(\varphi) \\ &\quad - 2n\sqrt{m^2+n^2-2mn\cos(\varphi)}\cos\left(\theta_{g,bs}\right) \end{aligned} \tag{7.4}$$

According to (7.4), we can obtain the cosine value of the angle $\theta_{g,bs}$ as follows.

$$\cos\left(\theta_{g,bs}\right) = \frac{n - m\cos(\varphi)}{\sqrt{m^2+n^2-2mn\cos(\varphi)}} \tag{7.5}$$

Hence, the reflection probability is

$$\begin{aligned} \mathscr{C} &= \mathbb{P}\left(\theta_{g,ris} \geq \theta_{g,bs}\right) \\ &\overset{(7.5)}{=} \mathbb{P}\left(\theta_{g,ris} \geq \cos^{-1}\left(\frac{n - m\cos(\varphi)}{\sqrt{m^2+n^2-2mn\cos(\varphi)}}\right)\right) \\ &\overset{(c)}{=} 1 - \frac{1}{\pi}\cos^{-1}\left(\frac{n - m\cos(\varphi)}{\sqrt{m^2+n^2-2mn\cos(\varphi)}}\right) \end{aligned} \tag{7.6}$$

where (c) is due to $\theta_{g,ris} \sim U(0,\pi)$.